KU LEUVEN

ARENBERG DOCTORAL SCHOOL
Faculteit Wetenschappen

Spectroscopic investigations of inhomogeneous barrier mechanisms of reversible photodegradation of aminoanthraquinone-doped polymer matrices

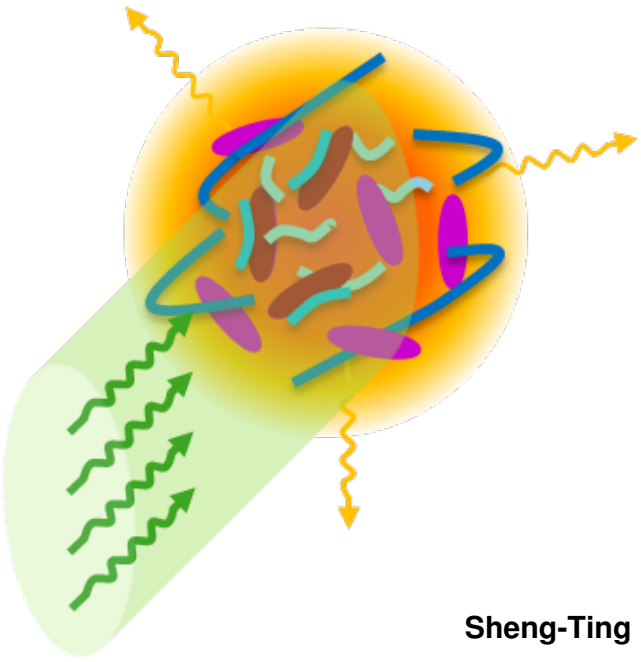

Sheng-Ting Hung

Supervisor:
Prof. Dr. Koen Clays
Prof. Dr. Mark G. Kuzyk
(Washington State University)

Dissertation presented in partial fulfillment of the requirements for the degree of PhD in Science

May 2015

Spectroscopic investigations of inhomogeneous barrier mechanisms of reversible photodegradation of aminoanthraquinone-doped polymer matrices

Sheng-Ting HUNG

Examination committee:

Prof. Dr. Koen Clays, supervisor, co-chair
Prof. Dr. Mark G. Kuzyk, supervisor, co-chair
(Washington State University)
Prof. Dr. Guy Koeckelberghs
Prof. Dr. Brian A. Collins
(Washington State University)
Prof. Dr. Matthew D. McCluskey
(Washington State University)

Dissertation presented in partial fulfillment of the requirements for the degree of PhD in Science

May 2015

Uitgegeven in eigen beheer, Sheng-Ting Hung, Afdeling Moleculaire Visualisatie en Fotonica, Celestijnenlaan 200D, B-3001 Heverlee (Belgium)

DEDICATION

To My Family

Ching Chi Hung

Chin Chu Wu

Hsin Yu (Beryl) Hung

Hsin Ying (Ami) Hung

Acknowledgements

First, I would like to thank my parents for their unconditional support in my life. I would like to thank my sisters for always supporting me and encouraging me. I would like to thank Prof. Chin-Hsien Wang for introducing me to the fascinating scientific research.

I would like to thank my advisors: Prof. Mark Kuzyk in Washington State University and Prof. Koen Clays in KU Leuven. I am very grateful to have your immense support and patience which provided me an excellent opportunity to explore various research possibilities and dive into a curiosity-driven research. I treasure all the excitement and the experience of years of " ... battles with frustration on a daily basis.", as once described by Prof. Kuzyk, in this journey that has enriched my life.

I would like to thank Prof. Matthew McCluskey for generously providing me the access to the Fourier transform infrared spectrometer in his laboratory and valuable discussions. Thanks also to his research group for the technical help.

I would like to thank Prof. Kirk Peterson in the Chemistry Department at WSU for his kind guidance and advice in quantum chemistry calculation, and the technical help that made it possible for me to conduct the study.

I would like to thank Prof. Brian Collins for introducing me useful experimental techniques that are currently applied to characterize dye-doped polymer materials through his collaboration with Prof. Mark Kuzyk and willing to be in my committee.

I would like to thank Prof. Guy Koeckelberghs for his valuable time and willing to participate in my dissertation as a committee member.

I would like to thank Prof. Javier Perez-Moreno for insightful discussions in quantum mechanics and non-linear optics. I am also indebted to Dr. Candy Mercado for invaluable discussions in molecular spectroscopy. I am thankful to both of you for sharing the excitement in the journey with me.

I would like to thank my past and present coworkers, especially Dr. Benjamin

Anderson in WSU for valuable discussions and criticism, Dr. Inge Asselberghs, Kasper Baert and Wim Libaers during the time I worked in KU Leuven, and Shiva Ramini, Xianjun Ye, Elizabeth Bernhardt, David Wyrick, Kyle Schademan, Prabodh Dhakal, Sean Mossman, Joseph Lanska and Nathan Rasmussen here in WSU, for valuable discussions and helps in experiments.

I would like to thank the staff members of the Chemistry Department in KU Leuven and the Physics Department in WSU for their tremendous help.

Last but not least, I would like to thank KU Leuven, WSU and Air Force Office of Scientific Research for supporting my research.

Abstract

Reversible photodegradation is a relatively new phenomenon observed mostly in dye-doped polymer materials. While the mechanism responsible for reversible photodegradation is not yet understood, a kinetic model describing the time-dependence of reversible photodegradation has been quantitatively examined with previous studies in disperse orange 11 doped in poly(methyl methacrylate) (DO11/PMMA) using amplified spontaneous emission (ASE) and transmittance image microscopy (TIM) techniques. However, we find that the latest kinetic model is inconsistent with new experimental results.

We hypothesize a mechanism responsible for reversible photodegradation of 1-substituted aminonanthraquinones doped in two polymers, PMMA and polystyrene. In this hypothesis, photodegradation of dye originates from (photo)chemical reactions between dye and thermally-degraded polymers, and recovery corresponds to the metastable reaction products returning back to the pristine dye. Reversible photodegradation of dye dissolved in liquid monomers and doped in polymers have been studied using ultraviolet-visible (UV-Vis) spectroscopy. The absorption spectra of proposed photodegraded species are obtained experimentally and compared with time-dependent density functional theory calculations. The change of molecular structures in reversible photodegradation is investigated with Fourier transform infrared spectroscopy. These results qualitatively verify the proposed mechanism.

New experimental results suggest inhomogeneous kinetics of photodegradation and recovery, and diffusion is proved to not be involved. Reversible photodegradation experiments probed with ASE and UV-Vis spectroscopy simultaneously confirm that new observations are the same processes as in previous studies probed with ASE. Comparing new results of photodegradation in DO11/PMMA with previous ASE studies, we find that the photodegradation rate may vary depending on whether the irradiation generates ASE, which results in disagreement between two studies. We also find that the temperature dependent photodegradation and recovery data supports an energy barrier scenario which contradicts the previous model, but does not fully agree with a simple energy barrier model. A possible cause is that the correct rate distribution

due to special heterogeneity is not yet found.

The proposed mechanism indicates that a key to improve the photo-stability of doped polymers is to eliminate the possibility of (photo)chemical reactions occurring between dopants and thermally-degraded polymers.

Contents

List of Figures

List of Tables

Chapter 1

Introduction

Degradation of materials caused by absorption of photons is referred to as photodegradation. Photodegradation is often undesirable, though in some cases it may be intended to prevent environmental pollution [1, 2] or utilized for photolithography [3–5]. Over the past decade, a vast variety of solid solutions, typically doped polymers, have been found to self-heal after photodegradation when kept in dark [6–18]. It is remarkable that self-healing takes place without intervention, but rather is a spontaneous process. The commonly observed self-healing phenomenon seems to contradict the second law of thermodynamics, which suggests that damage in materials is an irreversible process.

In this chapter, we begin with the motivation of this study, followed with the introduction of several self-healing phenomena observed from various materials in literature, and a review of previous studies on this topic. Then we discuss issues and challenges in past research as a motivation for the present studies.

1.1 Motivation

Organic dyes and polymers, which are the typical (but not the only) forms of materials exhibiting the self-healing phenomenon, have been widely applied in daily life such as textiles, paint, monitors and smart phones, and utilized and studied in various fields of research such as high-resolution fluorescence microscopy [19–22], second harmonic generation (SHG) microscopy [23–27], dye sensitized, organic and polymer solar cells [28–32], dye lasers [33–37], organic light emitting diodes [38, 39] and photodynamic therapy [40, 41]. Photostability of organic compounds and polymers is often a requirement for applications incorporating light-matter interaction [20–22, 36, 37, 42–46].

Fluorophores play a crucial role in biological science primarily in microscopy owing to resolution gains from imaging living matter tagged with fluorescence-emitting molecules [19–22]. Fluorophores are also π-conjugated molecules, as are the molecules in dye sensitized solar cells (DSSCs) [30–32], organic photovoltaics (OPV) [29–31], organic light-emitting diodes (OLEDs) [38, 39] and dye lasers [34–37]. Advances in optical techniques and fluorophores provide more precise measurements and powerful tools superior to conventional microscopy. Fluorescence microscopy is also much more sensitive than other microscopies, as it is a zero-background technique [24]. Two-photon and multiphoton microscopy have improved spatial resolution due to the nature of the nonlinear interaction between light and the molecules [20, 21]. By taking into account the photophysical and photochemical properties of fluorophores, super-resolution fluorescence microscopy achieved a resolution far beyond the diffraction limit [22]. However, photobleaching of fluorophores leads to reduced fluorescence signal and decreased resolution [20–22, 42, 43]. Improving photostability and avoiding phototoxicity of fluorophores in two-photon fluorescence microscopy, which requires excitation of fluorophores and thus causes photodegradation of fluorophores, can be achieved by using SHG microscopy, since excitation of the molecule is not required for harmonic light generation [23, 24]. This implies that dye molecules should be designed with rapid relaxation pathways, or with a large SHG signal and avoiding two-photon absorption to prevent excited states formation [23–27]. Thus, finding more about materials is one avenue for addressing photobleaching.

DSSCs utilizing organic dyes to generate photocurrent has strongly attracted industrial interest and has been an active research field [28]. Organic and polymer solar cells use π-conjugated molecules and polymers to harvest solar energy with advantages such as being free of toxic liquid electrolytes that can leak, having greater mechanical flexibility and ease of manufacturing thin film devices [30–32]. Exposure to sunlight can cause photodegradation of dyes or polymers, affecting durability and reliability of DSSCs, organic and polymer solar cells, which is their main disadvantage over conventional photovoltaic cells [44, 45].

Dye lasers, both in liquid solution and in the solid state, have nearly a half century of use in a wide range of research and technology [35–37]. Owing to the broad absorption and emission bands of dyes, dye lasers possess unique operational flexibility in a wide variety of excitation sources, great tunability of lasing wavelengths and capability of generating ultrashort pulses [34, 35]. Although liquid dye lasers have been well developed for decades and are still popular as light sources, the cumbersome design and the need of routinely changing large amounts of toxic dyes and organic solvents due to photodegradation prohibit their usage outside the laboratory. A solid state dye laser incorporating rhodamine 6G in a polymer matrix was developed just one year after the liquid dye laser was invented [33], which suggested a promising alternative. The main drawback is the poor photostability of organic dyes in

solid matrices and has been the main focus of research in developing robust solid state dye lasers [36, 37, 46].

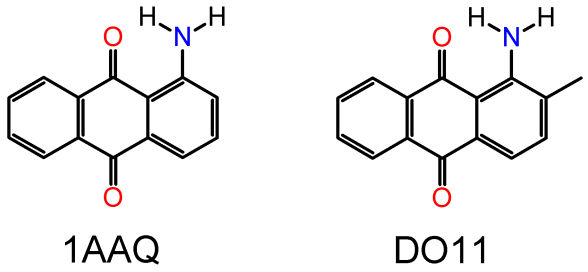

Figure 1.1: Dye molecules used in this study: 1-Aminoanthraquinone (1AAQ) and disperse orange 11 (DO11).

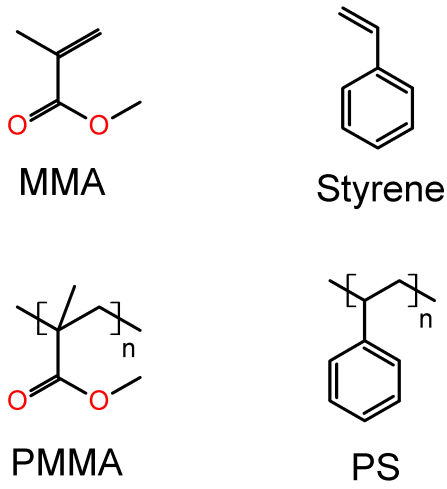

Figure 1.2: Monomers and polymers used in this study: methyl methacrylate (MMA), poly(methyl methacrylate) (PMMA), styrene and polystyrene (PS).

The observed reversible photodegradation in solid solutions and its potential for applications as mentioned above strongly motivated this study. This study aims to unveil the mechanism responsible for reversible photodegradation in aminoanthraquinones-doped polymer matrices with molecular structures shown in Figure 1.1 and 1.2, and shed light on the mechanism responsible for the potentially universal self-healing property of solid solutions.

1.2 Observations of reversible photodegradation

Photostability of a material is usually studied by exposing the material to light and recording a characteristic property of the material such as fluorescence, transmittance or refractive index. When a material undergoes photodegradation, its characteristic properties change over time, which is referred to as decay. For instance, the fluorescence intensity may decrease (or increase) monotonically due to photodegradation; the reverse change in the characteristic properties of the material is referred to as recovery. If photodegradation is an irreversible process, once the characteristic property of a material decays after light exposure, that property remains constant over time after the light source causing the damage is turned off. Over the past decade, the recovery process has been observed from a large variety of solid solutions with different experimental techniques when the photodegraded materials were kept in dark for a long enough time, typically many hours.

Fluorescence decay of rhodamine B- and pyrromethene-doped polymer optical fibers as a result of exposing to a 514 nm continuous wave (cw) laser was observed to recover completely or partially in the dark depending on the fluence of irradiation during decay, and the recovery could take several hours [6]. A series of polymethine dyes underwent photobleaching due to irradiation of a 532 nm picosecond laser, and the nonlinear optical absorption of polymethine dyes was observed to restore from photobleaching with a single rapid recovery on the order of seconds in ethanol solution, while in a solid poly(urethane acrylate) elastopolymer host the recovery was observed to possess a fast component on the order of minutes and a slow component on the order of hours to days, and the restoration was found to be incomplete after high optical pump exposure during decay [7]. Photoluminescence intensity of porous silicon nanoparticles embedded in a UV cured polymer recovered completely or partially in a single exponential fashion several hours after photoluminescence quenching caused by exposing the sample to a 488 nm cw laser irradiation, while the quenching was irreversible for nanoparticles alone [8]. Photoluminescence intensity of an organic light-emitting diodes containing 8-hydroxyquinoline aluminum was observed to partially recover in hours to days from photodegradation due to UV light or visible laser exposure [10]. A partial restoration in the performance of a DSSC device containing dye-sensitized nanoporous TiO_2 and gel electrolyte composed by mixing poly(methyl methacrylate) (PMMA), acetonitrile and propylene carbonate (a gelling solvent), was observed after keeping the device in the dark for 9 hours [11]. Two-photon fluorescence of AF455, an organic dye doped into PMMA, was observed to almost fully recover in the dark for 9 hours after being irradiated with a picosecond laser [12]. AF455 doped in PMMA (AF455/PMMA) was observed to not only heal from photodegradation caused by low fluence irradiation of a femtosecond laser, but laser ablated pits were found to heal after high fluence laser ablation with the same femtosecond laser, while no recovery was observed in damaged neat PMMA [13]. Full and partial recovery

of AF455/PMMA were observed 1-3 months after photodegradation and laser ablation, depending on fluence. PMMA polymer optical fibers doped with a polyfluorene conjugated polymer was observed to exhibit partial recovery of one- and two-photon-excited emission 24 hours after the decay due to irradiation of a femtosecond laser [17].

The causes of the above self-healing phenomena were undetermined, though some possible mechanisms were discussed by the authors without further study. Nonetheless, mechanisms responsible for the recovery process of some systems were investigated in the following studies. Femtosecond laser-induced refractive index change of amorphous soda lime glass completely recovered two years after micromachined (irradiated) by a femtosecond laser, and the healing process was proposed to be the recombination of trapped electron-hole pairs produced by electron ejection through a multi-photon absorption process under irradiation [13]. In contrast to soda lime glass, there was no recovery observed from SiC crystalline materials after femtosecond laser micromachining. The same hypothesis was applied to the healing of AF455/PMMA after photodegradation caused by femtosecond laser mentioned above, but the healing from laser ablation was unexplained. Fluorescence recovery from two-photon bleaching was observed in plasticizer added to dye-doped poly(vinyl alcohol) films, but not in pure dye-doped polymer films, and the recovery was attributed to dye diffusion [47]. However, diffusion may not apply to other observations since it was not observed in pure dye-doped polymer, which characterizes a majority of systems exhibiting the self-healing phenomenon. Single-walled carbon nanotube- (SWNT) adsorbed rhodamine B was reported to show complete recovery in fluorescence intensity when stored in the dark for several hours after photobleaching under 514 nm cw laser irradiation, and the mechanism causing decay and recovery of fluorescence intensity was ascribed to charge transfer between dye and SWNT [48]. Reversible photobleaching was only observed in the first layer of rhodamine B attached to SWNT while other dye molecules underwent permanent photooxidation. Although charge transfer may be applicable to other observations, the mechanism suggests full recovery which is not always observed from other systems in which dopants and hosts have more homogeneous mixture than SWNT-adsorbed dye. Recombination of trapped electron-hole pairs, diffusion and charge transfer may explain the self-healing phenomenon observed in some systems, but not all systems.

Amplified spontaneous emission (ASE) in 1-Amino-2-methylanthraquinone (1,2-AMAQ), also known as disperse orange 11 (DO11), doped in PMMA was observed to fully recover in the dark about 40 hours after photodegradation when irradiated by a 532 nm second harmonic ND:YAG picosecond laser [9]; however, no recovery was observed from ASE decay in DO11 dissolved in dimethylformamide liquid solution [49]. The self-healing phenomenon was also observed in various anthraquinone derivatives doped into PMMA [14, 16] and DO11 doped in MMA-styrene copolymers [15, 50]. Reversible photodegradation of DO11/PMMA has been studied with various experimental techniques [9,

16, 50–53], and will be further studied in this work. An example of reversible photodegradation in DO11/PMMA probed by ASE and linear absorption spectroscopy from this work is shown in Figure 1.3.

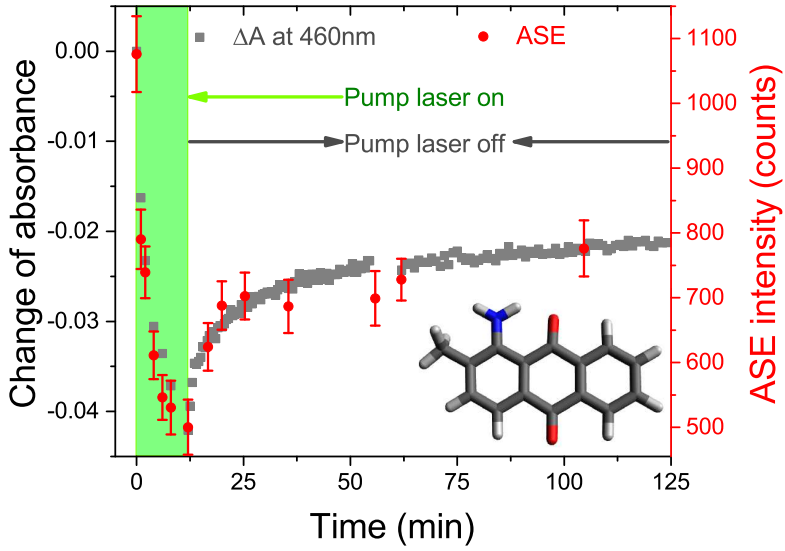

Figure 1.3: Reversible photodegradation of a DO11/PMMA thin-film sample. The sample was irradiated by a cw laser with wavelength 532 nm for 12 minutes, then left in the dark with pump laser turned off. The molecular structure represents DO11: black represents the carbon atom, gray is the hydrogen atom, red is the oxygen atom and blue is the nitrogen atom.

As described above, reversible photodegradation of solid solutions has been observed in a wide variety of dopants and polymer hosts over the past decade. While recombination of trapped electron-hole pairs, diffusion and charge transfer may explain reversible photodegradation for some specific systems, mechanisms causing reversible photodegradation for many other systems remain unsolved. Since most systems exhibiting reversible photodegradation have polymers as the host - the recovery time is typically between hours to days, and the degree of recovery often depends on fluence - there may be a universal mechanism responsible for reversible photodegradation phenomenon in solid solutions of which the observations in this study are special case.

1.3 Previous studies

Two possible mechanisms responsible for reversible photodegradation of DO11/P-MMA have been examined in early studies. Linear dichroism measurements

excluded orientational hole burning as the mechanism causing reversible photodegradation [51]. Spatially resolved ASE and fluorescence [54] and spatial image [52] studies indicated that diffusion/back diffusion is not responsible for reversible photodegradation. While the underlying mechanism is not yet known, some phenomenological models have been proposed based on quantitative studies of reversible photodegradation in AF455/PMMA and DO11/PMMA using various experimental techniques over the past decade [12, 16, 50, 51, 53, 55–57].

1.3.1 Non-interaction model

Based on two photon fluorescence (TPF) measurements of reversible photodegradation of AF455/PMMA, a simple model was proposed by considering a two species system where the fresh sample and reversibly-damaged species, produced under irradiation, convert into each other with a decay rate proportional to the pump intensity and a constant recovery rate [12]. The same model was adopted to explain ASE experimental results of DO11/PMMA by assuming that the fresh dye emits ASE after excitation and returns to a vibronic or tautomer ground state, then nonradiatively relaxes to the ground state of the fresh dye or forms dimers with another tautomer that does not produce ASE. Recovery is then characterized by a nonradiative decay of this long-lived dimer state to the ground state consisting of fresh dye [51]. In these experiments, the decay of TPF and ASE signals was observed to be a single exponential function, and the decay rate was assumed to be proportional to pump intensity I thus being denoted as αI. The recovery was observed to be a single exponential function of constant recovery rate β. Therefore the rate equation can be written as

$$\frac{dn_f(t)}{dt} = -\alpha I n_f(t) + \beta[1 - n_f(t)], \tag{1.1}$$

where $n_f(t)$ is the fraction of fresh dye as a function of time, i.e. $n_f(0) = 1$ for a fresh sample. The solution of the rate equation is

$$n_f(t) = \frac{\beta}{\beta + \alpha I} + \frac{\alpha I}{\beta + \alpha I} e^{-(\beta+\alpha I)t}. \tag{1.2}$$

For the recovery process, $I = 0$, and the fraction of fresh dye is given by

$$n_f(t) = 1 - [1 - n_f(t_0)]e^{-\beta(t-t_0)}, \tag{1.3}$$

with t_0 being the time at which the laser is turned off.

This phenomenological model fits the experimental decay data in TPF intensity of AF455/PMMA and ASE intensity of DO11/PMMA over a range of pump intensities and recovery data in both studies. In the TPF study, it was noticed that the recovery rate β obtained from fitting to decay process ($I \neq 0$) is larger than that from fitting to the recovery process ($I = 0$), but

both values appeared to converge at the limit of low pump intensity. The larger β obtained from decay data was attributed to the heating effect under irradiation, i.e. the recovery was accelerated at elevated temperatures. It was also discussed in the ASE study that recovery could be governed by a barrier process in which the reversibly-damaged species may return back to the pristine dye. The recovery rate should increase at higher temperature, but there was no available data except for preliminary results supporting the energy barrier hypothesis mentioned in the study. However, the model given by Equation 1.2 and 1.3 simply describes the decay as a function of time and pump intensity and recovery as a function of time without considering the effect of environment such as temperature, dye concentration and polymer host.

In addition, Equation 1.2 regresses to $\exp(-\alpha I t)$ for $\alpha I \gg \beta$, i.e. photodegradation only depends on αI, while recovery only depends on β. Though this seems to qualitatively agree with the fast decay and slow recovery observed in Figure 1.3, the long-time behavior of recovery exhibits a stretched exponential function instead of a single exponential function as will be seen in Chapter 8.

1.3.2 Correlated chromophore domain model

Based on additional quantitative studies of reversible photodegradation in ASE intensity of DO11/PMMA at various sample temperatures and concentrations, the correlated chromophore domain model (CCDM) was proposed which describes the observations that an increase in temperature leads to a decrease in recovery rate and an increase in concentration of dye leads to a decrease in decay rate and increase in recovery rate [53, 55]. These observations and the CCDM disagree with the energy barrier hypothesis discussed in the previous study [51]. The CCDM was later modified to account for dose-dependent studies using transmittance image microscopy (TIM), which monitors the change in transmitted light [50]. The model assumed that domain formation of pristine dye molecules, either mediated by polymer or dye aggregation alone [58, 59], results in a decay rate in inverse proportion to domain size and a recovery rate in proportion to domain size, and that the domain size is invariant, i.e. both pristine and reversibly-damaged molecules are counted in the domain originally formed by pristine dye, during decay and recovery at a constant temperature. The condensation model proposed that pristine dye and the reversibly-damaged species convert into each other, but that the rates depend on the domain size which decreases with temperature and promotes self-healing. For a domain including N dye molecules, the rate equation becomes

$$\frac{dn(t)}{dt} = -\frac{\alpha I}{N} n(t) + \beta N[N - n(t)], \tag{1.4}$$

where $n(t)$ is the number of undamaged (fresh) dye molecules in the domain and $N - n(t)$ is the number of reversibly-damaged species at time t. Integrating

Equation 1.4, we obtain the population of undamaged dye molecules as a function of time

$$n(t) = \frac{\beta N^2 + [(\beta N + \frac{\alpha I}{N})n(0) - \beta N^2]\exp[-(\beta N + \frac{\alpha I}{N})t]}{\beta N + \frac{\alpha I}{N}}, \tag{1.5}$$

for a domain of size N. The population of undamaged dye molecules during the recovery process can be obtained by integrating Equation 1.4 with $I = 0$,

$$n(t) = N + [n(t_0) - N]e^{-\beta N(t-t_0)}. \tag{1.6}$$

The observed ASE intensity and the transmittance are an ensemble sum of all domains. The distribution of domains $\Omega(N)$ is derived from a grand canonical partition function of a condensation model by minimizing the Helmholtz free energy, yielding

$$\Omega(N) = \frac{1}{z}\left[\frac{(1+2\rho z) - (1+4\rho z)^{1/2}}{2\rho z}\right]^N, \tag{1.7}$$

where $z = \exp(\frac{\mu}{k_B T})$, μ is the energy required for a dye molecule to join a domain, k_B is the Boltzmann constant, T is the temperature and $\rho = \Sigma_{N=1}^{\infty} N\Omega(N)$ is the total number of dye molecules in the system [53, 55]. The total number of undamaged dye molecules is then given by the ensemble average

$$\begin{aligned} \bar{n}(t;\rho,T,N,I) &= \sum_{N=1}^{\infty} n(t;N,I)\Omega(N;\rho,T) \\ &\approx \int_1^{\infty} n(t)\Omega(N)dN, \end{aligned} \tag{1.8}$$

which can be experimentally measured.

In this model, domain size is determined by the competition between thermal disorder and attractive forces between chromophores and/or between dye and polymer; thus, domain size increases with increasing concentration of dye but decreases with increasing temperature. As a result, the recovery rate decreases as temperature increases, which is opposite to an energy barrier model as discussed in the non-interaction model.

1.3.3 Further modifications on the CCDM

In previous models, it was assumed that the reversible photodegradation of dye-doped polymer matrices is due to pristine dye molecules and reversibly-damaged species converting into each other, which implies full recovery when samples are allowed to recover for long enough time. However, full recovery was

not always observed in ASE experiments. TIM experiments using a cw pump laser showed partial recovery, which indicated the presence of both reversible and irreversible species as decay products. The previous models only worked for the condition that irreversible damage is negligible. It was also observed in TIM measurements that an external electric field affects the kinetics of reversible photodegradation of DO11/PMMA due to the interaction among the electric field and dipole moments of fresh and damaged dye molecules and ions and radicals as possible damaged products [16, 56]. The CCDM was further modified by adding an irreversibly-damaged species, and taking into account the electric field's effect on the self-healing phenomenon [16, 57, 60]. The modified model describes the same concentration and temperature effects as the CCDM does, and it suggests that the external electric field breaks domains into smaller ones. The mathematical expressions describing this model are rather complicated and are not the focus in this work, so they are not presented here.

1.4 Issues and challenges

As mentioned in previous section, earlier studies on TPF from AF455/PMMA and ASE from DO11/PMMA suggested an energy barrier process for self-healing, but later studies using ASE and transmittance from DO11/PMMA led to the CCDM whose behavior was opposite to the prediction of a barrier process. There have been several inconsistent observations from previous and current studies:

1. ASE and TPF decay was assumed coming respectively from pristine DO11 and AF455 molecules, and exhibited a single exponential decay function even when ASE intensity decayed to about 20% of the initial intensity [9, 12, 51, 53, 55]. The change in transmittance of DO11/PMMA for all species during decay exhibited a fast and a slow decay process and was attributed to reversible and irreversible decay products that are formed at higher pump intensities [16, 57]. In current study of DO11/PMMA, ASE intensity and transmitted pump beam are recorded simultaneously. While ASE intensity exhibits a single exponential decay, the transmitted pump intensity shows a non-exponential decay processes as discussed in Chapter 8.

2. The ASE intensity of a 9 g/L DO11/PMMA sample recovers in about 30 hours to 90% of its initial value after about a 63% drop during degradation when using a picosecond laser [9]. The ASE intensity from a DO11/PMMA sample (concentration not specified) recovers to 90% in about 10 hours after about a 70-80% drop from the initial intensity when irradiated with a nanosecond laser [51]. Though the concentration of DO11/PMMA was not indicated for the later case, ASE quenching was noticed at concentration

higher than 9 g/L and the degree of recovery at 9 g/L was observed to be better than at lower concentrations in the same paper; thus, the concentration used for the recovery data in the later case was most likely 9 g/L.

3. The ASE intensity from a damaged DO11/PMMA sample recovered as a single exponential function in some measurements with relatively severe damage (ASE intensity reduced to about 20-37% of the initial intensity) [9, 51]. However, the recovery of the ASE intensity in other measurements with less damage (ASE intensity dropped to about 75-80% of initial intensity) fits best to a stretched exponential function which can be clearly seen by comparing the single-exponential-like CCDM fit [53] with the stretched exponential fit to the same ASE recovery data as discussed in Chapter 8. The degree of recovery in the first 100 minutes (approximately 50-60%) was found to be similar to that in the literature [51], where the ASE intensity dropped to about 75% of initial intensity after photodegradation, which suggests a similar stretched exponential recovery curve though the recovery after 100 minutes was not shown. The ASE intensity recovered fully in above measurements. Recovery in transmittance of DO11/PMMA using the TIM technique was observed to fit the single-exponential-like CCDM, which seemed to agree with ASE recovery from relatively severely damaged samples, but the full recovery was never observed [16, 50, 57]. Experiments using linear absorption spectroscopy suggest a stretched-exponential partial recovery, which will be presented in Chapter 8.

4. Measurements using the nonlinear optical process of ASE as a probe is more sensitive than linear optical techniques [53] such as fluorescence and transmittance. However, it was observed that even though the ASE intensity from DO11/PMMA fully recovered after burning with a nanosecond laser, a burn line was still visible under TIM as described in the literature [16].

5. It was concluded from ASE experiments that DO11/PMMA is more resistant to photodegradation at higher dye concentration, so the decay rate decreases as dye concentration increases [50, 51, 53, 55], but, experiments using linear absorption spectroscopy find the opposite concentration dependence, which will be described in Chapter 8.

6. ASE experiments found no recovery from DO11 dissolved in dimethylformamide liquid solution [49]. Recovery was only observed in dye-doped polymer matrices [9]. However, recovery of DO11 in liquid monomer is observed using linear absorption spectroscopy, which is described in Chapter 5.

These observations point to inconsistencies that need to be resolved. Secondly, the underlying mechanism responsible for reversible photodegradation of dye-

doped polymer matrices is not yet understood. However, the mechanisms of orientational hole burning and diffusion have been ruled out. A phenomenological model of the observations should be in agreement with the underlying mechanism, and understanding the mechanism will help to determine the kinetics of the self-healing phenomenon.

To investigate the underlying mechanism, our approach is to consider all possible photodegradation processes and molecular species formed that can recover or are irreversibly-damaged by reviewing similar systems and proposed mechanisms in literature. From these, we select the most likely candidate based on experimental data as described in Chapter 2. The experimental techniques employed in this work are described in Chapter 3. Since a stretched exponential time dependence of the undamaged population during recovery has been observed using linear absorption spectroscopy, we revisit the diffusion hypothesis, which was eliminated previously using only data that appeared to show a single exponential recovery of population. An analysis is given in Chapter 4. Reversible photodegradation studies of dyes dissolved in liquid monomer solutions as probed with linear absorption spectroscopy are described in Chapter 5, quantum chemistry calculations of the possible degraded species are carried out in Chapter 6, and reversible photodegradation studies of the dye-doped polymer matrix using Fourier transform infrared spectroscopy (FTIR) are presented in Chapter 7.

With the better understanding of the possible underlying mechanism, we then model the kinetics of the self-healing phenomenon. In addition to the amorphous nature of polymers, ASE intensity measurements require the pump laser to remain on, which could further damage a sample during recovery. Thus, it is difficult to reproduce experimental results from run to run even under identical experimental conditions. Although it is not possible to resolve all inconsistent results obtained by various researchers using different methods of probing the decay/recovery process, we have chosen to use the simple and reliable method of linear absorption spectroscopy, together with ASE measurements, to resolve some crucial issues such as the inconsistency between the observed single-exponential-like and stretched exponential behavior of the recovery kinetics, the temperature and concentration dependence of decay and recovery, and the nature of the phenomenological model. These are described in Chapter 8.

Chapter 2

Proposed mechanism

Most research reported in the literature on 1-substituted aminoanthraquinone derivatives focus on 1-Aminoanthraquinone (1AAQ) instead of DO11, the molecule studied most extensively in our laboratory. However, there should be no significant difference in photoinduced reactions between 1AAQ and DO11 with the same polymer host since the only difference between the two is a methyl group. Indeed, reversible photodegradation has been observed from both dyes doped in PMMA, as presented in Chapter 4, 6 and 8.

Anthraquinone exhibits a weak optical absorption band at 405 nm [61, 62], with an extinction coefficient about 60 $cm^{-1}M^{-1}$ which is often undetected [62]. Aminoanthraquinones, however, possess moderate to strong absorption bands in the visible region, which are absent in anthraquinone, and have been assigned to intramolecular charge transfer (ICT) between the amine group and the carbonyl groups [63, 64]. For example, DO11 dissolved in MMA is observed to show an absorption peak at 471 nm with the extinction coefficient about 8×10^3 $cm^{-1}M^{-1}$ in our lab. It is noticed that the calculated electron density of 1AAQ is also increased in the unsubstituted ring, in addition to the carbonyl groups, at the first excited state relative to the ground state [62]. This indicates that the carbonyl groups are not the only electron acceptors [62], which is consistent with the results reported by Inoue et al. that the calculated electron density of 1AAQ at the first excited state is increased in the carbonyl groups, the center ring and the unsubstituted ring, though they only mentioned the carbonyl groups in the text [63]. This is also in agreement with the quantum chemistry calculation conducted in this work as will be described in Chapter 6.

The absorbance of degraded 1AAQ/PMMA, DO11/PMMA and DO11/PS is hypsochromically (blue) shifted and has decreased magnitude with respect to that of fresh samples as presented in Chapter 4, 6 and 8; for example, the degraded DO11/PMMA is observed to have an absorption peak at around 450

nm with the extinction coefficient approximately 5.7×10^3 $cm^{-1}M^{-1}$. If the ICT in DO11 was completely disrupted due to photodegradation, the absorption spectrum of the damaged species in the visible regime would result in that similar to anthraquinone, which implies that the amplitude of the absorption band of the damaged species would be reduced to about 0.75% of the fresh DO11 spectrum, and the absorption peak would be hypsochromically shifted to about 405 nm; however, this is not observed. The measured absorbance of degraded aminoanthraquinones suggests that the ICT from the amine group to the carbonyl groups, the center ring and the unsubstituted ring is partially but not completely disrupted after photodegradation. Disruption of the ICT can occur by breaking the conjugated path; or lowering the electron donating power of the donor (by oxidation or protonation); or by lowering the electron accepting power of the acceptors (by reduction, or deprotonation if possible). For the concision of the text, we describe the ICT to be between the amine group and the carbonyl groups in this dissertation, though there are in fact multiple electron acceptors as described above. Note that "damage" (or "degradation") used in this dissertation is a phenomenological descriptor, protonation of the amine is not really "damage", but it stops the charge transfer.

Several photodegradation processes and molecular species formed that can recover or are permanently damaged in systems of or similar to aminoanthraquinones-doped polymer matrices have been observed or proposed without observation [51, 58, 59, 65–69]. These mechanisms and possible damaged dye species are discussed in this chapter to compare with the observed reversible and irreversible photodegradation in this study. Studies on relaxation of excited 1AAQ, thermal degradation of PS and PMMA, and photoinduced damage in dye-doped polymer matrices are summarized based on a literature survey. A possible mechanism responsible for the observed reversible and irreversible photodegradation of 1-substituted aminoanthraquinones doped in polymer matrices is proposed based on the literature survey, quantum chemistry calculation and experimental results that test these hypotheses.

2.1 Reversible photodegradation of dye

2.1.1 Intramolecular Proton transfer (IPT)

Photoinduced IPT tautomerization was proposed as a possible mechanism by Embaye et al. [51] This hypothesis posits that a DO11 molecule undergoes photoinduced IPT tautomerization via the transfer of a proton from the amine group to the adjacent carbonyl group to form a new O−H bond, leaving behind an N−H bond as shown in Figure 2.1(a). This proton transfer leaves the molecule in an excited IPT state that decays to the tautomer ground state by emitting a photon. Since the excited state is long lived, an excited population

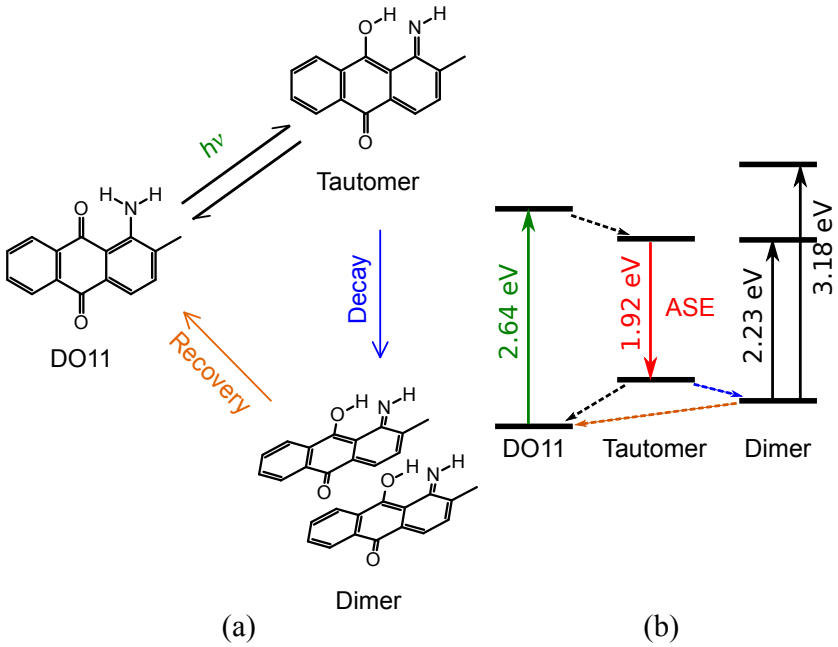

Figure 2.1: (a) Photoinduced IPT tautomerization in DO11 and the mechanism responsible for reversible photodegradation.(b) The corresponding energy level diagram.

of tautomers can be stimulated to emit coherent light by the emission of the photon. The ground state tautomer may then return to the ground state of the original DO11 molecule via nonradiative decay. Alternatively, it can undergo dimer formation with another tautomer or form a dimer via direct double proton transfer between two DO11 molecules, perhaps primarily by π-stacking as shown in Figure 2.1(a). It is proposed that dimers do not contribute to ASE by quenching any fluorescence, therefore they are the "degraded" species. The sample heals when the higher energy dimers gradually return to the lower energy individual DO11 molecules through nonradiative decay. The corresponding energy level diagram is shown in Figure 2.1(b).

While some hydroxy- and amino-anthraquinones were observed to exhibit excited-state intramolecular proton transfer (ESIPT) [70, 71], ESIPT was not observed in others, including 1AAQ [71, 72]. Nagaoka and Nagashima explained that ESIPT takes place for hydroxy- and amino-anthraquinones due to "the deformation of the aromatic ring skeleton instead of the motion of the hydrogen nucleus" [73]. The absence of ESIPT in 1AAQ is consistent with the visible absorption band of 1AAQ originating from ICT rather than IPT [63, 72].

Despite the earlier studies showing no evidence of ESIPT from 1AAQ,

dichroism of DO11 doped in PMMA was observed at room temperature originating from keto-enol phototautomerisation, in agreement with the observed photoinduced molecular reorientation [74], but at odds with the work of Embaye et al., who observed no evidence of orientational hole burning [51].

Given the proximity of the proton between the amine group and the adjacent carbonyl group, the tautomer structure could coexist with the structure of the ground state of 1AAQ (and DO11). It could be represented also as "the internal hydrogen bond present in the neutral molecule" as mentioned in the literature [75]. Thus, IPT in 1-substituted aminoanthraquinones may not require being photoinduced and the deformation of the aromatic ring skeleton. However, earlier studies suggested that aminoanthraquinones exist only in the amino form but not the tautomer structure [62].

2.1.2 Twisted intramolecular charge transfer (TICT)

Westfall and Dirk proposed TICT as being involved in reversible photodegradation of DO11 [65]. The amine group of a DO11 molecule can twist out of the molecular plane after photoexcitation as shown in Figure 2.2. The TICT state is found to be a long-lived excited state so the recovery process is associated with a relaxation from the TICT state to the ground state, accompanied with fluorescence or phosphorescence. Comparing IPT with TICT using semiempirical computational methods, they concluded that TICT is more energetically favorable than IPT in the gas phase of DO11, but did not consider solvent interactions, which can affect the result. However, phosphorescence is not observed in DO11/PMMA during recovery as expected when a TICT state is present.

However, the partial double bond (+)N=C ensures sp^2 hybridization for the nitrogen atom, which enforces both N−H to remain in the plane, and thus no twist can be invoked. In other words, a twist requires a single bond. Therefore, TICT state does not seem to be promising even though it is more energetically favorable than IPT state.

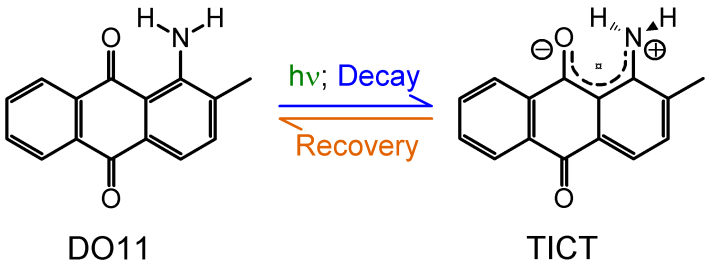

Figure 2.2: TICT in DO11 upon photoexcitation.

2.2 Reversible photodegradation of dyes in solvents

2.2.1 Anion formation

Reversible rhodamine dye anions were observed to form from photoreduction of the triplet state of rhodamine by thiols in aqueous solution, and the stability of the radical was ascribed to the delocalization of the free electron in a conjugated system, i.e. rhodamine dye [76]. Anthraquinones are used in industrial production of hydrogen peroxide (H_2O_2) [77]. Anthraquinones are good oxidants accepting electrons through the electron accepting carbonyls (C=O). With protons, the anthraquinone is reduced to anthrahydroquinons, with C−OH rather than C=O, but this is not stable and is being regenerated to the anthraquinone in the presence of air (O_2) to produce hydrogen peroxide [77]. In the other hand, anthraquinone anions were observed to be stable in aqueous alkaline solutions for more than one year in the absence of air, and the stability of the radical anion was attributed to the anthraquinone's symmetrical structure and to the delocalization of electrons [66].

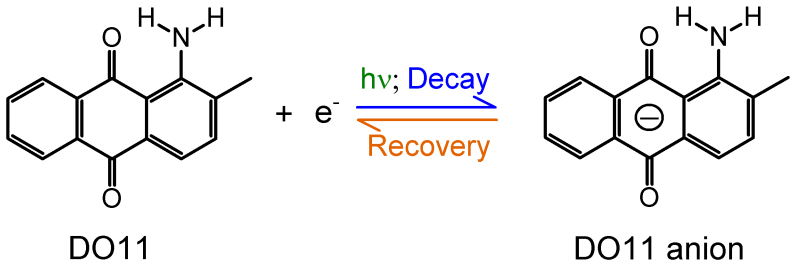

Figure 2.3: Anion formation of DO11 doped in polymer matrix.

PMMA can be regarded as a Lewis base owing to the carbonyl oxygens being basic (electron donor) sites [78]. It was also observed that DO11-doped PMMA has a propensity for free and trapped charges [16, 56]. Therefore, the formation of aminoanthraquinone anions in a polymer matrix could be a possible decay product, perhaps being formed when a dye molecule captures a free electron, an excited trapped electron, or an electron ejected by the polymer due to energy transfer from excited dye molecules through nonradiative relaxation [34, 79] as illustrated in Figure 2.3. Anions could gradually return to the neutral state by ejecting extra electrons, thus recovering from photodegradation. Measurements of photodegradation and recovery in the presence of an applied electric field suggests that a charged species may be involved [16, 56, 57], supporting the hypothesis that a charged or polarizable species is formed during photodegradation.

Alternatively, aminoanthraquinones are basic, and the -NH_2 electron

donating group can accept a proton becoming -$NH_3(+)$ [62, 75]. The protonated base results in a positively charged dye species. It is known that the protonated 1-substituted aminoanthraquinones are practically colorless [62], which can be understood since the ICT, which causes the visible absorption band, is disrupted due to the electron donor losing the electron donating power. Since the visible absorption band is still observed for degraded dye species, protonation is eliminated from the responsible mechanisms for reversible and irreversible photodegradation in 1-substituted aminoanthraquinones-doped polymers.

2.2.2 Domains

Hydrogen bonding between DO11 molecules or DO11 tautomers and the PMMA polymer were proposed to be responsible for domain formation [58, 59]. As described in Chapter 1, domains, which are hypothesized to drive recovery after photodegradation of DO11/PMMA in the correlated chromophore domain model (CCDM), might be associations of molecules along a common polymer chain held in place by hydrogen bonding between the amine group of DO11 and the carbonyl groups in PMMA, and/or between N−H and O−H of the DO11 tautomer and carbonyl groups in PMMA as illustrated in Figure 2.4. In this hypothesis, DO11 molecules and tautomers may co-exist; or, only one species exists in the pristine state. In either case, the tautomer is not considered to be a degraded product. The predicted hydrogen bond energy between a DO11 tautomer and PMMA, 0.30 eV, is within experimental uncertainty of the chemical potential determined from a fit of the data using the CCDM, 0.29±0.01 eV (28 ± 1 kJ/mol), though the bond energy could differ due to the environment, making it possible that other types of aggregation might be responsible for

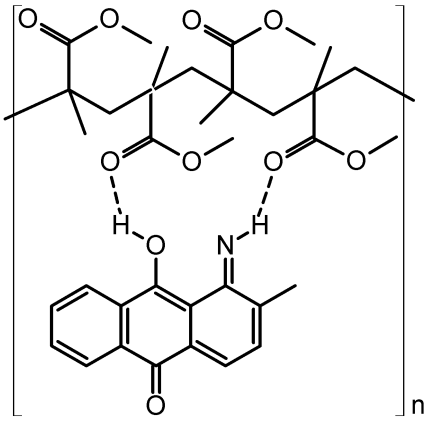

Figure 2.4: Domain formation of DO11 tautomer doped in PMMA. Dashed lines indicate hydrogen bonds.

domain formation [50, 53]. Nonetheless, domain formation is independent from the CCDM which is a kinetic model describing the reversible photodegradation of dye-doped polymer using the concept of domains.

Photodamage involves fragments dissociated from the parent dye molecules and/or tautomers after photoexcitation. Healing is the recombination of a damaged fragment and its counterpart, where the polymer keeps the damaged fragments in close enough proximity to increase the likelihood of recombination. Therefore, domains mediate the healing process.

2.2.3 Photochemical reaction between dye and solvents

Cycloaddition is a reaction in which unsaturated molecules (or parts of an unsaturated molecule) combine and form a cyclic adduct (see Figure 2.5). Photocycloaddition of 1AAQ to olefines was observed by visible light irradiation provided by an optically filtered ($\lambda > 420$ nm) 300 W high-pressure mercury lamp at 0 °C [67, 68]. Olefines are unsaturated hydrocarbon molecules, including dienes and styrene which is one of the molecules examined in the literature. Dienes are hydrocarbon molecules containing two carbon-carbon double bonds. It was proposed that the carbonyl group adjacent to the amine group of 1AAQ reacts under exposure of visible light as illustrated in Figure 2.5 with a diene (or olefine) to form the corresponding oxetane, which is a ring structure composed of one oxygen and three carbon atoms. The structures of some reaction products were confirmed by IR, NMR, and mass spectroscopy [67, 68]. Although there was no reaction observed between 1AAQ and monoenes, which are hydrocarbon molecules containing one carbon-carbon double bond such as methyl methacrylate (MMA, the monomer of PMMA as shown in Figure 1.2), the reason was not mentioned in the literature [67, 68].

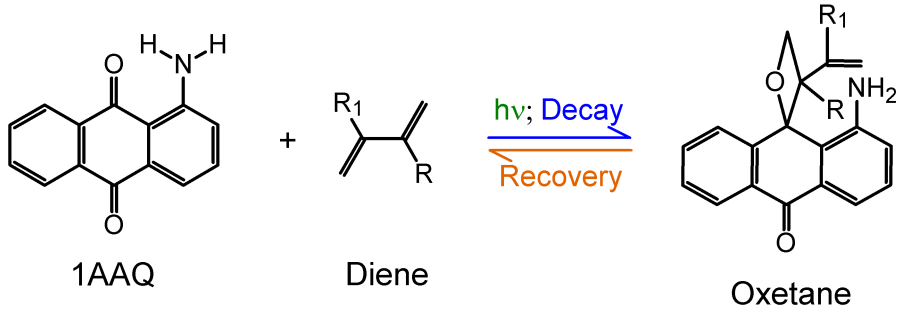

Figure 2.5: Reversible photocycloaddition of 1AAQ with a diene.

A possible explanation is that the light source used in the experiment did not provide enough intensity to show a measurable reaction rate, but if the solution is irradiated with a higher-powered light source such as a laser, the reaction

rate might be increased above the detection threshold. Another hypothesis is that the visible light source did not provide enough energy to overcome the activation energy for photocycloaddition of 1AAQ with monoenes at 0 °C. However, when irradiating the solution with a more intense light source such as a laser, the energy density in the vicinity of the irradiated dye molecules might be temporarily high due to nonradiative relaxation of excited dye molecules, thus, overcoming the activation energy of photocycloaddition. As pointed out in the beginning of this chapter, there should be no significant difference in photoinduced reactions between 1AAQ and DO11 in the same environment. Thus, photocycloaddition is likely to occur between DO11 and styrene and also between DO11 and MMA when exposed to a laser. The structures of photocycloaddition products between DO11 and styrene and DO11 and MMA are shown in Figure 2.6.

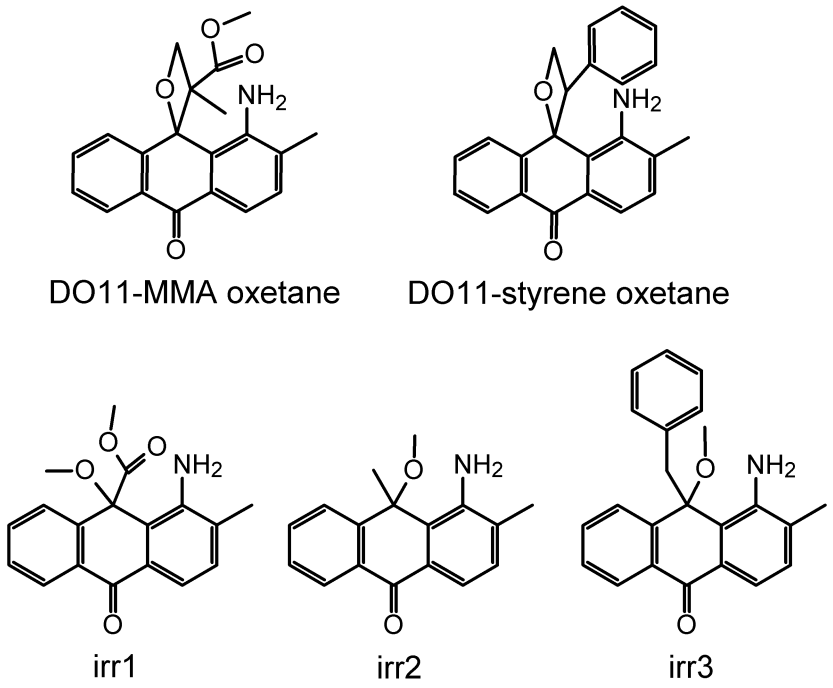

Figure 2.6: First row: Proposed reversibly-damaged DO11 biproducts made by photocycloaddition with MMA (left) and styrene (right). Second row: Illustration of possible irreversibly-damaged DO11 species.

Photocycloaddition was proposed to involve excited complex (exciplex) formation between an excited ICT state of 1AAQ and an olefine [69]. The photocycloaddition was unaffected by oxygen, and the reaction products were unstable in an environment of carbon dioxide, acid, light, and heat [67, 68].

Most importantly, the reaction products were found to gradually decompose into other compounds including 1AAQ itself at 30 °C [67]. The return of 1AAQ from the photocycloaddition products could be the recovery process observed in 1AAQ-doped polymer matrices if photocycloaddition occurs between 1AAQ (or DO11) and the polymer hosts or fragments of thermally degraded polymers, including depolymerized monomers due to locally accumulated heat via nonradiative relaxation of excited dye molecules. Compounds decomposed from photocycloaddition products other than 1AAQ (or DO11) would be the irreversibly-damaged species. This hypothesis, when applied to PMMA (with MMA being the depolymerized monomer), does not involve the two carbon-carbon double bonds, or a conjugated system, as is clear from the results and the proposed mechanism for styrene [67–69]. This implies that the same mechanism [69] might be valid for olefines in general, including MMA, and not restricted to dienes or a conjugated system. The possibility of thermal degradation of doped polymers will be discussed in Section 2.3. Some possible irreversibly-damaged DO11 species are illustrated in Figure 2.6.

We attribute the reversible photodegradation to photocycloaddition in this dissertation since it has be observed in similar systems in the literature as described above. However, before verifying the structure of reversibly-damaged dye species, we should not exclude the possibility that other (photo)chemical reactions, instead of photocycloaddition, take place between 1AAQ (or DO11) and thermally degraded polymers resulting in a metastable product which can gradually return to the fresh dye molecule. The important point is that the (photo)chemical reaction occurs due to the availability of thermally degraded polymers.

2.3 Irreversible photodegradation of a dye-doped polymer

Isosbestic points are found in an absorption spectrum when one species converts into another one. When one species converts into two other species, each at a different rate, isosbestic points are found under the following conditions: one species does not exhibit an absorption band overlapping with the other two in the wavelength range of interest; or, two of the three species possess the same absorption spectrum in the measured wavelength range. The approximate absorption spectra of irreversibly-damaged DO11/PS and DO11/PMMA requires exposing samples to laser radiation for long enough time so that the absorbance no longer changes, and the resulting peaks are blue shifted and reduced in magnitude relative to the absorption spectra of the fresh sample. Thus, reversibly-damaged DO11 species either has no absorption peak overlapping with both fresh and irreversibly-damaged species in the visible wavelength range, or has the same absorption spectrum as that of fresh or

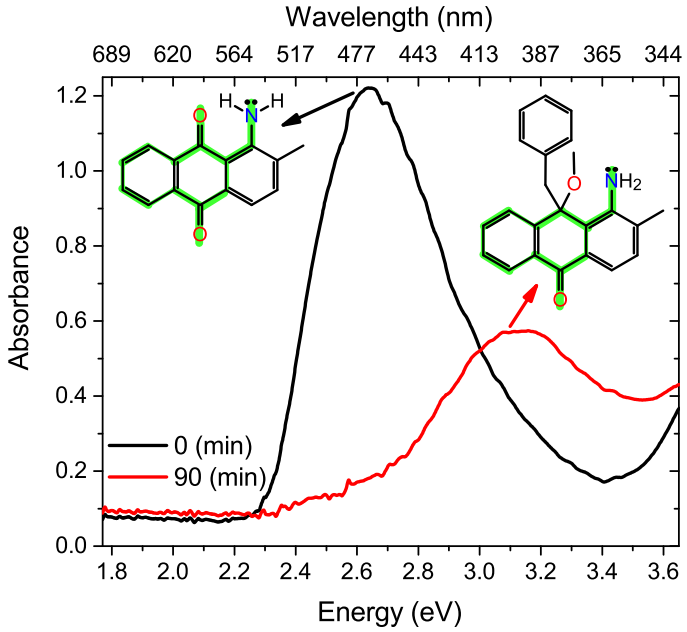

Figure 2.7: Absorption spectra of a 9 g/L DO11/PS thin film sample taken before (0 min) and after 90 minutes (90 min) of irradiation using a 532 nm wavelength cw laser with intensity 35.0 W/cm^2. The visible absorption band of pristine DO11 (0 min) is due to the ICT from the amine group to both carbonyl groups, the center ring and the unsubstituted ring as illustrated with thick green lines, and that of a possible irreversibly-degraded DO11 species (90 min) indicates partial ICT path remaining. The electron density of pristine DO11 and damaged species is calculated in Chapter 6 and plotted in Appendix B.

irreversibly-damaged species. Details about the absorption spectra of reversibly- and irreversibly-damaged species are discussed in Chapter 6 and Appendix A.

IPT, TICT, or anion formation do not produce an irreversibly-damaged dye species, i.e. these mechanisms suggest full recovery from photodegradation; thus, there must be another pathway to irreversible photodamage. Irreversible photodegradation of dye-doped polymer matrices could originate from the decomposition of pristine dye, decomposition from the reversibly-degraded dye species, or, photochemical reactions between dye and polymer. As described in the beginning of this chapter, the absorption band of 1-substituted aminoanthraquinones in the visible wavelength region is due to the ICT from the amine group to the two carbonyl groups, the center ring and the unsubstituted ring as illustrated in Figure 2.7 for pristine DO11/PS. The presence of a visible absorption band in the irreversibly-damaged DO11 species suggests that the ICT path is partially damaged as illustrated in Figure 2.7 for a

possible irreversibly-damaged DO11 species from photodegraded DO11/PS. The complication of having two mechanisms responsible for reversible and irreversible photodegradation with the simultaneous requirement that the absorption spectra of three species match in a way that the isosbestic points are present makes these three (reversible photodegradation) hypotheses unlikely. Indeed, quantum chemistry calculations exclude the IPT and anion formation hypotheses as will be described in Chapter 6, and the absence of phosphorescence during recovery after photodegradation in 1-substituted aminoanthraquinones-doped PS and PMMA eliminates the TICT hypothesis. On the other hand, domain formation or photochemical reaction between dye and polymer are viable hypotheses that provide an explanation for reversible and irreversible photodegradation in dye-doped polymers.

As described in Section 2.2.2, photodegradation of dye may be caused by decomposition of pristine dye molecules or tautomers following photoexcitation, and recombination of the decomposed fragments is assisted by the domain in which they reside. Nonetheless, the incident photon energy alone (2.33 eV and 2.54 eV used in this study) is insufficient to break the chemical bonds of an aminoanthraquinone molecule in vacuum. For example, the lowest average single bond energy in 1AAQ is 3.1 eV (300 kJ/mol) for C−N [80]. Therefore, decomposition of dye molecules is most likely mediated by local heating via nonradiative relaxation of photoexcited dye molecules. Nonradiative relaxation process can also transfer the absorbed photon's energy to the polymer causing damage. The damaged dye and polymer, which may contain radicals and/or ions, might react with each other to cause irreversible photodegradation of the dye.

As will be discussed in Chapter 7, the molecular structure of 1AAQ is confirmed from FTIR measurements and both the reversibly- and irreversibly-damaged products are associated with a change of the infrared (IR) peak attributed to the C=O group adjacent to the amine group, which is absent in the tautomer structure. 1AAQ (or DO11) and its tautomer may exhibit different absorption spectra, decay rates and recovery rates; thus, an isosbestic point during decay and recovery would be absent if both species were present in the fresh sample. It is possible that a domain is formed by interaction between pristine 1AAQ (or DO11) and PMMA, though the hydrogen bond energy is inconsistent with the chemical potential determined from previous ASE and TIM studies [50, 53] which agrees with the hydrogen bond energy between 1AAQ (or DO11) tautomers and PMMA as mentioned in Section 2.2.2. However, the local environment could change these energies, so the observation alone does not definitively rule out hydrogen bonding.

Recall that the CCDM predicts that the decay rate decreases as the concentration of dye increases, which contradicts the observation that will be described in Chapter 8. We posit that if reversible and irreversible damage of the dye is due to local heating, a sample with higher dye concentration should

decay faster due to a greater rate of heat accumulation around the dense regions of dye molecules, which is consistent with the observation in Chapter 8, but at odds with the CCDM.

The further decomposition from the products of photocycloaddition between dye and solvents as described in Section 2.2.3 provides another possible channel of irreversible photodegradation. Local heating due to nonradiative relaxation of photoexcited dye molecules could cause thermal degradation of the polymer in the vicinity of the excited dye molecules, resulting in generation of monomers, radicals and other thermally degraded polymer segments. Thus, photocycloaddition between 1AAQ (or DO11) and monomers becomes feasible when exposing 1AAQ- (or DO11-) doped polymers to light. As presented for DO11 in Figure 2.6, all reversibly- and irreversibly-damaged species involve breaking the carbon-oxygen double bond adjacent to the amine group and both carbon and oxygen atoms single-bonded to other components. Therefore, only the other carbonyl group remains as the electron acceptor of ICT in damaged species, which implies that all reversibly- and irreversibly-damaged DO11 species have the same visible absorption band.

Both hypotheses of domains and a photochemical reaction between dye and solvents are compatible with local heating through nonradiative relaxation of photoexcited dye, which causes the decomposition of dye molecules (the hypothesis of domains) and/or polymer scission (both hypotheses), resulting in both reversible and irreversible photodegradation of dye-doped polymer matrices. The fluorescence quantum yield of 1AAQ in several organic solvents was reported to be less than 10% [81, 82]. Thus, in 1AAQ, most of the absorbed photon energy is lost via nonradiative relaxation, leading to an accumulation of heat centered on the 1AAQ molecule. This local buildup of heat can cause decomposition of chemical bonds even when an individual photon's energy is too low to break a bond.

Thermal degradation of polymers has been studied extensively for several decades, and the dominant products of thermal degradation of PS and PMMA are known to be their monomers, styrene and MMA, respectively [83–85]. Mechanisms of thermal degradation such as depolymerization, scission of side chains, and dissociation of the polymer backbones take place depending on the environment, temperature, molecular weight, chain end groups, chain configuration, polymerization condition etc. [83–97] As such, the activation energy of thermal degradation can vary greatly. It is generally found to be between 1.87 eV and 3.34 eV for PS in an inert atmosphere or vacuum [86], and from 1.23 eV to 3.55 eV for PMMA in an inert atmosphere [85, 87–89, 92, 94–96]. The photon energies of lasers used in this study are 2.33 eV and 2.54 eV, which are within the reported range of activation energies for thermal degradation of PS and PMMA.

Photoinduced damage in dye-doped polymer matrices has been studied in

various systems for different applications [98–107]. Sensitized photodegradation and photooxidation of polymers can be induced by photoinitiators, in which polymer degradation or oxidation can be initiated by free radicals originating from photodegradation of sensitizers; or by photosensitizers, in which excited sensitizers transfer energy to the polymer or oxygen to initiate photodegradation or photooxidation [98]. Studies on photooxidation or photodegradation of various sensitized polymers have been reported including sensitized PS [98–101] and sensitized PMMA [102, 103]. Laser ablation of polymers can be induced with the assistance of photosensitizers using visible lasers at wavelengths of 351 nm [104], 488 nm [105], and 532 nm [106]. Fukumura et al. proposed that the photon energy absorbed by anthracene, the sensitizer, is converted into thermal energy in PS, the polymer host, causing thermal decomposition [104]. In a study of photodestruction of a solid-state dye laser composed of Rh6G-chloride dye doped in a modified PMMA gain medium, Popov attributed photobleaching of excited-state dye molecules to the permanent degradation of the lasing efficiency, and assigned the formation of carbon (char) in the polymer matrix to the polymer decomposition due to accumulated heat transferred from photoexcited dye molecules via direct vibrations and nonradiative relaxation of their singlet levels [107].

2.4 Proposed mechanism

Given the above reasoning that is guided by observations, we propose that a series of photothermal-induced chemical reactions (PTCR) between dye and polymer is a potential mechanism responsible for reversible and irreversible photodegradation of 1AAQ (and DO11) doped in PMMA and PS as follows:

1AAQ (and DO11) undergoes intramolecular charge transfer (ICT) when excited with visible light, and the absorbed photon energy can be transferred to a nearby polymer chain via nonradiative relaxation of the excited ICT singlet states. The transferred energy locally heats the polymer around the excited dye molecules, which leads to thermal degradation of the polymer including depolymerization, scission of side chains, and dissociation of polymer backbones. Since monomers are the major products of thermally degraded polymers (PS and PMMA), an excited dye molecule can undergo photocycloaddition with a monomer in its vicinity to form the reversibly photodegraded dye species. In addition to monomers, there are other decay products such as $\cdot CH_3$, $\cdot COOCH_3$, ·phenyl, and polymer chain radicals etc. which can attack ground- and excited-state dye molecules and reversibly-damaged dye species causing irreversible damage to dye molecules. While reversibly degraded dye species may gradually recover back to the original dye molecule with a monomer left behind in the polymer matrix, it may also further decompose to an irreversibly-damaged dye species or dye radicals and other fragments of radicals. Thus, the “recovered”

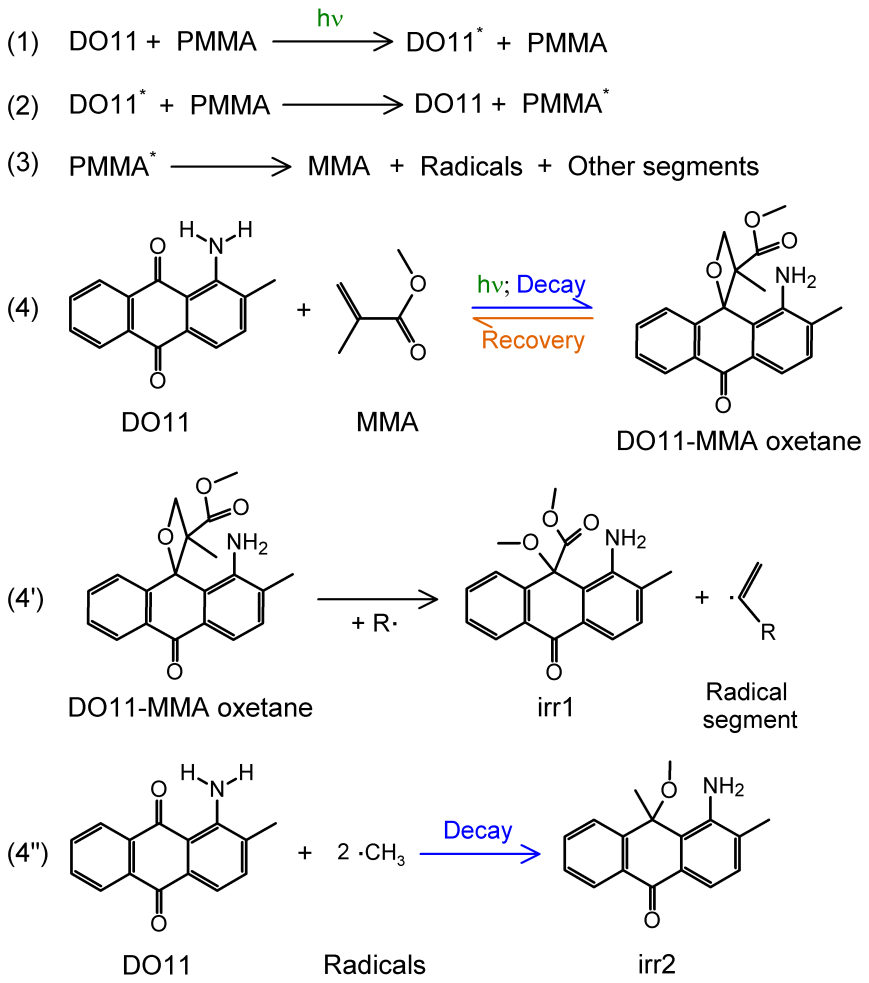

Figure 2.8: PTCR in DO11/PMMA. The asterisk indicates photoexcited DO11 or heated PMMA through nonradiative energy transfer from excited DO11. Reversible and irreversible degradation in DO11 starts after thermal degradation of PMMA (step (3)). Non-radical segments can also undergo thermal degradation similar to step (2) and (3) resulting in radicals. The reversibly-damaged species may undergo recovery (back reaction of step (4)) or decompose into irreversibly-damaged species and radical segments (step (4')). "irr1" and "irr2" are possible irreversibly-damaged dye species illustrated in Figure 2.6. There can be other irreversibly-damaged dye species depending on DO11's nearby radicals and polymer segments.

and thermally degraded monomers and radical fragments can react with each other or with decomposed polymer fragments, polymer chains and unsaturated polymer chain ends causing recovery of the polymer or changes in the polymer including the formation of small molecular weight polymer chains, cross linked polymer chains, and perhaps new species of polymer segments and chains.

In the PTCR hypothesis, dye undergoes (photo)degradation after the thermal degradation of polymer chains. The reversible degradation of dye requires at least two photons initially, but there can be multiple monomers available in the vicinity of dye molecules once the degradation of the polymer starts, so the reversible degradation of dye does not necessarily require two photons in average. On the other hand, the irreversible degradation of dye may be caused by radicals produced from at least one photon induced thermal degradation of the polymer. An illustration of PTCR is shown in Figure 2.8. We examine this proposed mechanism with all results obtained from linear absorption spectroscopy, quantum chemistry calculations and FTIR spectroscopy in this dissertation.

Chapter 3

Experimental Techniques

In this chapter, we describe details of sample preparation for experimental methods employed in this study including amplified spontaneous emission (ASE), linear absorption spectroscopy and Fourier transform infrared (FTIR) spectroscopy, followed by the basic principle and experimental setup of each experimental technique. ASE only occurs in pristine dyes and is a nonlinear process which will be described in this chapter, so it is the most sensitive method to measure population of pristine dyes. However, ASE requires a pump laser beam which may further damage the sample during recovery. As a consequence, ASE results are difficult to reproduce from run to run even under the same condition. Linear absorption spectroscopy requires a broad band white light source which is much weaker than a pump laser, therefore it is a more reliable method than ASE. FTIR spectroscopy is used to determine whether dissociation and formation of chemical bonds in dye molecules and polymer chains are involved in photodegradation and recovery of dye-doped polymers.

3.1 Sample preparation

1-Aminoanthraquinone (1AAQ) and 1-Amino-2-methylanthraquinone (DO11) with a purity of 97% and 95%, respectively; and methyl methacrylate (MMA) and styrene were purchased from Aldrich. MMA and Styrene were purified using two column flasks (one for each) filled with alumina powder to remove the inhibitors that prevent polymerization in the monomers. Commercially available PMMA (MW = 120, 000) purchased from Aldrich was also used in this study. Structures of dye molecules are shown in Figure 1.1, and that of monomers and polymers are shown in Figure 1.2.

3.1.1 Dye in monomer liquid samples

Appropriate proportions of dye and filtered monomer were mixed in a vial to make the desired concentration and sonicated for 30 to 60 minutes. The solution was subsequently filtered using 0.2 μm syringe filters and stored in the dark. All experiments using liquid samples were performed within 72 hours after the solutions were filtered.

3.1.2 Thin-film samples prepared from monomer

To make dye-doped PMMA samples, dye and purified MMA monomer were mixed in proportions to obtain the desired dye concentration and were sonicated for 30 minutes. After sonication, both butanethiol (chain transfer agent, CTA) and tert-butyl peroxide (initiator, INT) were added to the solutions in the proportion of 3.3 μl per ml MMA, and were sonicated for another 30 minutes. The sonicated solutions were filtered with 0.2 μm syringe filters and placed in an oven at 95 °C to initiate the polymerization reaction for at least 2 days resulting in dye-doped polymers. An appropriate volume of polymerized sample was pressed between two 2.5 cm $\times$ 2.5 cm glass substrates at 140 °C (well above the glass transition temperature where the polymer flows) with an uniaxial pressure of 110 ± 10 psi for 90 minutes to make a thin film. The pressure is gradually reduced while the sample is slowly cooling at an average rate about 1.5 °C/min.

For dye-doped PS samples, the same procedure as described above was used with 4.2 μl of INT added to 1 ml of styrene. The filtered solutions were placed in an oven at 95 °C for 4 days for complete polymerization. The glass transition temperature of dye-doped PS samples is lower than dye-doped PMMA samples, so the temperature for pressing thin films was reduced to 120 °C.

Thin-film samples obtained by this method have thicknesses in the range of 20 - 120 μm depending on the volume of polymerized sample pressed between glass slides.

3.1.3 Thin-film samples for Fourier transform infrared (FTIR) spectroscopy

Appropriate amounts of dye and PMMA in the desired ratio were dissolved into a solution composed of 33% γ-butyrolactone and 67% propylene glycol methyl ether acetate (PGMEA) with 10% solutes and 90% solvents by weight. The solution was stirred for 2 to 3 days to dissolve the dye and polymer, then filtered with a 0.2 μm syringe filter. The filtered solution was then spin-coated on a 2.5 cm $\times$ 2.5 cm glass substrates at 600 rpm for 90 seconds for performing

experiments using linear absorption spectroscopy. The filtered solution was also spin-coated on a 2.5 cm × 2.5 cm silicon wafer at 3000 rpm for 50 seconds for performing FTIR experiments. All spin-coated samples were stored in a vacuum oven at 100 °C for 90 minutes; then, the heater was turned off and the samples were kept in vacuum over night.

3.2 Amplified Spontaneous Emission (ASE)

3.2.1 Basic principle

In this section, we discuss the basic principles of spontaneous emission and ASE following the treatment in the book "Lasers" written by A. E. Siegman [108]. This treatment is based on a classical electron oscillator model, but the practical characteristics of ASE can be equally applied to a complex (molecular) system.

Consider a point electron with mass m and charge $-e$ revolving around the nucleus in an atom. The displacement $x(t)$ of the electron from its equilibrium position is linearly proportional to the electric force F exerted on the electron by the nucleus

$$F = -Kx(t), \tag{3.1}$$

and the corresponding potential U is

$$U = \frac{1}{2}Kx^2(t), \tag{3.2}$$

where t is time and K is the force constant.

The equation of motion for the electron subjected to an applied electric field $\xi_x(t)$ due to the incident light wave is given by

$$m\frac{d^2x(t)}{dt^2} = -Kx(t) - e\xi_x(t). \tag{3.3}$$

By defining the oscillator's resonance frequency $\omega_a \equiv \sqrt{K/m}$, Equation 3.3 can be expressed as

$$\frac{d^2x(t)}{dt^2} + \omega_a^2 x(t) = -\frac{e}{m}\xi_x(t). \tag{3.4}$$

The resonance frequency of the oscillator is equivalent to the electronic transition frequency of the atom. For example, $\omega_{12} = (E_2 - E_1)/\hbar$ with E_n being the energy of the n^{th} eigenstate of the electron in the atom.

The oscillator in a real atom can release the energy after excited by the incident light, hence a damping term should be added to the equation of motion,

$$\frac{d^2x(t)}{dt^2} + \gamma\frac{dx(t)}{dt} + \omega_a^2 x(t) = -\frac{e}{m}\xi_x(t), \tag{3.5}$$

where γ is the damping rate for this oscillator. The solution of Equation 3.5 without the applied electric field (during relaxation) is given by

$$x(t) = x(0) \exp\left[\left(-\frac{\gamma}{2} + i\omega_b\right) t\right], \tag{3.6}$$

where $\omega_b = \sqrt{\omega_a^2 - (\gamma/2)^2} \approx \omega_a$ since the damping rate is much smaller than the resonance frequency as we will see in the later discussion. The energy of the oscillator can be written as

$$\begin{aligned} U(t) &= \frac{1}{2} K |x(t)|^2 + \frac{1}{2} m |v_x(t)|^2 \\ &= U(0) \exp(-\gamma t) \\ &\equiv U(0) \exp(-t/\tau), \end{aligned} \tag{3.7}$$

where $v_x(t)$ is the velocity of the electron, $\tau \equiv \gamma^{-1}$ is the energy decay time constant of the oscillator and γ is also the energy decay rate of the oscillator. For a real atom or molecule in the excited state, energy can be released by emitting a photon, which is called spontaneous emission or fluorescence; or, it can be transferred to the surroundings via nonradiative decay such as heat or inelastic collisions with surrounding materials. Note that we consider only the singlet to singlet electronic transition, i.e. the singlet to triplet transition is not under consideration here. Thus, the energy decay rate is the sum of the radiative decay rate γ_{rad} and nonradiative decay rate γ_{nr},

$$\gamma = \frac{1}{U}\frac{dU}{dt} = \gamma_{rad} + \gamma_{nr}. \tag{3.8}$$

The radiative decay rate for an electron oscillator can be calculated using classical electromagnetic theory. The sinusoidally oscillating electron radiates electromagnetic energy in the same way as an oscillating dipole antenna, and the total power radiated by a sinusoidally oscillating dipole $\mu_x(t) = \mu_0 \cos(\omega_a t)$ is given by

$$P = \frac{\omega_a^4 \mu_0^2}{12\pi\epsilon v^3}, \tag{3.9}$$

where $\mu_0 = ex_0$ is the dipole moment of the electron oscillator at the equilibrium position x_0, ϵ is the permittivity and v is the speed of light in the material [109]. Using Equation 3.8, 3.9 and $U = \frac{1}{2} m\omega_a^2 x_0^2$ for an electron oscillator, the radiative decay rate is obtained as

$$\gamma_{rad} = \frac{\omega_a^2 e^2}{6\pi\epsilon m v^3}, \tag{3.10}$$

assuming no nonradiative decay. Equation 3.10 can be re-arranged using the refractive index $n = c/v$, with c being the speed of light in vacuum, and the

frequency of oscillation $f = 2\pi\omega_a$ measured in Hz,

$$\gamma_{rad} = \frac{2\pi e^2}{3\epsilon mc^3} n^3 f^2. \tag{3.11}$$

The radiative decay rate of a classical electron oscillator has a value $\gamma_{rad} \approx 10^8$ s^{-1} when excited by visible light with $\omega_a \approx 4 \times 10^{15}$ s^{-1}.

The spontaneously emitted light can be amplified from a distribution of excited molecules in a state of inverted population with a gain that is sizable in the direction of other excited molecules, hence the medium acts as a mirror-less laser. Consider a long slender rod of excited molecules of length L and diameter $2a$ as illustrated in Figure 3.1. Each small volume of the slender rod emits photons into all directions due to spontaneous emission. Assuming for simplicity that there is no non-radiative decay and the inverted population density is N, the total emitted power per unit volume is given by $N\gamma_{rad}\hbar\omega_a$.

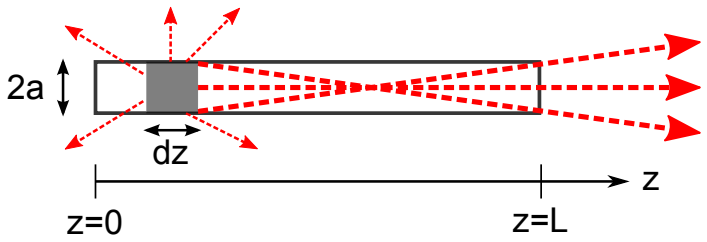

Figure 3.1: Amplified spontaneous emission generated along a slender rod.

When $L \gg a$, the contribution to the intensity of spontaneous emission dI at the output end of the rod at $z = L$ from any small length dz at z is

$$dI = \frac{\pi a^2}{4\pi L^2} N\gamma_{rad}\hbar\omega_a \exp\left[2\alpha_m (L - z)\right] dz, \tag{3.12}$$

where $2\alpha_m = N\sigma_m$ is the power amplification coefficient of the material, and σ_m is the transition cross section. The total intensity of ASE exiting the rod to the right can be approximated by integrating Equation 3.12 over the entire rod

$$\begin{aligned} I_{ASE} &\approx \frac{a^2}{4L^2} N\gamma_{rad}\hbar\omega_a \exp\left(2\alpha_m L\right) \int_0^L \exp\left(-2\alpha_m z\right) dz \\ &\approx \frac{a^2\gamma_{rad}\hbar\omega_a}{4\sigma_m L^2} \left[\exp\left(N\sigma_m L\right) - 1\right]. \end{aligned} \tag{3.13}$$

Notice that the ASE intensity is an exponential function of population density, not a linear function as in fluorescence.

3.2.2 Experimental method - ASE

The experimental setup that we use to measure ASE is schematically shown in Figure 3.2. An Nd:YAG nanosecond laser with fundamental wavelength 1064 nm and 10 Hz repetition rate is used to pump a second harmonic crystal that generates the 532 nm light that is used for the photodegradation and recovery experiment. The fundamental 1064 nm beam is removed with a set of dichroic mirrors after the second harmonic crystal. The pump beam is focused with a cylindrical lens onto a dye-doped polymer thin-film sample such that the horizontal excitation line is perpendicular to the vertically polarized pump beam

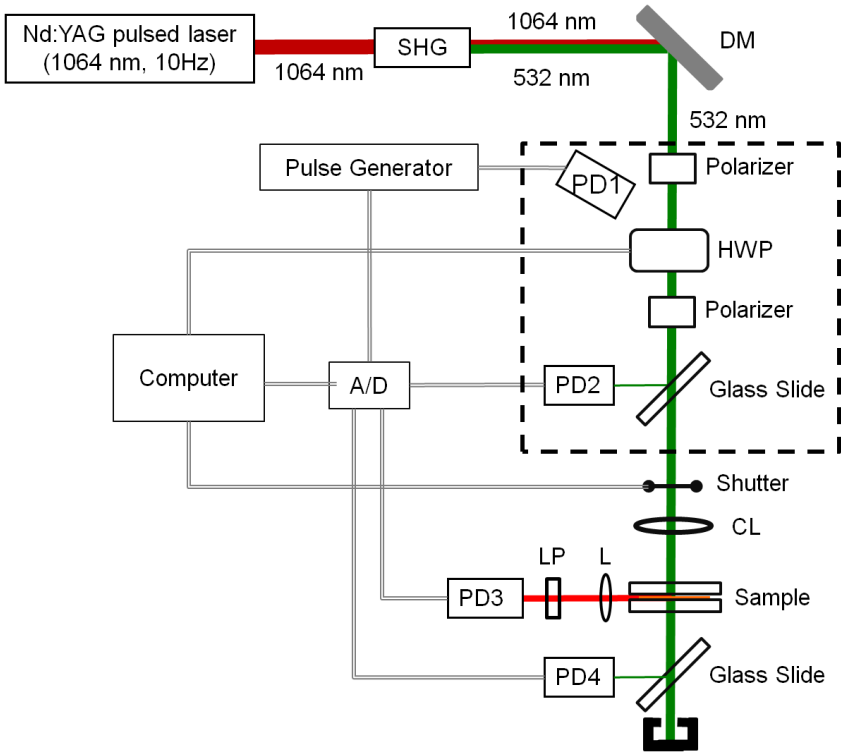

Figure 3.2: ASE experimental setup. Both polarizers allow vertically polarized pump beam to pass. SHG is the second harmonic generation crystal, DM is a set of dichroic mirrors, HWP is a half-wave-plate, CL is a cylindrical lens, L is a set of convex lens, LP is a longpass filter, A/D is the analog-to-digital converter, PD1 to PD4 are photodetectors, and the dashed line is a black box to block strong scattering light. PD1 collects the scattered pulsed laser light to trigger ADC. PD2 monitors the intensity of the pump beam. PD3 collects ASE signal. PD4 collects the transmitted pump laser light.

to yield dipole radiation along the excitation line, thus generating ASE with maximum efficiency as shown in Figure 3.3. ASE is collected from one edge of the thin film and the signal is sent to an analog-to-digital converter (ADC) and recorded by computer. An ADC gate is controlled by a pulse generator which is triggered by the photodetector PD1. A small portion of the pump beam is directed to the photodetector PD2 by a glass slide and monitored by the computer to ensure a constant pulse energy by controlling the half-wave-plate. The components within the dashed rectangle in Figure 3.2 thus stabilize the laser power.

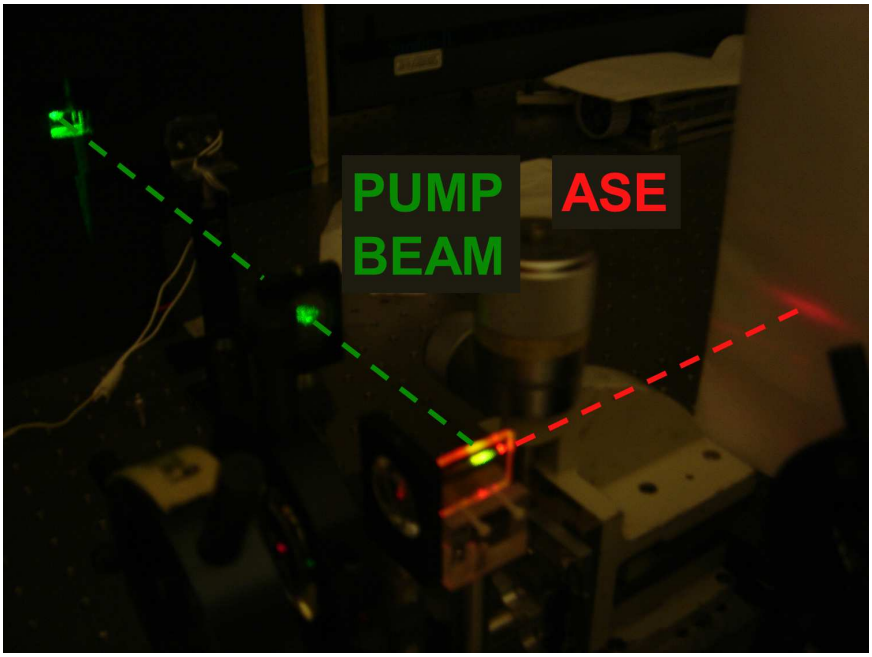

Figure 3.3: ASE generated by a pulsed laser beam with wavelength 532 nm focused with a cylindrical lens onto a dye-doped polymer thin-film sample. The excitation line is perpendicular to the polarization of the pump beam to yield ASE along the excitation line with maximum efficiency.

3.3 Linear Absorption spectroscopy

3.3.1 Lambert-Beer law

The absorption of light by matter can be described by the Lambert-Beer law, which states that the absorbance is proportional to the concentration c and the

thickness l of a sample,

$$A(\lambda) = \varepsilon(\lambda)\, cl, \tag{3.14}$$

where A is the absorbance, λ is the light wavelength and ε is the absorptivity which is a proportionality constant at each wavelength. Absorbance is defined as the logarithm of the ratio of incident light intensity I_0 and transmitted light intensity I,

$$A(\lambda) = \log \frac{I_0(\lambda)}{I(\lambda)} = -\log \frac{I(\lambda)}{I_0(\lambda)}. \tag{3.15}$$

Thus, the transmitted light intensity can be expressed as

$$I(\lambda) = I_0 \exp\left[-(\ln 10)\, \varepsilon(\lambda)\, cl\right] = I_0 \exp\left[-(\ln 10)\, \sigma(\lambda)\, l\right], \tag{3.16}$$

where $\sigma(\lambda) = \varepsilon(\lambda)\, c$ is the absorption cross section.

Each distinct molecule has its own characteristic absorption spectrum due to the unique molecular electronic transitions in each. The absorption spectrum of a sample can be obtained by measuring the incident and transmitted light intensity according to Equation 3.15. When a molecule converts into another species, the absorption spectrum changes accordingly, hence we can monitor the conversion between species through the absorption spectrum. Note that when c and ε depend on depth, e.g. during photodegradation, $A(\lambda) = \sum_{l_i} \varepsilon(\lambda, \Delta l_i)\, c_i \Delta l_i$.

3.3.2 Experimental method - linear absorption spectroscopy

The experimental set up is shown in Figure 3.4. A cw argon ion laser or a cw solid state laser were used to provide pump beams at wavelengths 488

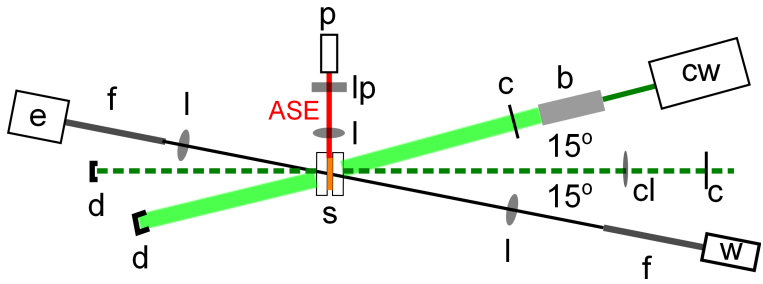

Figure 3.4: Experimental set up. The pump beam comes from a cw laser and is expanded 5 times in diameter. The dashed line represents the pulsed laser beam focused with a cylindrical lens onto the sample. (cw) CW Laser. (b) 5× beam expander. (c) Shutter. (d) Beam dump. (w) White light source. (f) Optical fiber. (e) Spectrometer. (l) Convex lens. (cl) Cylindrical lens. (s) Sample. (lp) longpass filter. (p) Photodetector.

nm and 532 nm, respectively, to cause the photodegradation of dye/monomer solutions and dye-doped polymers. Two light sources were used for absorption measurements: an Ocean Optics PX2 Xenon pulsed lamp and an Ocean Optics LS1 tungsten halogen lamp. The spectrometer was an Ocean Optics SD2000. ASE was generated by pumping the sample with a 532 nm nanosecond pulsed laser and utilized as a probe. The detailed ASE set up is shown in Figure 3.2. Figure 3.5 illustrates the overlap of pump and probe beams on the sample.

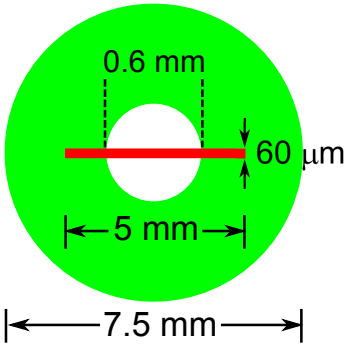

Figure 3.5: Illustration of the cross sections of pump (green disk) and probe (white disk) beams at the sample. The 532 nm cw laser was expanded to a diameter of 7.5 mm. The white light source was focused to 0.6 mm in diameter. The pulsed laser was focused to 60 μm (red line) in width and centered on the masked glass substrate with a 5 mm wide open window.

Both angles between the cw pump beam and the normal of the glass substrate and from the white light path to the normal of the glass substrate were about 15°. The 532 nm pump laser beam passed a 5× beam expander so the 1/e diameter becomes 7.5 mm. The 488 nm cw laser beam was not expanded and the 1/e diameter was 1.23 mm. The focus of the white light had diameter 0.6 mm. The white light probe was centered on the cw pump beam at the sample. Both cw laser beams had much larger diameters than the white light, so the pump intensity is approximately a constant at the point of peak intensity. The sample was mounted on a translation stage so we could re-take the reference spectrum through air in proper time intervals during recovery to ensure the change of absorbance is not due to drift of the white light intensity.

While the cw laser is causing photodegradation in the sample, the absorption spectra and ASE signals are recorded with the pump laser temporarily blocked. After the desired irradiation time for photodegradation, the cw laser was turned off and absorption spectra and ASE signals were recorded in preset time intervals to monitor recovery. The pulsed laser was blocked when ASE was not being measured.

A thin mask was stuck on the surface of the glass substrate with an open

aperture of 5mm in width and centered on the pump beam to ensure the ASE light was generated from a uniformly damaged/recovering area of the sample. When ASE measurements were not performed, the sample surface was oriented perpendicular to the white light path, and the cw laser beam replaced the path of the pulsed laser beam.

3.4 Fourier transform infrared spectroscopy

3.4.1 FTIR spectrometry

In this section, the basic principle of FTIR spectrometry is introduced following the book "Fourier Transform Infrared Spectrometry" written by Griffiths, P. R. and de Haseth, J. A. [110] The basis of FTIR spectroscopy is the Michelson interferometer as schematically shown in Figure 3.6. It consists of a beam splitter and two mutually perpendicular plane mirrors. One of the mirrors can move along the normal axis of the mirror. A beam from an external source is partially reflected by the beam splitter to the fixed mirror and partially transmitted to the movable mirror. The two beams that return from the two mirrors are again partially reflected by and partially transmitted through the beam splitter. Some of the light travels back to the light source and the rest towards the detector.

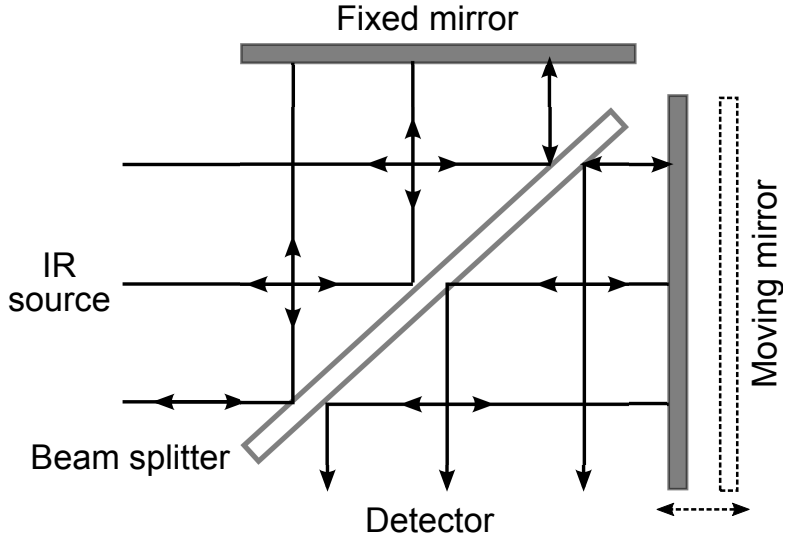

Figure 3.6: Michelson interferometer.

Two beams arriving at the detector interfere constructively when the optical path difference δ is an integral multiple of the wavelength λ, thus the intensity

of the beam at the detector is the maximum. For other values of δ, the intensity at the detector $I'(\delta)$ for each wavenumber, k, is given by

$$I'(\delta) = \frac{B(k)}{2}\left[1 + \cos\left(2\pi k\delta\right)\right], \tag{3.17}$$

where $k \equiv 1/\lambda$, $B\left(k\right)$ is the intensity of the source and it is assumed that the reflectance and transmittance of the beam splitter are 50%/50%. The amplitude of the modulated component of $\frac{B(k)}{2}\cos\left(2\pi k\delta\right)$ is referred to as the interferogram $B\left(\delta\right)$ and is of importance in spectrometric measurements. The amplitude of the interferogram can be affected by the beam splitter efficiency, detector response and amplifier characteristics, therefore the interferogram for each wavenumber can be written as

$$B_k\left(\delta\right) = I\left(k\right)\cos\left(2\pi k\delta\right), \tag{3.18}$$

where $I\left(k\right)$ is the intensity of the source corrected for instrumental characteristics. For a broadband source, the interferogram can be described with the integral

$$B\left(\delta\right) = \int_{-\infty}^{\infty} I\left(k\right)\cos\left(2\pi k\delta\right)dk, \tag{3.19}$$

and the corrected intensity is obtained by the cosine Fourier transformation of $B\left(\delta\right)$

$$I\left(k\right) = \int_{-\infty}^{\infty} B\left(\delta\right)\cos\left(2\pi k\delta\right)d\delta. \tag{3.20}$$

In practice, $d\delta$ is a finite sampling interval and δ has a finite boundary Δ which results in a finite resolution. The simplest correction of Equation 3.20 is to multiply by a truncation function

$$\begin{array}{ll} D\left(\delta\right) = 1, & -\Delta \leqslant \delta \leqslant \Delta \\ D\left(\delta\right) = 0, & \delta > \left|\Delta\right|, \end{array} \tag{3.21}$$

and we obtain the recorded intensity

$$G\left(k\right) = \int_{-\infty}^{\infty} B\left(\delta\right)D\left(\delta\right)\cos\left(2\pi k\delta\right)d\delta. \tag{3.22}$$

Mathematically, the right-hand-side of Equation 3.22 is the Fourier transform (FT) of the product of two functions and can be rewritten as the convolution of the FT of each function. The FT of $B\left(\delta\right)$ is the true spectrum $I\left(k\right)$, and the FT of $D\left(\delta\right)$ is referred to the instrument line shape (ILS) function $f\left(k\right)$. The convolution of $I\left(k\right)$ and $f\left(k\right)$ is given by

$$G\left(k\right) = I\left(k\right) * f\left(k\right) = \int_{-\infty}^{\infty} I\left(k'\right)f\left(k - k'\right)dk'. \tag{3.23}$$

The spectral resolution is affected by the shape of the ILS function which is determined by the choice of the truncation function.

Similar to linear absorption spectroscopy, the Lambert-Beer law can be applied to FTIR spectroscopy. Since infrared (IR) light is resonant with the vibration modes of nuclei in a molecule, as the electronic transitions in a molecule are resonant with visible light, FTIR gives information about chemical bonds.

There are two types of infrared detectors to record the intensity: thermal detectors and quantum detectors. Thermal detectors sense the change of temperature of an absorbing material resulting in a thermal electromotive force (thermocouples), a change in resistance of a conductor (bolometer) or semiconductor (thermistor bolometer), or the movement of a diaphragm due to the thermal expansion of a gas (pneumatic detector), which can lead to the change in illumination of an auxiliary photocell (Golay detector). Thermal detectors usually respond to radiation slower than quantum detectors and are used for the far-infrared wavelength range. The Golay detector and pyroelectric bolometer are the most popular ones among thermal detectors.

In a quantum detector, electrons can be excited to a higher energy state by the absorption of incident photons. Phototubes and photomultipliers can be used for ultraviolet, visible and near-infrared (to about 1 μm), in which electrons in the light-absorbing material are given enough energy to escape from the surface and flow through a vacuum to give a current. Semiconductors are used for mid-infrared wavelengths detection, where electrons in the valence band are excited to the conduction band. Examples are PbS, PbSe, mercury cadmium telluride (MCT) etc. Quantum detectors require cooling to reduce electrical noise, for instance, an MCT has to be maintained at liquid nitrogen temperatures (77 K).

3.4.2 Experimental method - FTIR spectroscopy

Figure 3.7 schematically shows the set up for the FTIR experiment. IR spectra were obtained from a DA8 Bomen FTIR spectrometer equipped with a water-cooled globar broadband light source (200 to 10000 cm^{-1}), a KBr beam splitter (450 to 5000 cm^{-1}), and a liquid nitrogen cooled MCT detector (400 to 5000 cm^{-1}). The pressure inside the FTIR spectrometer was kept below 0.2 torr throughout the entire experiment. The aperture was set at 10.0 mm, the speed of the moving mirror was 0.5 cm/s, and the resolution was 4 cm^{-1}. The customized sample holder has 3 windows allowing light to pass and each of them is 5 mm in diameter, so we can load up to three spin-coated (dye-doped) polymer samples simultaneously. The 532 nm pump beam generated from a cw solid state laser was expanded with a 5× beam expander giving the diameter of the pump beam on the sample of 7.5 mm.

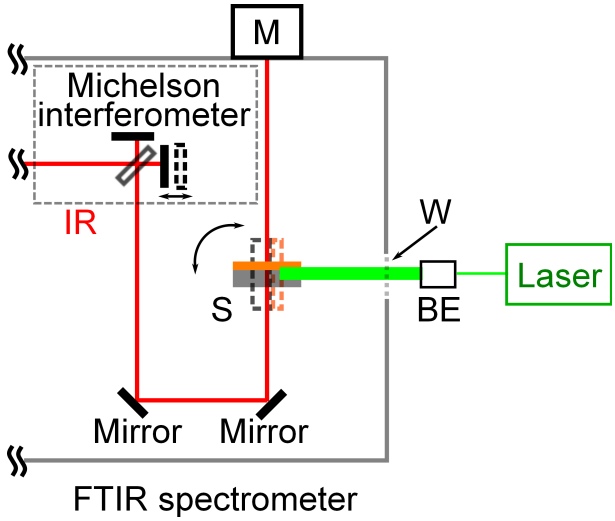

Figure 3.7: FTIR setup. BE is the 5× beam expander, M is the MCT detector, S is the sample, and W is the quartz window. The sample can be rotated during the experiment. The window is covered and the laser beam is blocked while taking IR spectra.

Each IR spectrum of a silicon wafer, a spin-coated PMMA film on a silicon wafer, and fresh dye-doped PMMA spin-coated on a silicon wafer was averaged over 6000 scans, which takes about 66 minutes. The dye-doped polymer sample was rotated 90° for laser irradiation, and rotated back to the original position for taking IR spectra after 30 minutes of irradiation. In order to observe possible changes during recovery, each IR spectrum was averaged over 1500 scans (about 16 minutes) during the first 400 minutes of recovery, 3000 scans (about 32 minutes) or 6000 scans (about 66 minutes) afterward. The actual number of scans is reported in the results section of Chapter 7. The window on the side of the FTIR spectrometer was covered and the laser beam was blocked while the IR spectra were taken.

Rotating the sample and reducing the number of scans adds uncertainties in addition to the noise of comparing IR spectra obtained at different times. These uncertainties were determined prior to the experimental runs by simulating the procedure without irradiating the sample. Each trial IR spectrum was averaged over 1000 scans (about 10 minutes) to compare it with the changing IR spectra relative to the fresh sample obtained in experimental runs, and the results are presented in Chapter 7.

Chapter 4

Diffusion?

Although "normal" diffusion has been excluded in earlier studies of single-exponential-like recovery [52, 54], it has not yet been examined whether diffusion is involved in the observed stretched exponential recovery. The "normal" diffusion is referred to the diffusion process described by Fick's law and thus it exhibits a single exponential time dependence. When the diffusion does not exhibit a single exponential time dependence, it is referred to the "anomalous" diffusion.

Tetracene, which has a structure similar to an anthraquinone, was observed to exhibit anomalous diffusion in a PS matrix at 9.5 K below its glass transition temperature, T_g, and the anomalous diffusion was modeled with a combination of a stretched exponential and a single exponential functions [111]. Diffusion of both 9,10-phenanthrenequinone dye (PQ) and polymer chain (of PMMA with covalently bounded PQ after photobleaching) in PMMA were studied from 20 K below T_g to well above T_g, and the amount of refractive index modulation was described as a combination of two stretched exponential functions [112]. If diffusion is involved in the stretched exponential recovery from photodamaged dye-doped polymers as observed in ASE and linear absorption spectroscopy experiments, the "recovery" may come from a combination of normal diffusion and recovery of the molecule, or a combination of anomalous diffusion and molecular recovery, or purely anomalous diffusion. Therefore, the possibility that diffusion is responsible for the observed stretched exponential recovery should be examined.

All samples studied using linear absorption spectroscopy possess isosbestic points during decay and recovery. The presence of isosbestic points suggests that diffusion is most likely not responsible for the self-healing phenomenon, unless the damaged species diffuses away from the probed region at the same rate as undamaged dye molecules diffuse back to the probed region. Alternatively,

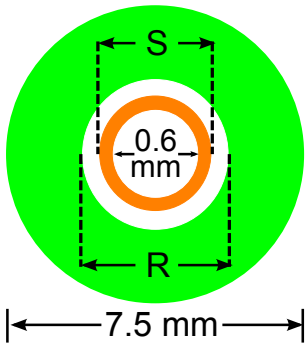

Figure 4.1: Illustration of the pump and probe beams overlapping in the sample. The white light probe has a diameter R and at the focus $R_{focus} = 0.6$ mm. The sample with a diameter S was moved to a position where $R_{focus} < S < R$ to perform the photodegradation and recovery experiments. The pump beam was expanded to 7.5 mm in diameter.

both diffusion and recovery are present with coordinated diffusion and recovery rates after photodegradation. Since there are several ways that diffusion might behave in a way similar to recovery, we seek to answer the question of whether diffusion has taken place after photodegradation before modeling the specific mechanisms.

A simple experiment that excludes all forms of diffusion during decay and recovery is performed using linear absorption spectroscopy with the apparatus described in Section 3.3.2 with the following modifications. An 1AAQ/PMMA thin-film sample is sandwiched between two glass slides with a film diameter about 1 to 2 mm, which is larger than the focus of the white light source as schematically shown in Figure 4.1. The sample was placed at the focus of the white light and the absorbance was less than 1 OD (optical density) to ensure that the Lambert-Beer law is obeyed [113]. The sample was then translated along the white light beam path until the diameter of the white light source was larger than the sample and the absorption spectrum was still clearly resolved as shown in Figure 4.2. The 5× expanded cw pump laser beam of wavelength 532 nm was centered at the sample to induce photodegradation. After 31 minutes of irradiation, the laser was turned off and the absorption spectra were continuously recorded. Since the sample size is smaller than the white light probe beam width, diffusion beyond the probed region is not possible, so the diffusion mechanism is eliminated. Thus the observed changes in the absorption spectrum will be due only to changes in the molecular structure of the dopant or host polymer.

Absorption spectra during decay and recovery are shown in Figure 4.2. The change of absorbance in both decay and recovery measurements has the same

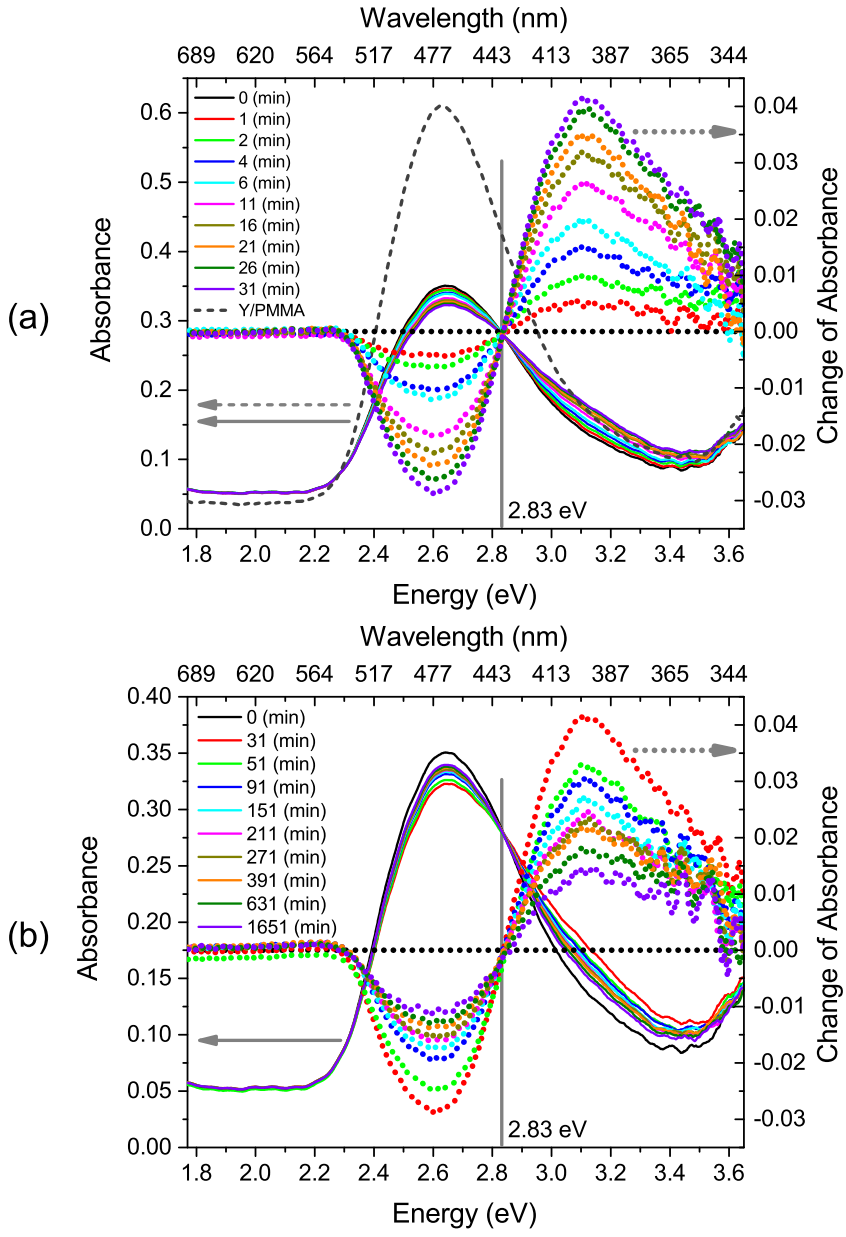

Figure 4.2: (a) Absorption spectrum of 1AAQ/PMMA during decay. The dashed spectrum was taken when the white light was focused on the sample. The solid curves are spectra in which the white light source's transverse width is larger than the sample's diameter. The dotted spectra are the changing absorbance relative to the fresh spectrum taken before irradiation (0 min). (b) Absorbance of 1AAQ/PMMA during recovery.

isosbestic point (2.83 eV) as in the samples with larger diameters (2.84 eV) that will be presented in Chapter 5 within experimental uncertainty. As such, we conclude that diffusion is not responsible in these cases. The absorbance as a function of time also follows a stretched exponential function as do observations on the same (1AAQ/PMMA) but larger thin-film samples in which only a limited area is irradiated by the cw pump laser. The results clearly exclude diffusion and anomalous diffusion as mechanisms contributing to the decay and recovery processes.

Chapter 5

Reversible photodegradation of liquid dye solutions

1AAQ was observed to undergo photocycloaddition with olefines when irradiated by visible light at 0 °C in solutions with ethanol and benzene as solvent [67–69]. The reaction products (after being separated from the solution for analysis) were observed to gradually decompose into other species including pristine 1AAQ at 30 °C; however, photocycloaddition between 1AAQ and monoene was not observed [67, 68]. As we discussed in Chapter 2, a stronger visible light source, such as a laser, may cause photocycloaddition between 1AAQ (or DO11) and monoene, such as MMA, and we further proposed that photocycloaddition of 1AAQ (or DO11) and monomers can take place in 1AAQ-(or DO11-)doped polymers owing to photothermal-induced depolymerization. To explore this possibility, the degradation and recovery of dye in monomer solutions, including MMA (a monoene), must first be established. In this chapter, we exam the photodegradation of 1AAQ dissolved in styrene and MMA and DO11 dissolved in styrene solutions, and compare their absorption spectra with the ones obtained from photodegradation in 1AAQ/PMMA and DO11/PS. The absorption spectra of these liquid samples are continuously monitored for a few hours after photodegradation, and these observations lead to the conclusion that dye molecules dissolved in liquid monomers also undergo reversible photodegradation.

5.1 Liquid dye solution experiment

The preparation of dye dissolved in monomer solutions is described in Section 3.1.1. Each dye/monomer solution is filled in a quartz cell with 10.0 mm width

and 0.1 mm depth. The height of the solution in the cell is approximately 5 mm. The cell is placed in the setup of linear absorption spectroscopy as described in Section 3.3.2 such that the white light source has a cross section of diameter approximately 2 mm and the pump beam is expanded to 7.5 mm in diameter. The overlap of the pump and probe beam on the sample is illustrated in Figure 5.1. After taking the absorption spectrum of a fresh dye/monomer solution, the sample is irradiated for the desired time to observe a clear change in absorbance, at which time the pump laser is turned off.

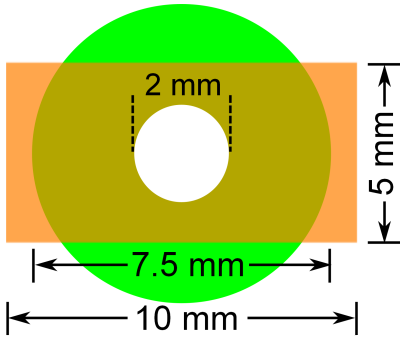

Figure 5.1: Illustration of the pump (green) and probe (white) beams overlapping on a liquid dye/monomer solution (orange). The pump beam is a cw laser with 532 nm wavelength.

The quartz cell is unfortunately wider than the diameter of the pump beam, thus diffusion of dye and damaged dye can not be completely excluded. However, the depth is much thinner than the width of the cell, so the fresh dye diffusing into the probed volume and the damaged dye diffusing out from the probed volume are expected to be slow on experiment time scale so that the observed change in absorbance after the pump turned off is mainly due to changes in molecular structures in the solution. The observation of isosbestic points in the absorption spectra during recovery confirms this hypothesis.

5.2 Reversible photodegradation of liquid dye solutions

In earlier studies, ASE signal from DO11 dissolved in dimethylformamide solution was found not to recover after photodegradation [49] but was found to recover in solid DO11/PMMA [9]. However, this observation does not imply that photodegradation of DO11 in all liquid solvents, including monomers like MMA and styrene, is irreversible. In the proposed photothermal-induced chemical reactions (PTCR) mechanism, reversible photodegradation of DO11 (or 1AAQ) in monomer solutions may be possible depending on the stability

of the reversibly-damaged DO11 (or 1AAQ) species, in which all molecules have higher mobility and are thus susceptible to diffusion. Additionally, the reversibly- and irreversibly-damaged dye species in dye-doped polymer matrices could be the same as or similar to those in dye-dissolved monomer solutions according to the PTCR hypothesis as described in Chapter 2.

5.2.1 1AAQ/styrene

Figure 5.2 shows the absorbance and change in absorbance of 1AAQ in styrene solution exposed to a 532 nm cw laser of intensity 0.0045 W/cm^2 for 5 minutes, then kept in the dark. Though the isosbestic point is noisy during decay, it indicates that the change in absorbance is mostly due to 1AAQ being converted into the damaged species under irradiation but not diffusion. After irradiation, the isosbestic point and the spectrum in the higher energy region becomes too noisy to distinguish, possibly due to the small signal-to-noise (S/N) ratio (the absorption spectrum drift $\leq$ 0.002 OD) and/or further degradation of intermediate degraded dye species. A DO11/styrene experiment, described in a later section, makes clear that diffusion is negligible when a weak pump intensity is used. Thus, the restoration of absorbance in the low energy region after irradiation indicates the recovery of 1AAQ, or further degradation of intermediate degraded dye species, or both.

5.2.2 1AAQ/MMA

Figure 5.3 shows the absorbance and change in absorbance of 1AAQ in MMA solution exposed to a 532 nm wavelength cw laser with intensity 0.23 W/cm^2 for 38 minutes then kept in the dark. Notice that the pump intensity used here is about 51 times and the dose is about 388 times stronger than those used for 1AAQ in styrene solution. There is no well-defined isosbestic point during decay, but the changing absorbance exhibits clear increasing or decreasing trends at various regions of the spectrum indicating actual photodegradation, i.e. pristine 1AAQ converts into other species under irradiation though the photodegradation may not necessarily be the photocycloaddition of 1AAQ to MMA. This result indicates that photodegradation of 1AAQ in MMA (a monoene) requires a stronger pump intensity and higher dose, or consequently, a greater amount of induced heat than in styrene as posited in Chapter 2. The greater amount of heat can accelerate the diffusion of dye and damaged species in the volume under irradiation. The observed change in absorbance does not have well-defined isosbestic points, suggesting that diffusion accompanies photodegradation in 1AAQ/MMA under irradiation. The change in amplitude of the absorbance in the high energy region (larger than 3 eV) is about a half the change at low energy region (between about 2.4 to 3 eV). In contrast, 1AAQ/PMMA is often observed to have approximately the same change in amplitude in both regions,

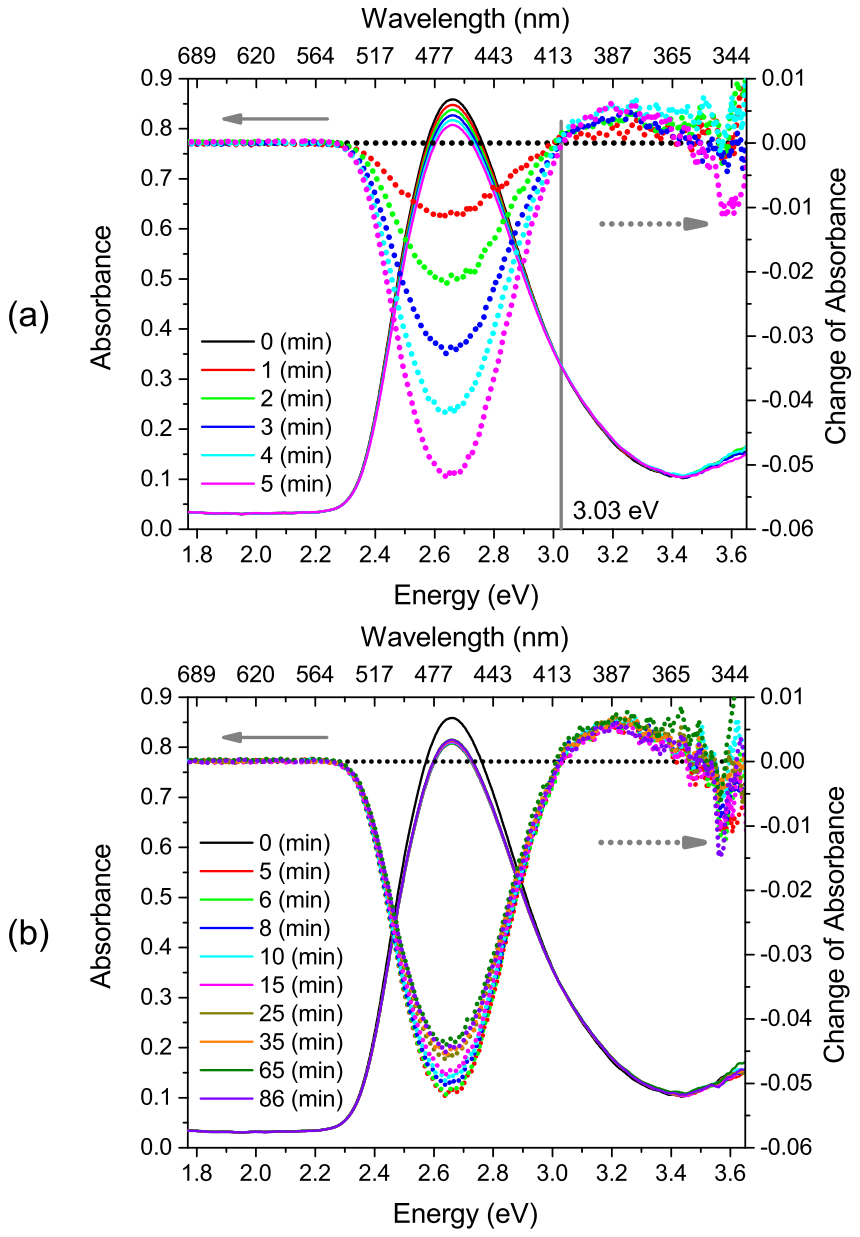

Figure 5.2: Absorbance and changing absorbance of 1AAQ in styrene as a function of time (a) under irradiation of a 532 nm wavelength cw laser, and (b) after 5 minutes of irradiation.

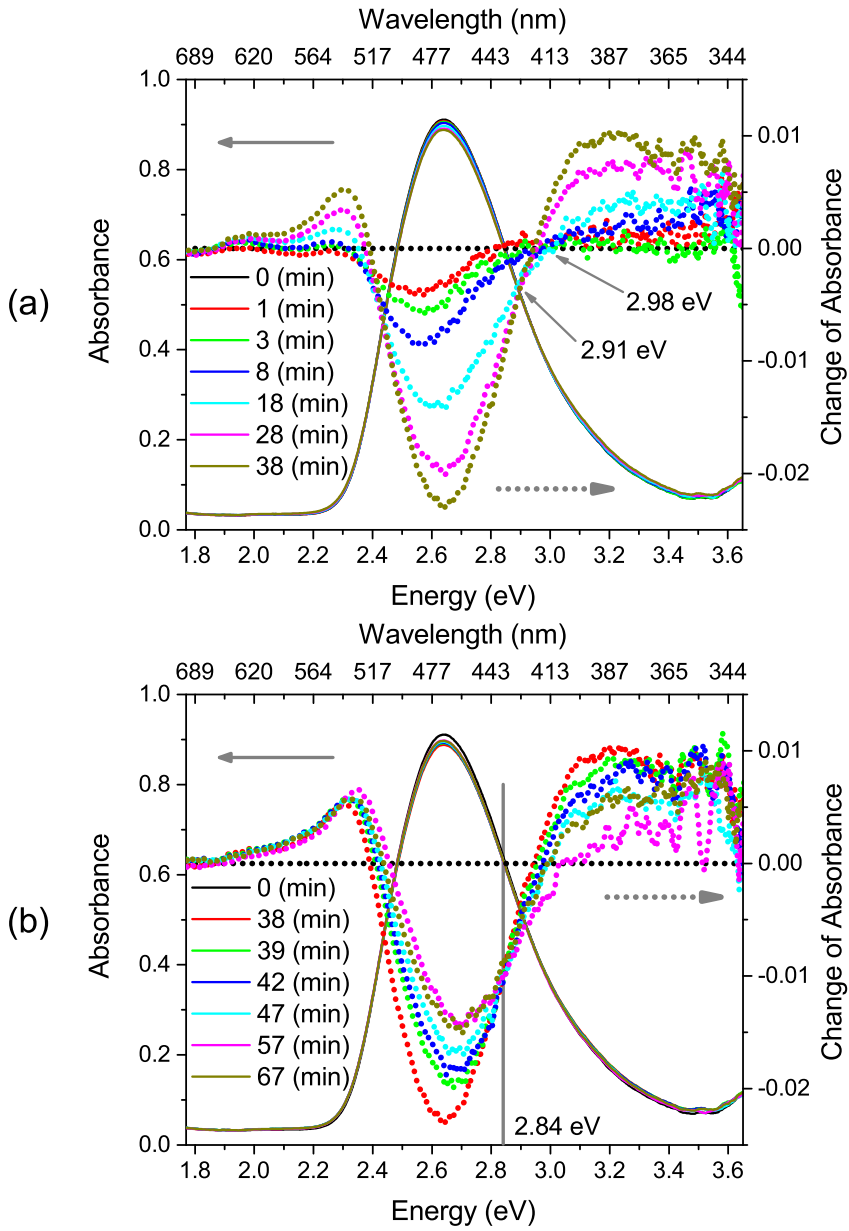

Figure 5.3: Absorbance and change in absorbance of 1AAQ in MMA as a function of time (a) when irradiated with a 532 nm wavelength cw laser, and (b) after 38 minutes of irradiation. Spectra taken after the 57^{th} minute fluctuate between that at the 57^{th} and the 67^{th} minute and are not shown here except for the one at the 67^{th} minute.

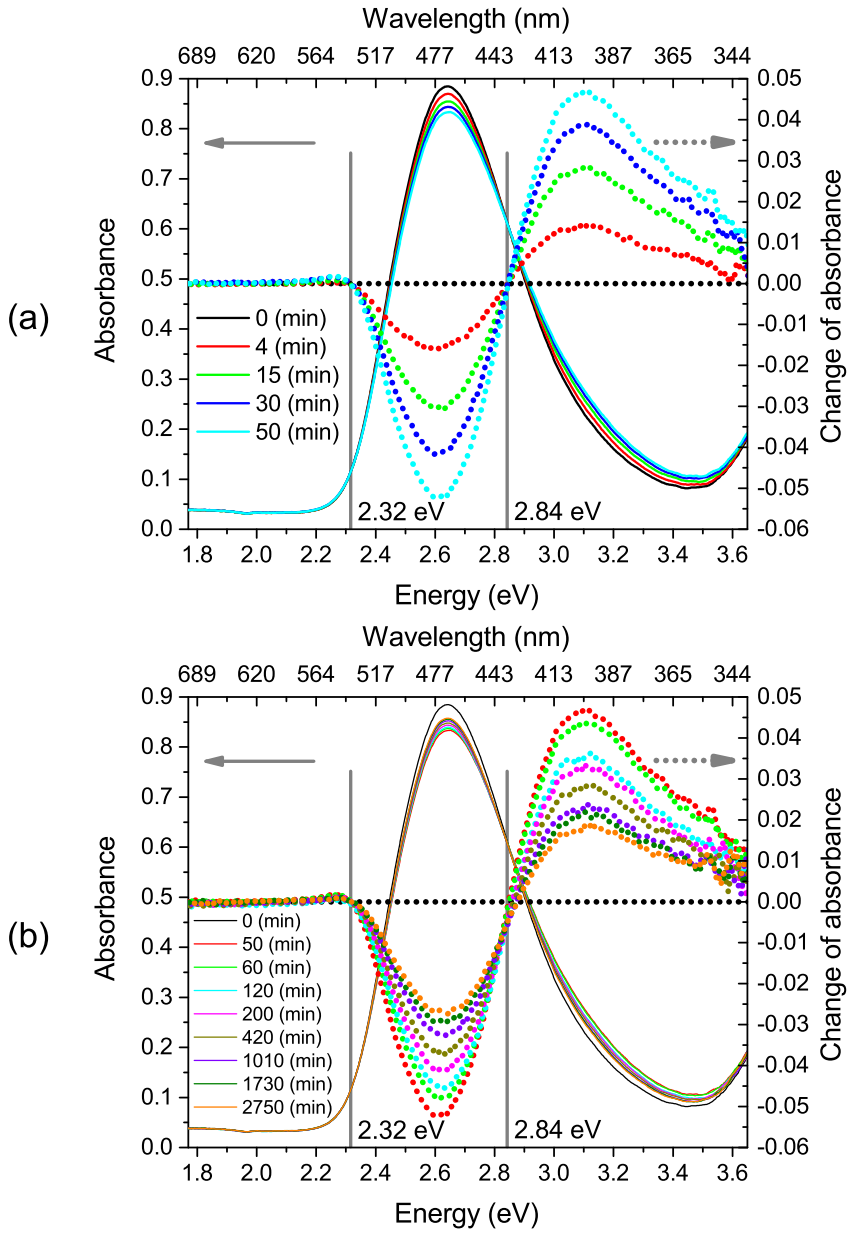

Figure 5.4: Absorbance and change in absorbance of 1AAQ/PMMA with concentration 8.5 g/L (a) when irradiated by a 532 nm wavelength cw laser with intensity 1.71 W/cm^2, and (b) during recovery after 50 minutes of irradiation.

as shown in Figure 5.4. This may result from a combination of photodegradation and fresh dye diffusing away from the probed volume under irradiation, i.e. the change of absorbance in 1AAQ/MMA may be similar to that in 1AAQ/PMMA if there were no diffusion. There is a small peak, though not well defined, that appears during degradation at around 2.3 eV. This small peak is often observed when 1AAQ- (or DO11-)doped PMMA is irradiated with a strong pump intensity or high dose.

During recovery, an isosbestic point is observed at 2.84 eV as shown in Figure 5.3(b), though it is noisy. No isosbestic point is observed in the lower energy region in Figure 5.3(b). We plot the change in absorbance with respect to the absorption spectrum taken at the end of irradiation, the 38$^{\text{th}}$ minute in Figure 5.5, and obtain two isosbestic points. Similarly, the change of absorbance relative to the absorption spectrum taken at the end of irradiation for 1AAQ/PMMA is plotted in Figure 5.6. Comparing Figure 5.5 and Figure 5.6, we find that the isosbestic points are at the same position, within the experimental uncertainty, and the positions of the absorption peaks are similar, which suggest a similar conversion product in both MMA and PMMA. This also indicates that back diffusion is negligible when the solution is in the dark since there is no heating due to the laser beam.

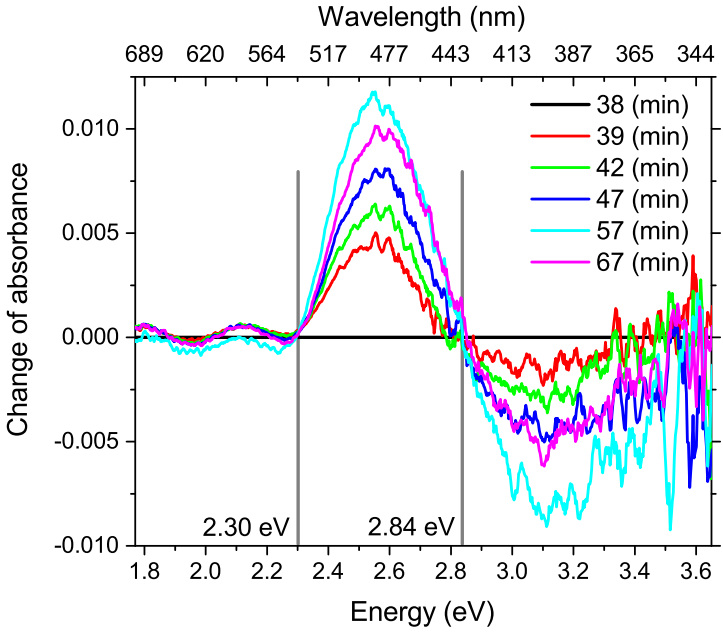

Figure 5.5: Change in absorbance of 1AAQ/MMA relative to the absorption spectrum at the 38$^{\text{th}}$ minute, the end time of irradiation. Spectra taken after the 57$^{\text{th}}$ minute fluctuate between that at the 57$^{\text{th}}$ and the 67$^{\text{th}}$ minute and are not shown here except for the one at the 67$^{\text{th}}$ minute.

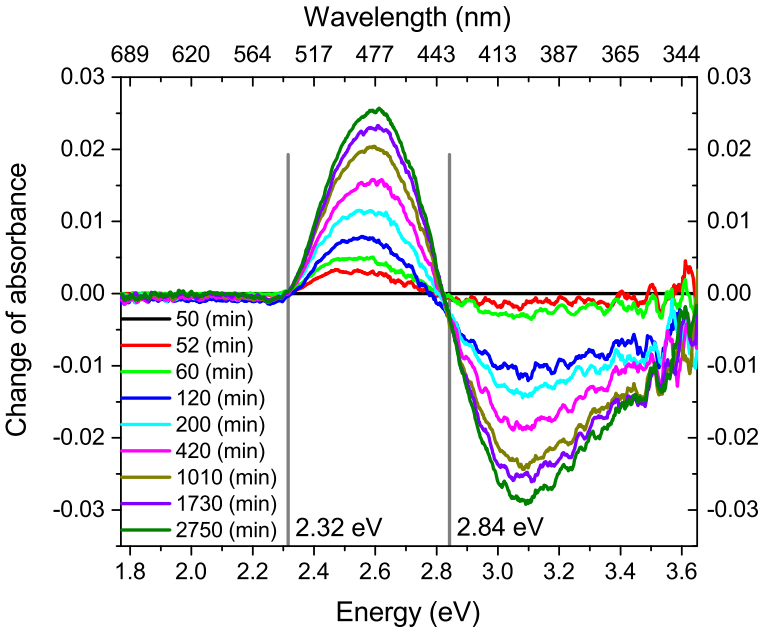

Figure 5.6: Change in absorbance of 1AAQ/PMMA relative to the absorption spectrum at the 50^{th} minute, the end time of irradiation.

The lower energy peak of the change in absorbance in 1AAQ/MMA (Figure 5.5), is at 2.57 eV while it is at 2.61 eV for 1AAQ/PMMA (Figure 5.6). In addition to the relatively large noise, the difference may also rise from the solvent effect (liquid MMA and solid PMMA) on the (reversibly-)damaged dye molecules, which have higher polarity than the pristine ones - as will be described in Chapter 6. The fluctuations in the change of absorbance in the higher energy region is also large. Nonetheless, these results indicate that 1AAQ dissolved in MMA solution also recovers from photodegradation, not only when doped in PMMA. Judging from the agreement of isosbestic points and the peak positions in 1AAQ/MMA and 1AAQ/PMMA, the same or similar reversible photodegradation products appear to be found in 1AAQ/MMA and 1AAQ/PMMA.

5.2.3 DO11/styrene

The absorbance and change in absorbance of DO11/styrene irradiated for 17 minutes using a 532 nm wavelength cw laser with intensity 0.011 W/cm^2 is presented in Figure 5.7. The isosbestic point at 3.01 eV indicates that diffusion is negligible at this pump intensity so the DO11 molecule is converting into

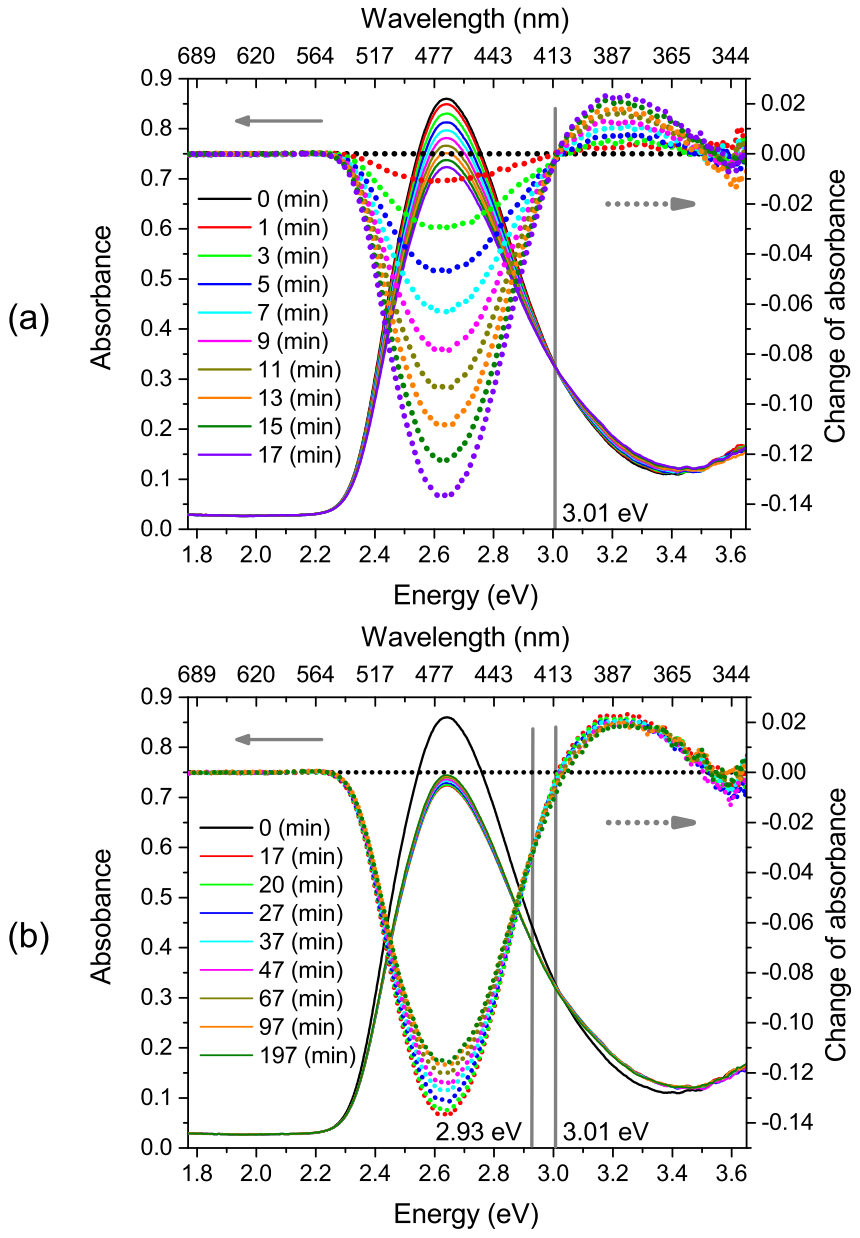

Figure 5.7: Absorbance and change in absorbance of DO11 in styrene (a) when irradiated with a 532 nm wavelength cw laser, and (b) during recovery after 17 minutes of irradiation.

other species under irradiation. After irradiation, when the sample is recovering, the isosbestic point in the absorbance shifts to 2.93 eV. Comparing with the results obtained from DO11/PS shown in Figure 5.8, the change in absorbance of DO11 behaves the same way in both liquid styrene solution and solid PS matrix.

The change in absorbance of DO11/styrene and DO11/PS during recovery relative to the absorption spectrum taken at the end of irradiation are shown in Figure 5.9 and 5.10, respectively. The shift of the isosbestic point after irradiation results from recovery accompanied with further degradation of reversibly-damaged dye species as described in Appendix A. The excellent agreement of the evolution of the absorption spectrum change between DO11/styrene and DO11/PS during decay and recovery leads us to conclude that DO11 undergoes the same reversible photodegradation process in styrene as in PS.

A higher pump intensity and dose is required to cause the same degree of damage in DO11 than in 1AAQ, and diffusion is likely observed while irradiating 1AAQ/MMA. Therefore, photodegradation of DO11/MMA may be accompanied by diffusion and thermal expansion under irradiation, and so was not tested. However, as we have seen from the above results, 1AAQ/styrene and DO11/styrene share the same reversible photodegradation process, which agrees with the assumption in Chapter 2 that 1AAQ and DO11 undergo the same reaction in the same environment. Thus, DO11/MMA is expected to follow the same reversible photodegradation process as 1AAQ/MMA.

All the above results indicate that DO11/styrene and 1AAQ/MMA have in common the same reversible photodegradation processes as DO11/PS and 1AAQ/PMMA, respectively, as posited in the PTCR hypothesis in Chapter 2. In Appendix A, we further investigate photodegradation at various degrees of damage and recovery to calculate the possible absorption spectra of reversibly-damaged dye-doped polymers.

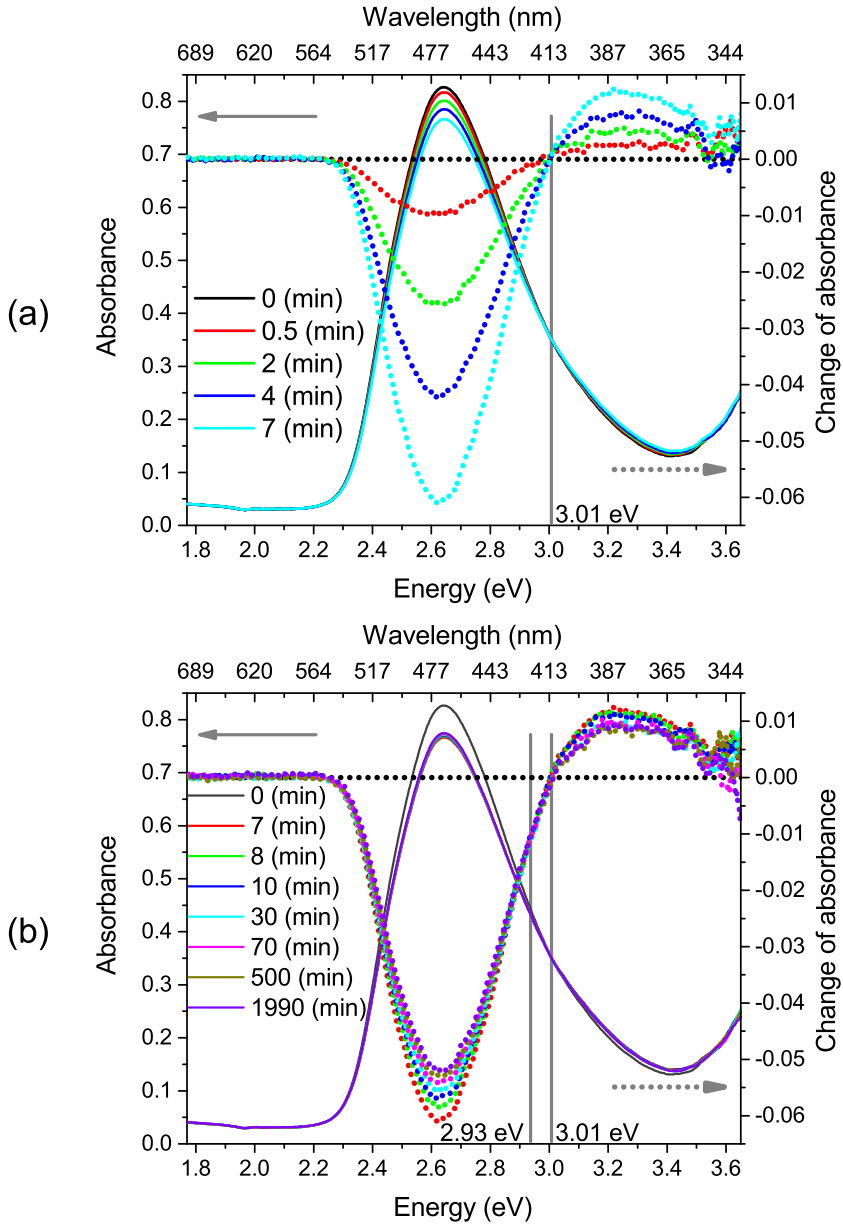

Figure 5.8: Absorbance and change in absorbance of a 9 g/L DO11/PS thin film sample (a) when irradiated with a 532 nm wavelength cw laser of intensity 0.43 W/cm^2, and (b) during recovery after 7 minutes of irradiation.

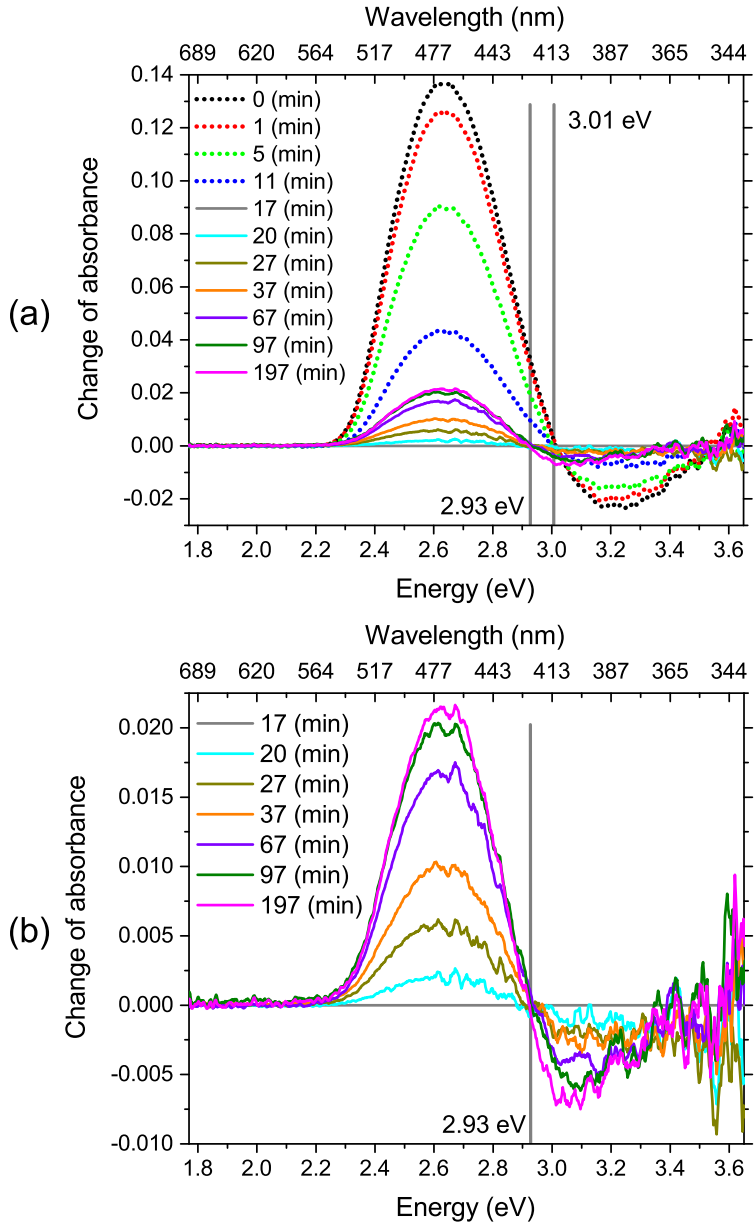

Figure 5.9: (a) Change in absorbance of DO11 in styrene during photodegradation and recovery relative to the absorption spectrum at the 17^{th} minute. (b) Same as (a) but only the ones during recovery.

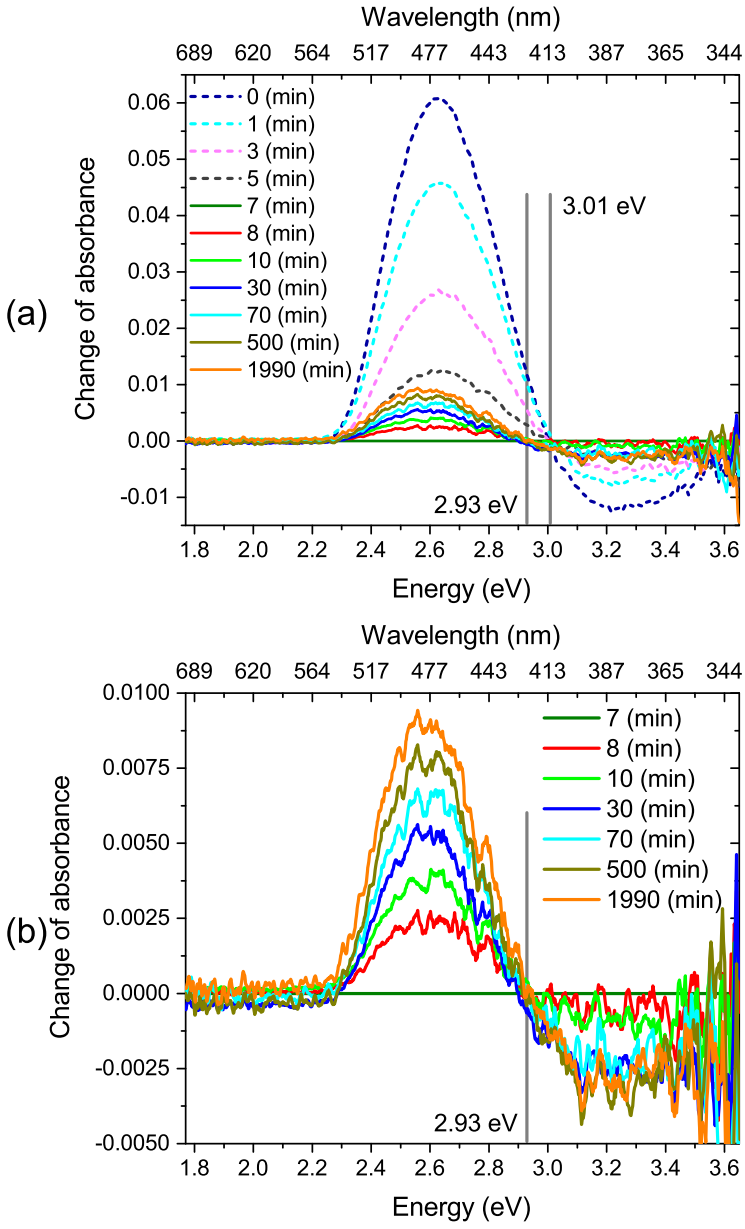

Figure 5.10: (a) Change in absorbance of DO11/PS during photodegradation and recovery relative to the absorption spectrum at the 7^{th} minute. (b) Same as (a) but only the ones during recovery.

Chapter 6

Quantum chemistry calculation

Density functional theory (DFT) is a computational quantum mechanical method widely applied to investigate the electronic structure of many body systems including atoms, molecules and condensed matter phases in their ground states [114–116]. As an extension of DFT, time-dependent density functional theory (TD-DFT) describes the excited states of many electron systems [114–116], therefore the absorption spectrum of these systems can be estimated. A brief introduction to the theory and computational methods employed in this work will be described, then the calculated absorption spectra of pristine and damaged dye species will be presented and compared with experimental results.

6.1 Density functional theory

Electronic structure problems are conventionally treated using wavefunctions that are found from approximate solutions of the Schrodinger equation. The Born-Oppenheimer approximation expresses the total wavefunction of a molecule as a direct product of nuclear and electronic wavefunctions. The electronic Schrodinger equation of an isolated N-electron molecule can be expressed as

$$\hat{H}\Psi_e = E\Psi_e, \tag{6.1}$$

where E is the electronic energy, Ψ_e is the electronic wavefunction and $\hat{H}$ is the Hamiltonian operator given by,

$$\hat{H} = \sum_{i=1}^{N}\left(-\frac{1}{2}\nabla_i^2\right) + \sum_{i=1}^{N} v\left(\mathbf{r}_i\right) + \sum_{i<j}^{N}\frac{1}{r_{ij}}, \tag{6.2}$$

where $\mathbf{r}_i$ is the spatial coordinate of the i^{th} electron, $r_{ij} \equiv |\mathbf{r}_i - \mathbf{r}_j|$, and the external potential exerted on the i^{th} electron due to nuclei of charges Z_α is

$$v(\mathbf{r}_i) = -\sum_\alpha \frac{Z_\alpha}{r_{i\alpha}}. \tag{6.3}$$

The first term on the right-hand side of Equation 6.2 describes the kinetic energy of electrons, and the last term is the electron-electron interaction potential. The Schrodinger equation can not be solved exactly due to the presence of the electron-electron interaction.

The variational theory states that an upper bound to ground state energy E_0 of a system can be obtained by considering trial ground state wavefunctions $\tilde{\Psi}$,

$$E_0 \leq E\left(\tilde{\Psi}\right) = \left\langle \tilde{\Psi} \middle| \hat{H} \middle| \tilde{\Psi} \right\rangle, \tag{6.4}$$

and the minimum, E_0, is found when the trial ground state wavefunction $\tilde{\Psi}$ equals the exact ground state wavefunction $\Psi_{0e} \equiv \Psi$. By imposing the Pauli exclusion principle, the trial wavefunction (and the true electronic wavefunction) is an antisymmetric product of N orthonormal electron spin-orbitals $\psi_i(\mathbf{r})$, and can be constructed by taking the direct product of a single particle spatial wavefunction $\phi(\mathbf{r})$ and a spin function $\alpha(s)$, where the Slater determinant

$$\tilde{\Psi}(\mathbf{r}_1, \mathbf{r}_2, \cdots, \mathbf{r}_N) = \frac{1}{\sqrt{N!}} \begin{vmatrix} \psi_1(\mathbf{r}_1) & \psi_2(\mathbf{r}_1) & \cdots & \psi_N(\mathbf{r}_1) \\ \psi_1(\mathbf{r}_2) & \psi_2(\mathbf{r}_2) & \cdots & \psi_N(\mathbf{r}_2) \\ \vdots & \vdots & & \vdots \\ \psi_1(\mathbf{r}_N) & \psi_2(\mathbf{r}_N) & \cdots & \psi_N(\mathbf{r}_N) \end{vmatrix}, \tag{6.5}$$

assures antisymmetry.

DFT is a method that approximates the solution to the Schrodinger equation based on the Hohenberg-Kohn theorems [117]. For the exact ground state wavefunction $\Psi(\mathbf{r}_1, \mathbf{r}_2, \cdots, \mathbf{r}_N)$ of an N-electron system, the non-degenerate electron density $\rho(\mathbf{r})$ in the ground state is defined as

$$\rho(\mathbf{r}) = N \int |\Psi(\mathbf{r}, \mathbf{r}_2, \cdots, \mathbf{r}_N)|^2 \, d\mathbf{r}_2 \cdots d\mathbf{r}_N. \tag{6.6}$$

The first theorem states that for a stationary many electron system, the external potential $v(\mathbf{r})$ is a unique functional of $\rho(\mathbf{r})$, apart from a trivial additive constant. Consider $v(\mathbf{r})$ of an N-electron system being determined by $\rho(\mathbf{r})$ for the non-degenerate ground state with wavefunction Ψ and corresponding Hamiltonian operator $\hat{H}$. Assume that there exists another potential $v'(\mathbf{r})$ with ground state wavefunction Ψ' and corresponding Hamiltonian operator $\tilde{H}$ giving the same $\rho(\mathbf{r})$. Notice that $\Psi \neq \tilde{\Psi}$ since they satisfy different Schrodinger equations unless $v'(\mathbf{r}) = v(\mathbf{r}) + const$. Taking $\tilde{\Psi}$ as the trial wavefunction,

$$E_0 = \left\langle \Psi \middle| \hat{H} \middle| \Psi \right\rangle < \left\langle \tilde{\Psi} \middle| \hat{H} \middle| \tilde{\Psi} \right\rangle = \left\langle \tilde{\Psi} \middle| \tilde{H} \middle| \tilde{\Psi} \right\rangle + \left\langle \tilde{\Psi} \middle| \hat{H} - \tilde{H} \middle| \tilde{\Psi} \right\rangle, \tag{6.7}$$

we obtain

$$E_0 < E' + \int \left[v\left(\mathbf{r}\right) - v'\left(\mathbf{r}\right)\right] \rho\left(\mathbf{r}\right) d\mathbf{r}. \tag{6.8}$$

Similarly, if Ψ is taken as the trial wavefunction, we find that

$$E' < E_0 + \int \left[v'\left(\mathbf{r}\right) - v\left(\mathbf{r}\right)\right] \rho\left(\mathbf{r}\right) d\mathbf{r}. \tag{6.9}$$

Adding Equation 6.8 and 6.9, we obtain a contradiction

$$E_0 + E' < E' + E_0, \tag{6.10}$$

so there can not exist different v giving the same ρ. Thus, ρ determines all observables such as v, the total number of electrons, N, and all properties of the ground state. The second theorem [117] is the variational principle which states that the ground state energy E_0 is the minimum value of the ground state energy functional $E\left[\rho\right]$ for the correct ρ. To prove this theorem [114, 117, 118], we express the ground state energy as a functional of ρ,

$$E\left[\rho\right] = \int v\left(\mathbf{r}\right) \rho\left(\mathbf{r}\right) d\mathbf{r} + \frac{1}{2} \int \frac{\rho\left(\mathbf{r}\right) \rho\left(\mathbf{r}'\right)}{\left|\mathbf{r} - \mathbf{r}'\right|} d\mathbf{r} d\mathbf{r}' + F\left[\rho\right], \tag{6.11}$$

and

$$F\left[\rho\right] \equiv T_s\left[\rho\right] + E_{xc}\left[\rho\right], \tag{6.12}$$

where $T_s\left[\rho\right]$ is the kinetic energy of non-interacting electrons in the ground state and $E_{xc}\left[\rho\right]$ is called the exchange correlation energy which includes the effect of correlations on the kinetic energy of the interacting electrons and non-classical electron-electron interactions. The second term on the right-hand side of Equation 6.11 is the classical Coulomb repulsion between pairs of electrons. A trial density $\tilde{\rho}$ determines $\tilde{v}$, $\tilde{H}$ and $\tilde{\Psi}$ of the N-electron system. Thus, taking the trial wavefunction $\tilde{\Psi}$, we obtain

$$\begin{aligned} E\left[\tilde{\rho}\right] &= \left\langle \tilde{\Psi} \left| \hat{H} \right| \tilde{\Psi} \right\rangle \\ &= \int v\left(\mathbf{r}\right) \tilde{\rho}\left(\mathbf{r}\right) d\mathbf{r} + \frac{1}{2} \int \frac{\tilde{\rho}\left(\mathbf{r}\right) \tilde{\rho}\left(\mathbf{r}'\right)}{\left|\mathbf{r} - \mathbf{r}'\right|} d\mathbf{r} d\mathbf{r}' + F\left[\tilde{\rho}\right] \\ &\geq E\left[\rho\right]. \end{aligned} \tag{6.13}$$

Though the functional form of F[ρ] was not specified in the Hohenberg-Kohn theorems, the Kohn-Sham method was later developed to calculate F[ρ] [119, 120]. It assumes a system composed of N non-interacting electrons with electron density

$$\tilde{\rho}\left(\mathbf{r}\right) = \sum_{i=1}^{N} \left|\tilde{\Psi}_i\left(\mathbf{r}\right)\right|^2. \tag{6.14}$$

The corresponding single particle Schrodinger equation is given by

$$\left(-\frac{1}{2}\nabla^2 + v\left(\mathbf{r}\right) - \varepsilon_j\right)\varphi_j\left(\mathbf{r}\right) = 0, \tag{6.15}$$

with the ground state energy of the N particle system given by

$$E = \sum_{j=1}^{N}\varepsilon_j, \tag{6.16}$$

where φ and ε are the wavefunction and eigenenergy of the single non-interacting electron.

The Hohenberg-Kohn variational principle in Equation 6.13 for such a system is given by

$$E\left[\tilde{\rho}\right] = \int v\left(\mathbf{r}\right)\tilde{\rho}\left(\mathbf{r}\right)d\mathbf{r} + T_s\left[\tilde{\rho}\left(\mathbf{r}\right)\right] \geq E. \tag{6.17}$$

The Euler-Lagrange Equation applied to Equation 6.17 gives

$$\delta E\left[\tilde{\rho}\right] = \int \delta\tilde{\rho}\left(\mathbf{r}\right)\left\{v\left(\mathbf{r}\right) + \left.\frac{\delta T_s\left[\tilde{\rho}\left(\mathbf{r}\right)\right]}{\delta\tilde{\rho}\left(\mathbf{r}\right)}\right|_{\tilde{\rho}=\rho} - \varepsilon\right\}d\mathbf{r} = 0. \tag{6.18}$$

For the interacting N-electron system, the Euler-Lagrange Equation applied to Equation 6.13 yields,

$$\delta E\left[\tilde{\rho}\right] = \int \delta\tilde{\rho}\left(\mathbf{r}\right)\left\{v_{eff}\left(\mathbf{r}\right) + \left.\frac{\delta T_s\left[\tilde{\rho}\left(\mathbf{r}\right)\right]}{\delta\tilde{\rho}\left(\mathbf{r}\right)}\right|_{\tilde{\rho}=\rho} - \varepsilon\right\}d\mathbf{r} = 0, \tag{6.19}$$

with

$$v_{eff}\left(\mathbf{r}\right) \equiv v\left(r\right) + \int \frac{\tilde{\rho}\left(\mathbf{r}'\right)}{\left|\mathbf{r}-\mathbf{r}'\right|}d\mathbf{r}' + V_{xc}\left(\mathbf{r}\right) \tag{6.20}$$

and

$$V_{xc}\left(\mathbf{r}\right) \equiv \left.\frac{\delta E_{xc}\left[\tilde{\rho}\left(\mathbf{r}\right)\right]}{\delta\tilde{\rho}\left(\mathbf{r}\right)}\right|_{\tilde{\rho}=\rho}. \tag{6.21}$$

Equation 6.19 is identical to 6.18 if the non-interacting electrons are placed in an external effective potential v_{eff}. Equations 6.14, 6.20, 6.21 and the single particle Schrodinger equation in an external effective potential given by

$$\left(-\frac{1}{2}\nabla^2 + v_{eff}\left(\mathbf{r}\right) - \varepsilon_j\right)\varphi_j\left(\mathbf{r}\right) = 0, \tag{6.22}$$

have to be solved self-consistently to optimize ρ. These self-consistent equations are also known as the Kohn-Sham equations. The ground state energy is then given by [119, 120]

$$E = \sum_{j=1}^{N}\varepsilon_j - \frac{1}{2}\int\frac{\tilde{\rho}\left(\mathbf{r}\right)\tilde{\rho}\left(\mathbf{r}'\right)}{\left|\mathbf{r}-\mathbf{r}'\right|}d\mathbf{r}d\mathbf{r}' + E_{xc}\left[\tilde{\rho}\left(\mathbf{r}\right)\right] - \int V_{xc}\left(\mathbf{r}\right)\tilde{\rho}\left(\mathbf{r}\right)d\mathbf{r}. \tag{6.23}$$

The estimated ground state energy clearly depends on the accuracy of $E_{xc}[\tilde{\rho}(\mathbf{r})]$, therefore a proper functional has to be chosen to approximate $E_{xc}[\tilde{\rho}(\mathbf{r})]$ for the actual system.

DFT has been extended to TD-DFT which takes into account the time-dependence of the electron density in a many electron system [115, 121]. The analogue of the Hohenberg-Kohn theorem in time-dependent problems is the Ruge-Gross theorem, which states that the external potential exerted on a single electron $v(\mathbf{r},t)$ uniquely determines electron density $\rho(\mathbf{r},t)$ for a given initial wavefunction [121]. The Ruge-Gross theorem can also be used to establish the exchange correlation potential $V_{xc}[\rho(\mathbf{r},t)]$ and the Kohn-Sham equations in time-dependent problems [115, 121]. Thus, the Ruge-Gross theorem sets the foundation for TD-DFT. Using TD-DFT, the linear response of a many electron system can be calculated and further used to determine the excited state energies of the system [115, 122].

6.2 Computational method

Ultraviolet-visible (UV-Vis) spectra of various organic molecules including anthraquinone derivatives have been calculated using TD-DFT calculations and the results are found to be in good agreement with experiments if the appropriate basis set of wavefunctions and functionals are chosen [123–132]. In order to obtain a qualitative estimate of absorption spectra of possible photodegraded dye molecules within a reasonable computing time, one of the methods that produce reasonably good predictions for visible spectra of anthraquinone derivatives is adopted [123]. We use Gaussian 03 to perform the TD-DFT calculations. Geometry optimization of pristine DO11 and all possible damaged DO11 species discussed in Chapter 2, except for the twisted intramolecular charge transfer (TICT) state and DO11 tautomer due to intramolecular proton transfer (IPT), was implemented with the 6-31G(d,p) basis set and the B3LYP functional for each species in vacuum. The 6-31G(d,p) basis set utilizes Gaussian-type functions added with polarization functions to describe the atomic orbitals [133]. B3LYP is a hybrid functional containing a portion of the exact exchange energy evaluated from the Kohn-Sham single-particle orbitals and some portions of exchange and correlation energies approximated using DFT and empirical methods [134, 135]. TD-DFT calculations were carried out with the optimized ground state geometry using the same basis set and functional, and the polarizable continuum model (PCM) to account for the solvent effects. In PCM, the solution is divided into a solute portion located inside a cavity and a surrounding structureless solvent portion characterized by its dielectric constant and other parameters[136–138]. Photodegradation experiments were performed in PS and PMMA polymer matrices that have dielectric constants of 2.6 and

2.6 – 3.1 [139], respectively, which are close to toluene's value of 2.38 [139]. Thus, toluene was selected as the PCM solvent.

Geometry optimization failed for the DO11 tautomer structure shown in Figure 2.1, which indicates that the tautomer structure has higher energy than the ground state DO11 structure. Thus, the tautomer ground state geometry was optimized by placing the hydrogen atom on the other side of the oxygen, i.e. rotating the C−OH group in the tautomer by 180° as shown in Figure 6.1(a), and using the same basis set and functional. The C−OH was then rotated 180° from the optimized geometry as shown in Figure 6.1(b) to conduct the TD-DFT calculation with the same procedure described above. Although the geometry may be affected by intramolecular hydrogen bonding between O−H and N−H of the DO11 tautomer, it may not drastically change the UV-Vis absorption peak and the oscillator strength.

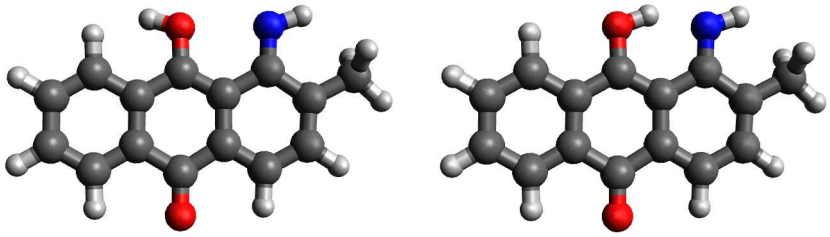

Figure 6.1: Colors in molecular structures: black represents the carbon atom, gray is the hydrogen atom, red is the oxygen atom and blue is the nitrogen atom. (a) The modified DO11 tautomer structure used for ground state geometry optimization. (b) The DO11 tautomer structure obtained by rotating the C−OH group by 180° from the optimized geometry.

Geometry optimization also failed for the TICT structure because its geometry change may be too subtle to capture, thus it was not computed here.

6.3 Computational and experimental results

The lowest absorption peak of all species calculated using TD-DFT corresponds to the excitation from the highest occupied molecular orbital (HOMO) to the lowest unoccupied molecular orbital (LUMO), except for the anion of DO11, which includes contributions from other transitions but mainly from the HOMO-LUMO transition. The distribution of electron clouds for HOMO and LUMO of each species is plotted in Appendix B.

The calculated oscillator strength and the corresponding excitation energy of the reversibly-damaged species are expected to be similar to that of the irreversibly-damaged species according to the PTCR hypothesis described in Chapter 2 and discussions in Appendix A. Though the absorption spectra of the damaged dye species can not be determined directly from the experiment as a result of (at least) three species involved in the photodegradation process, the absorption spectra of the irreversibly-damaged DO11 dye can be approximated by exposing the pristine DO11-doped polymers to the laser beam for long enough time such that the spectra approach steady state if there is a major irreversibly-damaged species or all irreversibly-damaged species have similar absorption spectra as described in Appendix A.

Figure 6.2 shows the UV-Vis absorption spectra of pristine and irreversibly photodegraded DO11/PS, the oscillator strength of the possible reversibly-damaged species calculated with toluene as the solvent, and the change in absorbance of DO11/PS during decay. The calculated lowest energy absorption peak position of pristine DO11 agrees with the measured absorption spectrum as expected. The peak corresponding to the change in absorbance at 2.64 eV indicates that the amount of fresh DO11 decreases during decay. On the other hand, the appearance of a peak at 3.22 eV indicates reversibly- and irreversibly-damaged dye species forming during decay, though only the irreversibly-damaged species is present after 90 minutes of irradiation. Therefore, the calculated absorption peaks of reversibly- and irreversibly-damaged dye species should be located at 3.22 eV. Comparing the calculated absorption energies and the oscillator strength with experimental results in the visible regime, the DO11-styrene oxetane is the only proposed reversibly-damaged species that agrees with the observation. Note that even if taking into account the uncertainty in the calculation of tautomer due to the modification of its ground state geometry optimization, the effect is unlikely large enough to shift the absorption peak from 2.40 eV (517 nm) to 3.22 eV (385 nm), the position of the peak associated with the damaged species.

Similar to Figure 6.2, we plot the same experimental results with the calculated oscillator strength of DO11-styrene oxetane and the irreversibly-damaged species proposed in the PTCR hypothesis in Figure 6.3. The calculated results are in agreement with the experiment. Besides, the calculation indicates that the reversibly-damaged species has a similar absorption spectrum in the visible regime as does the irreversibly-damaged species. It also suggests that as long as the carbon-oxygen double bond adjacent to the amine group of DO11 is broken, and the carbon and oxygen atoms form single bonds with fragments (which may be different from the proposed ones) thermally-degraded from PS, the visible absorption spectra of damaged DO11 species may all be similar due to the partial damage of the intramolecular charge transfer (ICT) pathway as illustrated in Figure 2.7 and confirmed with the calculated electron density of the pristine DO11 and damaged species shown in Appendix B.

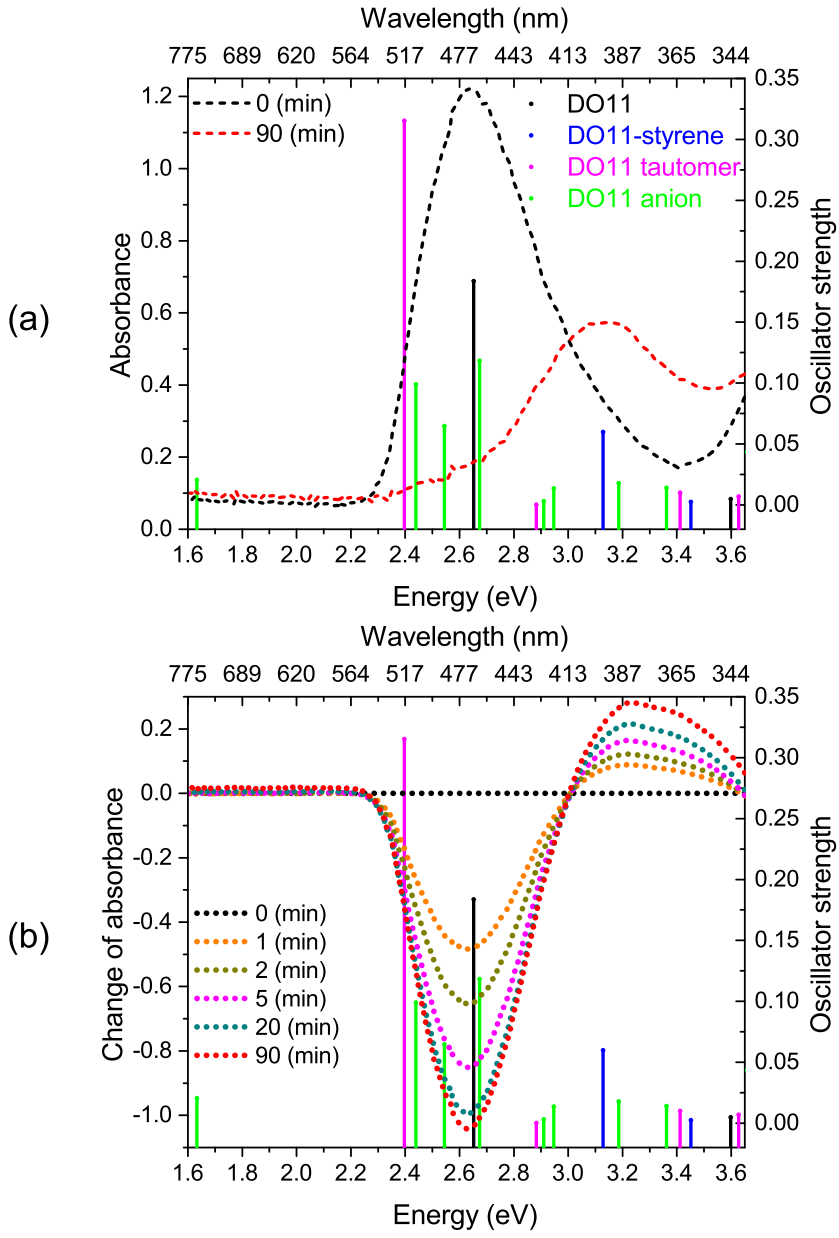

Figure 6.2: (a) UV-Vis absorption spectrum of pristine DO11/PS, the spectrum taken after 90 minutes of irradiation (dashed curves), and the oscillator strength of the possible reversibly-degraded species (vertical lines). (b) Change of absorbance during decay with respect to the pristine sample (dotted curves) and the oscillator strength of the possible reversibly-degraded species (vertical lines).

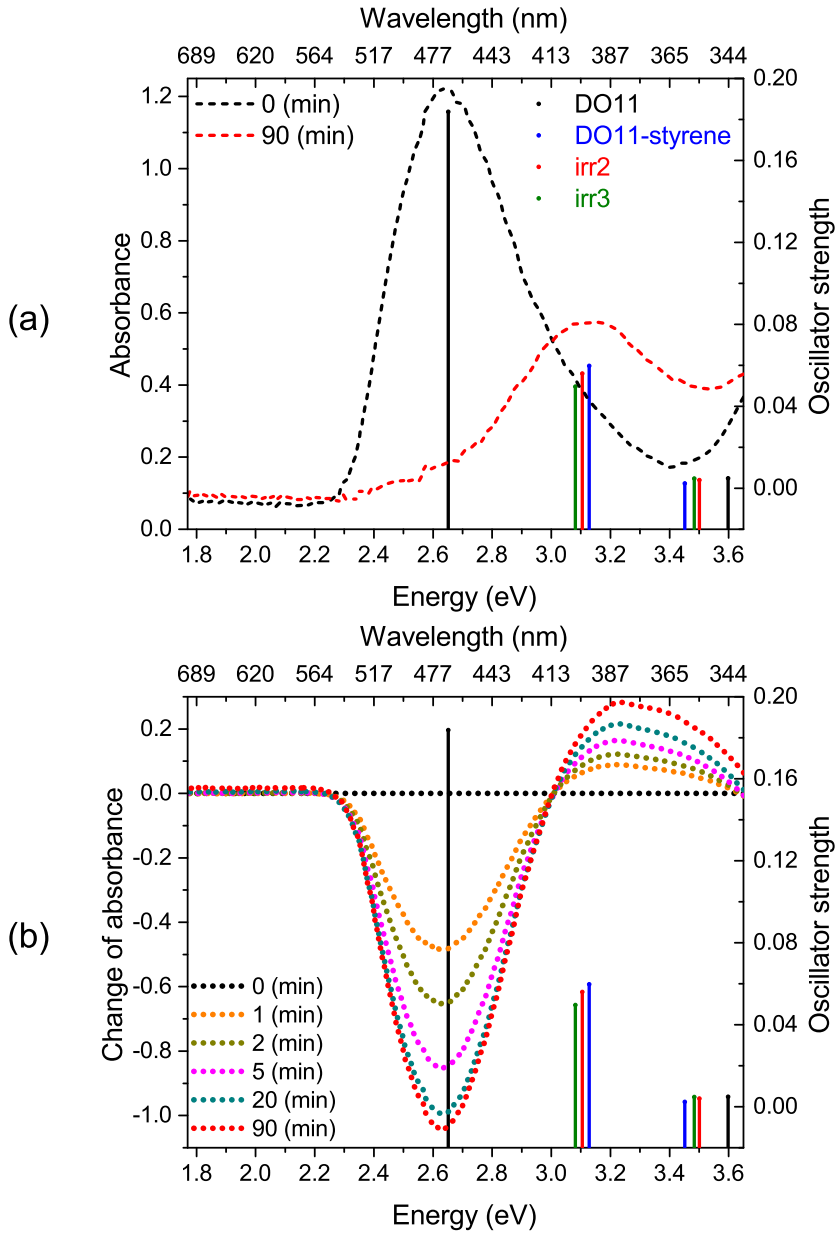

Figure 6.3: (a) UV-Vis absorption spectrum of pristine DO11/PS, the spectrum taken after 90 minutes of irradiation (dashed curves), and the oscillator strength of the possible irreversibly-degraded species (vertical lines). (b) Change of absorbance during decay with respect to the pristine sample (dotted curves) and the oscillator strength of the possible irreversibly-degraded species (vertical lines). The oscillator strength of the DO11-styrene oxetane is also plotted in both graphs for comparison.

Figure 6.4 shows the UV-Vis absorption spectra of fresh and irreversibly photodegraded DO11/PMMA, the calculated oscillator strength of the possible reversibly-damaged species dissolved in toluene, and the change in absorbance of DO11/PMMA during decay. Similar to the results in DO11/PS, the computed results of both anion and tautomer of DO11 disagree with the experimental results. Only DO11-MMA oxetane is in agreement with the change in visible absorption spectrum during photodegradation, thus DO11-MMA oxetane is the most likely reversibly-damaged species among the three computed candidates.

Figure 6.5 shows the same experimental results with the calculated oscillator strength of DO11-MMA oxetane and the proposed irreversibly-damaged species. DO-11/PMMA has better photoresistance than DO11/PS so the absorbance after 59 minutes of irradiation with a similar pump intensity may not be as close to that of the irreversibly-damaged species obtained in DO11/PS, but the experiment was stopped due to the increasing instability of the white light source. In addition, the structure of toluene, the solvent chosen for the TD-DFT calculation, is similar to a unit of PS but different from a unit of PMMA. Therefore the agreement between the computational and experimental results for DO11/PMMA may not be as good as DO11/PS. Besides, the calculated dipole moment of damaged species is larger than the pristine DO11 as listed in Appendix B, therefore the damaged species may interact more strongly with PMMA than PS due to the $COOCH_3$ group in PMMA. Nonetheless, the blue shift in the absorption spectrum and the change of absorption peaks qualitatively agree with the calculated oscillator strength and the corresponding energy for DO11-MMA oxetane. DO11-MMA oxetane also exhibits similar oscillator strength and absorption peak positions in the visible region as does the irreversibly-degraded species. Thus, the conclusion drawn from the results of DO11/PS is also true in DO11/PMMA.

By comparing the computational and experimental results, both IPT and anion formation are ruled out and the proposed PTCR hypothesis is the most possible mechanism responsible for reversible photodegradation. As presented in Appendix B, TD-DFT results confirm that all reversibly- and irreversibly-damaged species proposed in the PTCR hypothesis have similar absorption spectra in the visible region due to the partial damage in ICT path as illustrated in Figure 2.7, and these results also qualitatively agree with the absorption spectra of the reversibly-damaged dye species in PS and PMMA calculated using a simple model and experimental results as described in Appendix A.

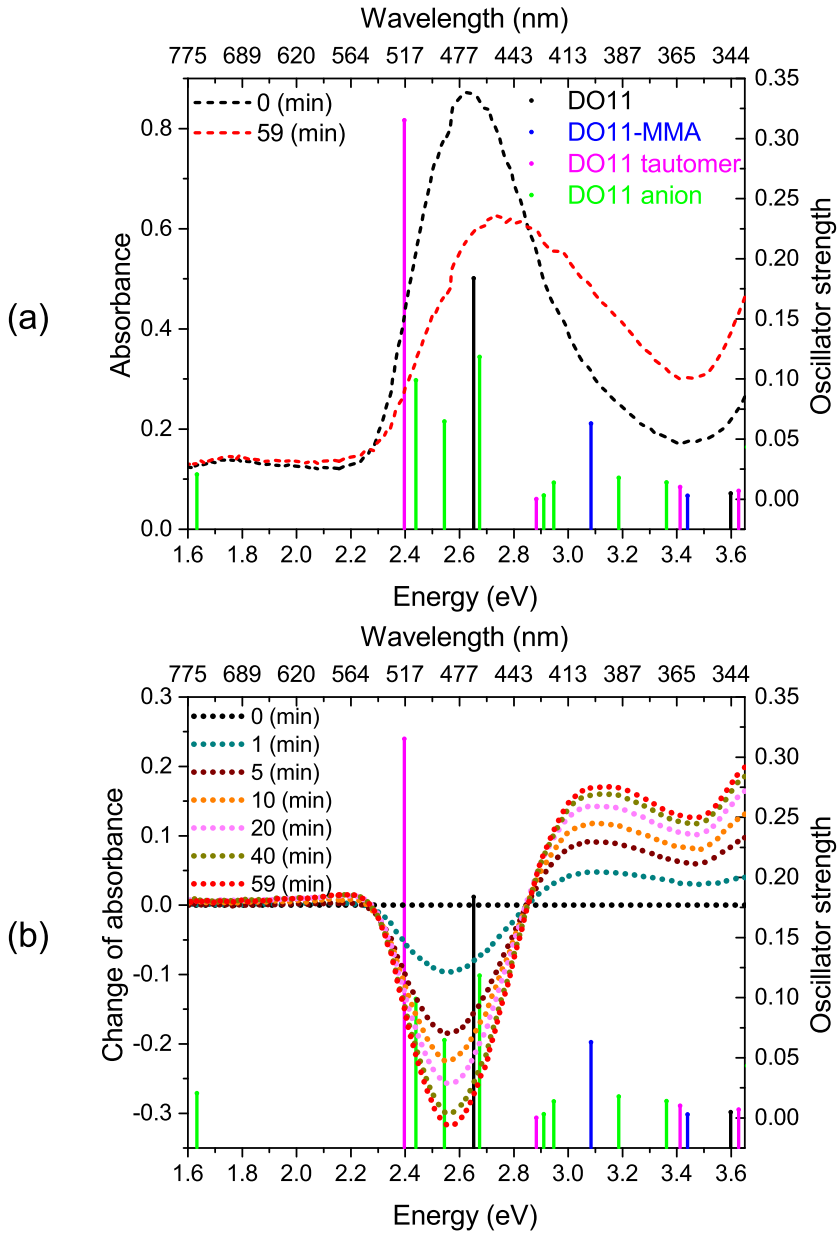

Figure 6.4: (a) UV-Vis absorption spectrum of pristine DO11/PMMA, the spectrum taken after 59 minutes of irradiation (dashed curves), and the oscillator strength of the possible reversibly-degraded species (vertical lines). (b) Change of absorbance during decay with respect to the pristine sample (dotted curves) and the oscillator strength of the possible reversibly-degraded species (vertical lines).

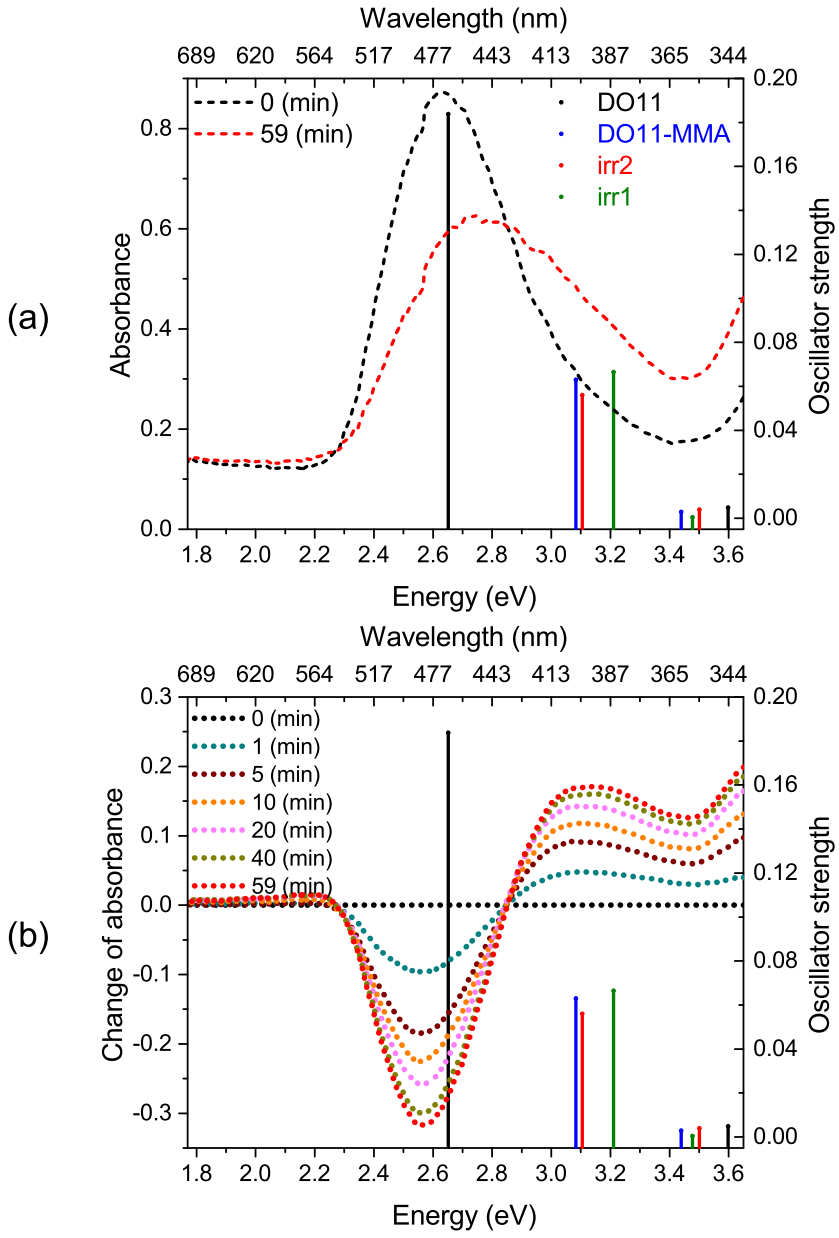

Figure 6.5: (a) UV-Vis absorption spectrum of pristine DO11/PMMA, the spectrum taken after 59 minutes of irradiation (dashed curves), and the oscillator strength of the possible irreversibly-degraded species (vertical lines). (b) Change of absorbance during decay with respect to the pristine sample (dotted curves) and the oscillator strength of the possible irreversibly-degraded species (vertical lines). The oscillator strength of the DO11-MMA oxetane is also plotted in both graphs for comparison.

Chapter 7

Fourier transform infrared spectroscopy

A UV-Vis absorption spectrum shows peaks due to the dyes in a dye-doped polymer; but since PS and PMMA are transparent in this wavelength range, the contribution from the host polymer is negligible. However, infrared (IR) absorption spectroscopy allows the study of both dye and polymer. Thus, we apply Fourier transform infrared (FTIR) spectroscopy to monitor the change of chemical bonds in the dye molecules and in the host polymer to study their role in reversible and irreversible photodegradation.

1AAQ/PMMA was chosen for FTIR characterization studies because of the abundant literature on 1AAQ. In contrast, the literature on DO11 is sparse. It is reasonable to assume no significant differences in photoinduced reactions between 1AAQ and DO11 when incorporated in the same polymer host, as described in Chapter 2 and 5. PS was not studied in the FTIR experiments due to the small amount of dye recovery, which would be difficult to distinguish from noise. A polymerized sample sandwiched between two glass substrates can not be used in FTIR experiments, because glass absorbs IR radiation in the region of interest. Silicon wafers, on the other hand, provide a good IR window for this study. Spin-coating is used to make thin samples that allow us to observe the evolution of IR spectra. However, IR absorption from the bonds in the dye molecules is much weaker than for PMMA due to the low dye concentration used in samples polymerized from a dye-dissolved monomer solution. For example, a typical polymerized 1AAQ/PMMA sample has a concentration of 8.5 g/L, which corresponds to about 0.3% number density of 1AAQ in MMA monomer. In order to observe possible changes in the IR spectrum from both dye and polymer, the concentration of 1AAQ/PMMA was increased to 105 g/L, about 4.0% number density of 1AAQ in MMA monomer, resulting in a dye concentration more

than 12 times higher than a typical polymerized sample. With such a drastic change in dye concentration and the method of sample preparation from the usual experimental protocol, it is necessary to confirm that the same reversible photodegradation can be observed. Thus, 1AAQ/PMMA sample was also spin-coated on glass substrates and studied with linear absorption spectroscopy. The thickness of 1AAQ/PMMA spin-coated on a glass slide is about 0.6 μm estimated using the same method described in Appendix C for DO11/PMMA thin films. The thickness of 1AAQ/PMMA spin-coated on a silicon substrate is not measured, but it is thinner than 0.6 μm since the spin speed is 5 times faster than the sample spin-coated on a glass slide. The role of air in reversible photodegradation will be discussed since spin-coated samples are open to the air in the linear absorption spectroscopy measurements.

7.1 Observations in UV-Vis spectrum

1AAQ/PMMA was spin-coated on a glass substrate and irradiated with a 532 nm wavelength cw laser at a peak power of 2.09 W/cm^2 for 30 minutes and probed using linear absorption spectroscopy to confirm that reversible photodegradation takes place for spin-coated samples. Figure 7.1 shows the absorption spectra and the change in absorbance during decay and recovery. In the decay process, the absorption peak of the fresh sample, the peaks of changing absorbance, and the isosbestic points at 2.84 eV and 2.31 eV agree within the experimental uncertainty with those observed from the polymerized sample as shown in Figure 5.4. The fact that no significant difference observed between spin-coated (open to the air) and polymerized (sandwiched between two glass slides) samples during decay suggests that air is unlikely involved in the decay process.

In the recovery process, shown in Figure 7.1(b), the change in absorbance near 2.3 eV behaves similar to but is not as drastic of a change as the 1AAQ/MMA liquid sample as shown in Figure 5.3(b). The reason for the similar behavior may be due to the larger amount of free space left in the spin-coated samples by evaporated solvent. In contrast, the sample polymerized from monomer may have less free space and more polymer entanglements, which increase the possibility of recombination of thermally decomposed polymer fragments and stop the diffusion of dye and thermally decomposed polymer products during irradiation. As a result, more MMA monomers and other fragments accumulate than in a polymerized sample. Thus, the local environment becomes a mixture of small amounts of liquid solution and polymer. The isosbestic point at 2.81 eV in Figure 7.1(b) is slightly shifted from the 2.84 eV peak in the recovery spectra of the polymerized sample shown in 5.4(b). The change of absorbance during recovery in Figure 7.2 agrees with that observed from polymerized sample in Figure 5.6, except that the isosbestic point near 2.3 eV

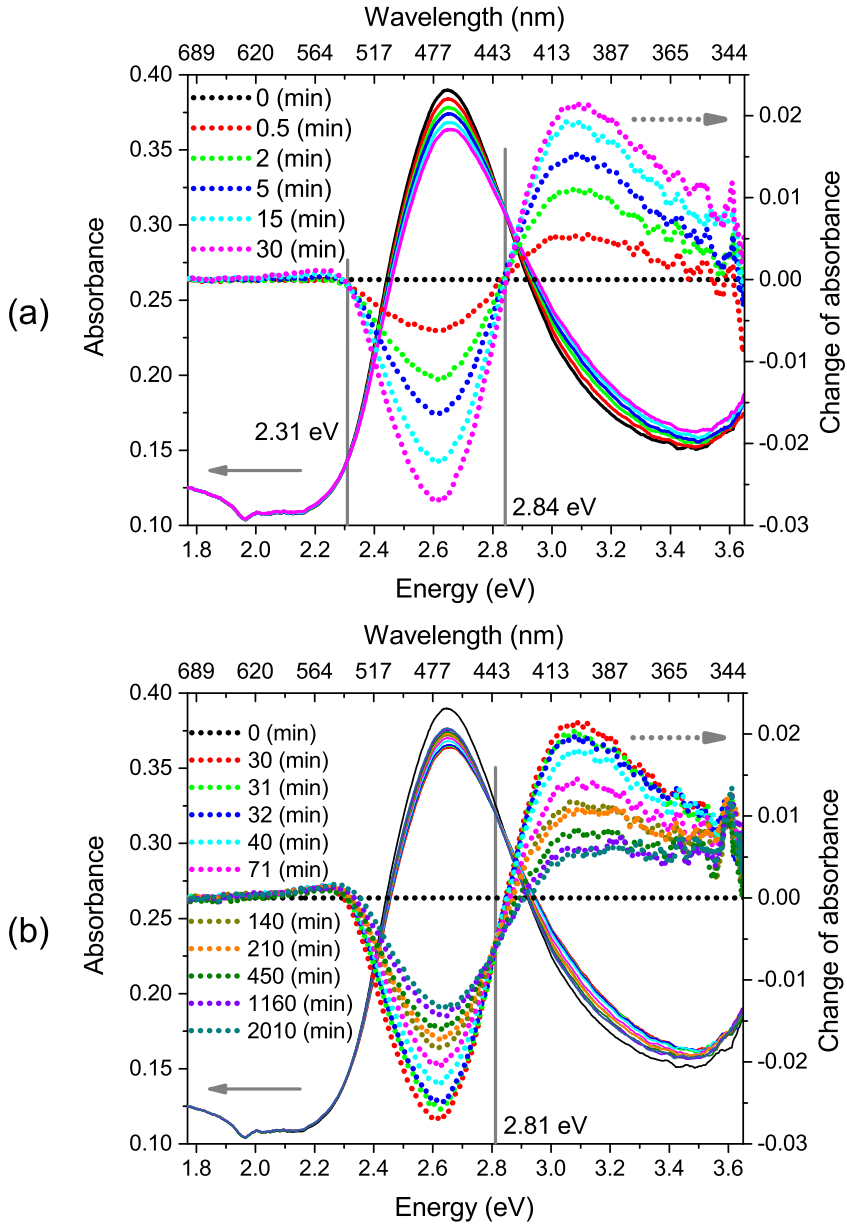

Figure 7.1: Absorption spectrum and the change of absorbance relative to the pristine sample of 1AAQ/PMMA as a function of time during (a) decay and (b) recovery.

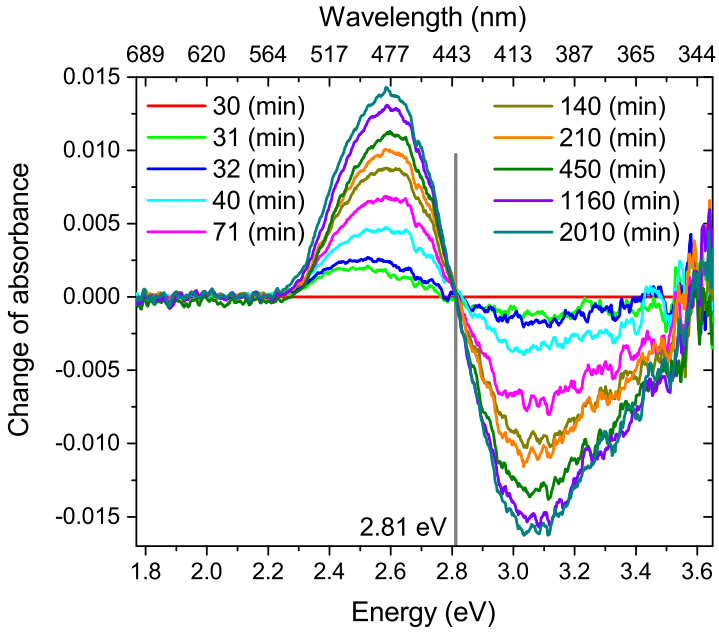

Figure 7.2: The Change in absorbance of 1AAQ/PMMA relative to the spectrum taken at the 30$^{\text{th}}$ minute, the time at which the pump laser turned off.

of the spin-coated sample is not discernible. The change in the character of the isosbestic points may be due to experimental uncertainty and/or the conversion of some portion of reversibly-damaged species into the irreversibly-damaged species similar to the cases described in Appendix A for DO11. The low energy peak position of the change in absorbance during recovery in Figure 7.2 shifts from around 2.5 eV to 2.6 eV, suggesting that some of the reversibly-damaged species converts into irreversibly-damaged species in addition to recover back to the fresh 1AAQ, which agrees with the observation from the polymerized sample discussed in Appendix A for DO11. The agreement between spin-coated (open to the air) and polymerized (sandwiched between two glass slides) samples during recovery indicates that air may not significantly affect the process of the reversibly-damaged species converting into the irreversibly-damaged species or back to fresh 1AAQ.

Our current experimental configuration does not allow for the entire decay and recovery experiment to be run in vacuum. However, the decay experiment can be run in vacuum followed by the recovery experiment in air. If photodegradation in air differs from that in vacuum - for example, containing different kinds of damaged products or different amounts of reversibly- and irreversibly-damaged products - the process during recovery should behave differently even when measured under the same conditions.

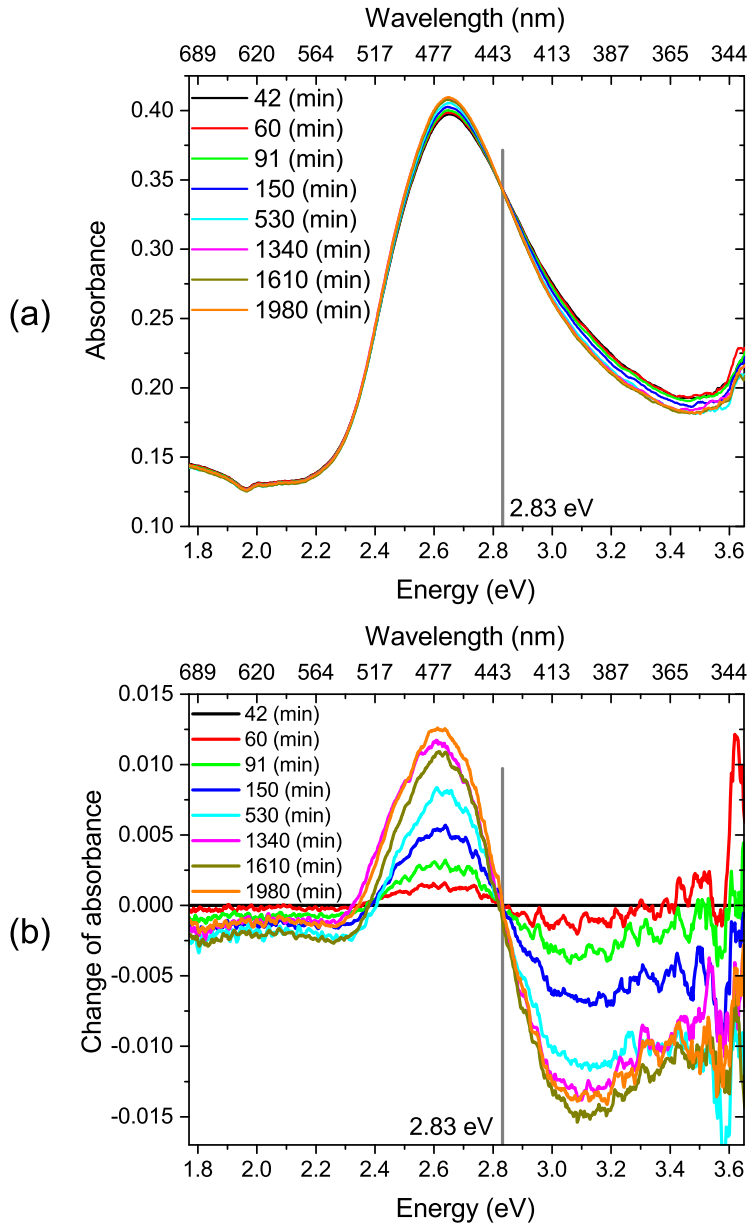

Figure 7.3: (a) Absorption spectra of 1AAQ/PMMA during recovery after irradiated in the FTIR setup for 30 minutes. The first spectrum was taken at the 42$^{\text{nd}}$ minute, 12 minutes after the irradiation. (b) The change in absorbance relative to the spectrum taken at the 42$^{\text{nd}}$ minute.

To test the effect of air, a sample spin-coated on a glass substrate was irradiated in the FTIR setup in vacuum under the same pump conditions (approximately the same pump intensity) as previously done in air, then transferred to the linear absorption spectroscopy experiment to record the recovery starting from the 42nd minute. The transfer took 12 minutes. The absorption spectra and the change in absorbance during recovery are shown in Figure 7.3. To insure that the damaged area was probed after the transfer, the sample was positioned such that the diameter of the white light probe was about 2 mm. While this increases experimental uncertainties, the same isosbestic point at 2.83 eV and peak positions were observed within experimental uncertainty as those in Figure 7.1.

The change of absorbance at 2.61 eV for both experiments described is plotted in Figure 7.4. The black circular dots represent measurements in the linear absorption spectroscopy setup, and the red hollow squares represent recovery measurements subsequent to the photodegradation experiment performed in vacuum with the FTIR setup using the linear absorption spectroscopy setup. The recovery data are adjusted to be the same at the 42nd minute. A meaningful comparison between the two runs assumes that the spin-coated samples made

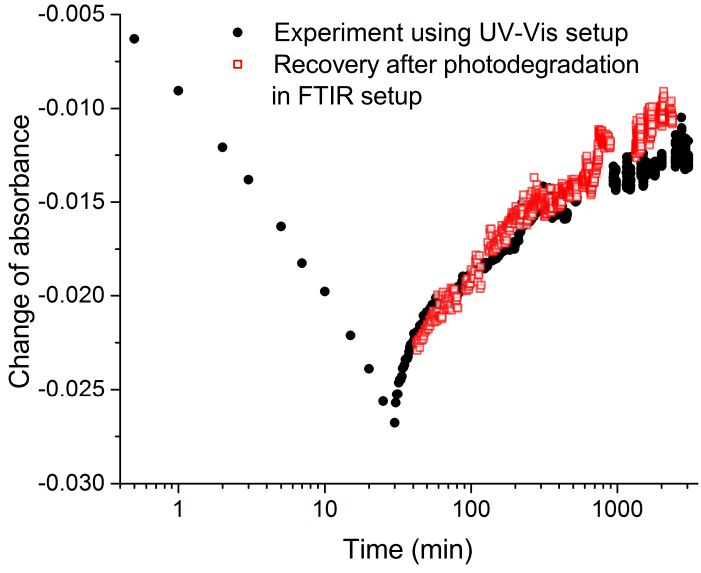

Figure 7.4: Black dots: Change of absorbance relative to the pristine 1AAQ/PMMA at 475 nm (2.61 eV) measured in air. Red hollow squares: Change of absorbance relative to the 1AAQ/PMMA absorbance taken at the 42nd minute, where the data is shifted so that the values obtained at the 42nd minute match. The decay experiment was performed in vacuum and the recovery was recorded in air.

under the same conditions have the same thickness.

It may be possible that air is involved in photodegradation and/or recovery processes but only on the surface of the film, if air can not diffuse into the polymer matrix easily. In this case, the effect of air is negligible in all experiments conducted with dye-doped polymers since the same photodegradation and recovery processes are observed in vacuum and air.

Since spin-coated samples from polymer/dye solution undergo the same reversible photodegradation as samples polymerized from dye dissolved in monomer, we use spin-coated samples in FTIR study to study the mechanism responsible for reversible photodegradation in samples prepared using both methods.

7.2 FTIR

In the FTIR experiment, the 1AAQ/PMMA sample needs to be rotated 90° for laser irradiation and rotated back to its original position for taking IR spectra during recovery. This introduces uncertainties in addition to the noise when comparing spectra during recovery to the spectrum of the fresh sample taken before it is rotated. We examined the uncertainty by simulating the experiment without irradiating the sample as follows. 1AAQ/PMMA with a concentration of 105 g/L is spin-coated on a silicon wafer and used in this test. An IR absorption spectrum is acquired at room temperature by averaging 6000 scans. The sample is then rotated 90° (without laser irradiation) and rotated back to the original position. Subsequently 1000 scans are averaged to obtain a spectrum and the procedure is repeated. 45 minutes after taking the second spectrum, another spectrum averaging 1000 scans is acquired. The change in IR absorption spectrum is obtained by subtracting the first spectrum taken before rotating the sample from the later ones. The results of two full cycles of rotation are plotted as “test 1” and “test 2”, and the one taken 45 minutes after “test 2” is plotted as “test 3” in Figure 7.5.

To study the reversible photodegradation of 1AAQ/PMMA with FTIR, we prepared as controls a plain silicon wafer, spin-coated PMMA on a silicon wafer, and 105 g/L concentration 1AAQ/PMMA spin-coated on a silicon wafer. To minimize the uncertainty, all three samples were fixed on the sample holder and placed in the vacuum chamber for the entire experiment.

All IR spectra were acquired at room temperature and averaged over 6000 scans before irradiation. The 1AAQ/PMMA sample was irradiated using 532 nm wavelength cw laser light with approximate peak power of 2.09 W/cm^2 for 30 minutes. IR spectra of 1AAQ/PMMA acquired after irradiation were averaged over 1500 scans during the first 400 minutes, 3000 scans for the 540$^{\text{th}}$ minute, and 6000 scans afterward. The IR absorption spectra of PMMA and

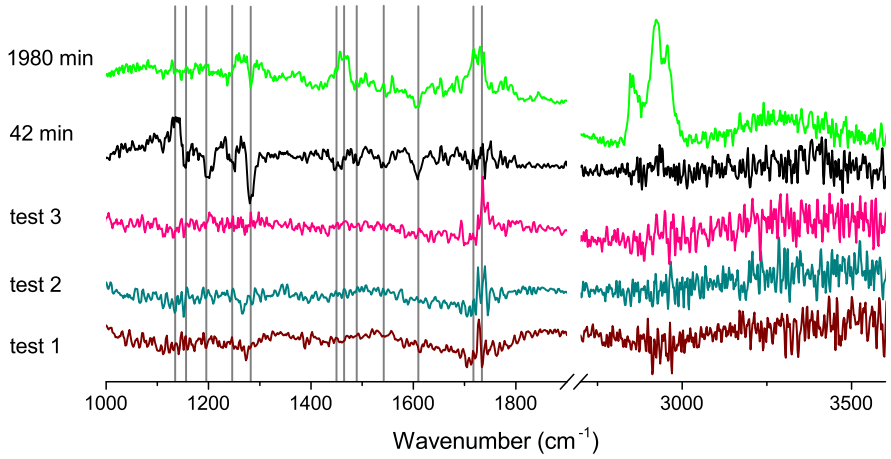

Figure 7.5: Comparison of noise and the change in IR absorbance of 1AAQ/PMMA during recovery after being irradiated with a 532 nm wavelength cw laser for 30 minutes. The vertical lines correspond to the varying IR absorption bands shown in Figure 7.6 and discussed in the text.

1AAQ/PMMA were obtained by subtracting the spectrum of each sample from that of the silicon wafer as shown in Figure 7.6(a) and 7.7(a). The IR absorption peaks of the dye are much weaker than that of PMMA as can be seen by comparing the amplitudes of IR spectra in Figure 7.6(a). Though the dye concentration is about 12 times higher than polymerized samples used in other experiments, the polymer contribution to the IR absorption is larger. The change of IR spectrum with respect to fresh 1AAQ/PMMA during recovery is plotted in Figure 7.6(b) and 7.7(b) at various time intervals, and the first and last spectra are also plotted in Figure 7.5, which shows that the change of IR spectra are distinguishable from noise except for the peak near 1731 cm^{-1} due to the nearly saturated absorbance at 1731 cm^{-1}.

We assign observed IR absorption peaks that change over time in Figure 7.6 and 7.7 according to literature and tabulate them in Table 7.1. According to Nagai et al., the bands at 1150 and 1194 cm^{-1} are associated with coupled vibrations of skeletal stretching and internal C−H deformation modes, and the band at 1244 cm^{-1} is associated with the coupled C−C−O and C−O stretching vibrations [140, 141]. However, the bands between 1150 and 1300 cm^{-1} have been attributed later to strong coupling between stretching vibrations of C−C−O and C−O or C−O−C and C−O of the ester group (R_1−COO−R_2) [142–144]. We adopt the more current assignment for the bands at 1150, 1194 and 1244 cm^{-1} to be coupled C−C−O−C stretching vibrations. The bending vibrations of CH_2, α-CH_3 (in which α represents the first carbon atom that is attached to the functional group $COOCH_3$) and (O)CH_3 strongly overlap around the band

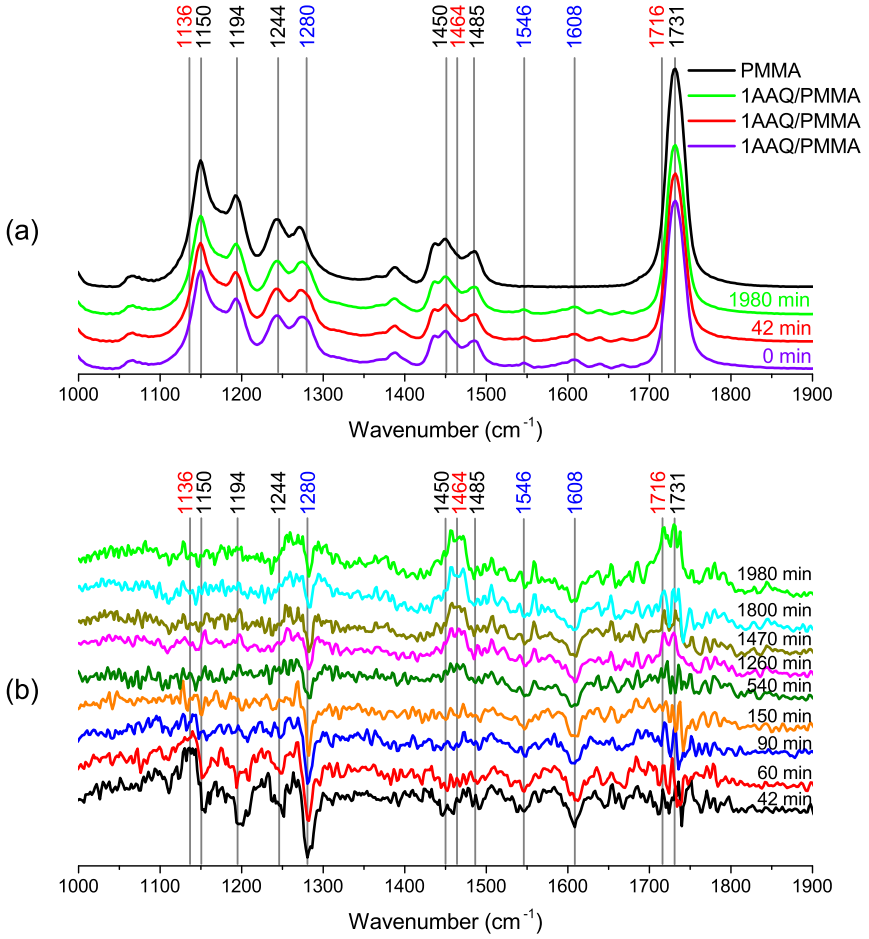

Figure 7.6: Peaks in the FTIR spectra are labeled: black for PMMA, blue for 1AAQ and red for absorption peaks that do not belong to PMMA and 1AAQ. (a) IR absorbance of PMMA and 1AAQ/PMMA at 0, 42 and 1980 min. (b) Change in the IR absorbance of 1AAQ/PMMA relative to the pristine spectrum (0 min) as a function of time after being irradiated by a 532 nm wavelength cw laser for 30 minutes.

at 1450 cm^{-1} [140, 141, 145]. The peak at 1485 cm^{-1} can be assigned to the α-CH_3 asymmetric deformation vibration of PMMA [140, 141, 145]. While the peak at 1136 cm^{-1} may be a new peak, it is also possible that this peak is a result of a frequency shift of the 1150 cm^{-1} peak under irradiation that recovers after the laser is turned off.

The peak at 1280 cm^{-1} is about the same magnitude as the 1244 cm^{-1} peak

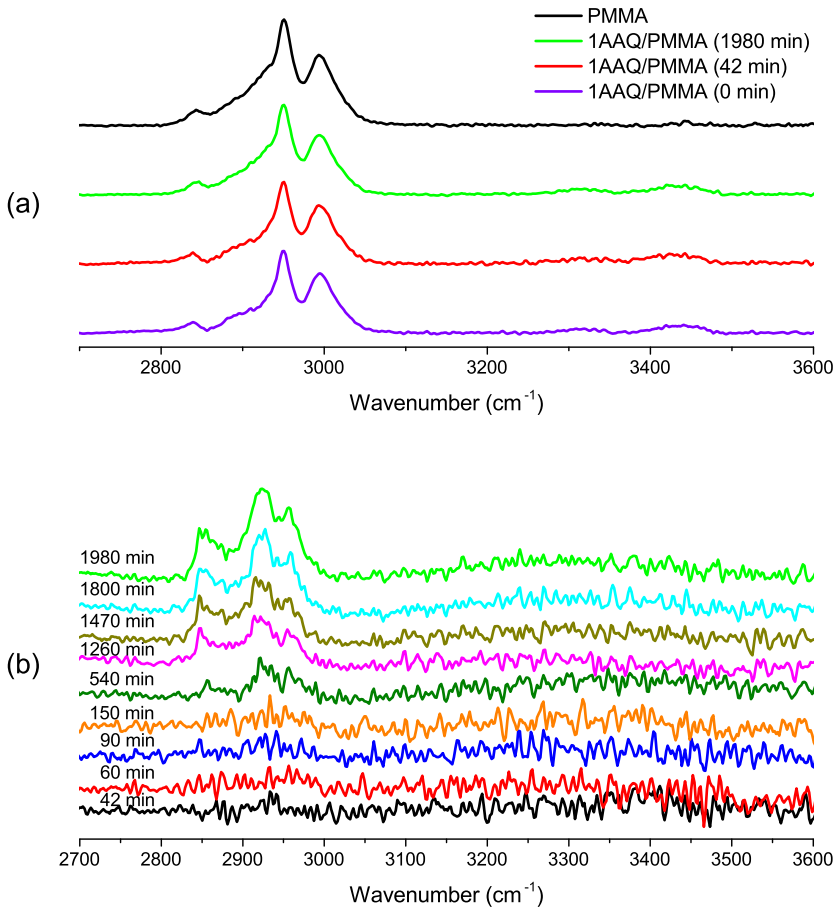

Figure 7.7: (a) IR absorbance of PMMA and 1AAQ/PMMA at 0, 42 and 1980 min. (b): Change in the IR absorbance of 1AAQ/PMMA relative to the pristine spectrum (0 min) as a function of time after being irradiated by a 532 nm wavelength cw laser for 30 minutes.

in the IR spectrum of pristine 1AAQ/PMMA in Figure 7.6(a), but 1280 cm^{-1} is located at the shoulder of the IR absorption peak of PMMA at 1270 cm^{-1}, which is smaller than the 1244 cm^{-1} peak in the pure PMMA IR spectrum, so the peak at 1280 cm^{-1} comes from 1AAQ and can be attributed to C−C−C stretch of ketones, i.e. C−C(=O)−C [143]. The peak at 1546 cm^{-1} can be assigned to the in-plane NH_2 scissoring of 1AAQ, though is 34 cm^{-1} lower than the usual frequency range in organic compounds [143], which could be caused by the intramolecular hydrogen bond. The band at 1608 cm^{-1} can be attributed

Wavenumber (cm^{-1})	Molecule	Corresponding vibration
1150, 1194, 1244	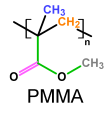 PMMA	C−C−O−C stretching
1450		CH_2, α-CH_3 and (O)CH_3 bending
1485		α-CH_3 asymmetric deformation
1731		C=O stretching
1280	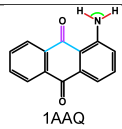 1AAQ	C−C−C stretch of ketones
1546		in-plane NH_2 scissoring
1608		C=O stretching
3320, 3440		N−H stretching
1136	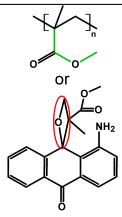	See text
1464		CH_2 scissoring
1716		C=O stretching
2850-3000		sp^3 CH stretching

Table 7.1: The assignment of IR absorption bands with each assignment colored in the corresponding molecular structure. The molecular structures shown for molecules other than PMMA and 1AAQ are merely illustrations for the corresponding IR bands, not necessarily the actual molecules. Details of the assignment of the IR bands are described in the text.

to the vibration of C=O adjacent to the amine group [146] of 1AAQ. It is worth noticing that the band at 1667 cm^{-1}, which can be assigned to the vibration of the other C=O group of the 1AAQ molecule [146], is observed as can be found in Figure 7.6, and there is no change at this band after irradiation (therefore not indicated in the figure). The symmetric and asymmetric N−H stretching modes of the amine group at about 3320 cm^{-1} and 3440 cm^{-1} [146] are too noisy to determine whether they changed after irradiation.

Some changes in the IR absorption peaks that do not belong to PMMA and 1AAQ are found to be the changes in the background of the system. The peak at 1464 cm^{-1} is known to be the CH_2 scissoring band of hydrocarbons [143, 147]. The band at 1716 cm^{-1} originates from the C=O stretching vibration [143] that belongs to neither aminoanthraquinones, which possess frequency of C=O stretch in 1610∼1680 cm^{-1} [146], nor PMMA, which exhibits the C=O stretch

near 1731 cm^{-1} [78]. The change of IR absorption bands between 2850 and 3000 cm^{-1} are known to be sp^3 CH stretching vibration [143, 147]. These peaks are compared with the changes in the background of the system in Appendix D.

Possible mechanisms described in Chapter 2 will be examined with the above observation in what follows.

7.2.1 Possible mechanisms

Reversible photodegradation of dye

With the above observations, both twisted intramolecular charge transfer (TICT) and anion formation are unlikely to be the possible mechanisms responsible for reversible photodegradation due to the following reasons. Both TICT and anion formation in 1AAQ do not involve dissociation of chemical bonds. According to the study comparing C=O vibrations of 1AAQ, 1-methylamino- and 1-dimethylamino-anthraquinone [146], the C=O vibration band at 1608 cm^{-1} shifts toward higher frequency and the C=O vibration band at 1667 cm^{-1} shifts toward lower frequency as the extent of the resonance (due to intramolecular charge transfer) decreases. Hence, both TICT and anion formation in 1AAQ may cause shifts in C=O vibration modes due to the change in the extent of the resonance, instead of the observed decrease in the amplitude of C=O vibration at 1608 cm^{-1} alone.

As described in Section 2.1.1, the intramolecular proton transfer (IPT) hypothesis proposes that a dimer of two tautomers is the reversibly-damaged dye species [51]. When 1AAQ converts into its tautomer, the C=O vibration peak at 1667 cm^{-1} remains unchanged, and another C=O vibration peak at 1608 cm^{-1} reduces its magnitude. The tautomer of 1AAQ should exhibit one N−H stretching vibration band near 3320 cm^{-1}, as observed at 3270 cm^{-1} for 1-methylamino-anthraquinone [148], and an O−H stretching vibration band. The O−H stretch, possibly around 3350 cm^{-1}, could be buried in the noise or suppressed by hydrogen bonding, as observed in 1-substituted hydroxyanthraquinones [146]. The observed decrease of the C=O vibration peak at 1608 cm^{-1} and in-plane NH_2 scissoring band at 1546 cm^{-1} may be a result of IPT, which may result in the observed reduction of the C−C−C stretch mode of the ketone group at 1280 cm^{-1}. Thus, the IPT hypothesis can not be eliminated with the FTIR results alone if the IPT hypothesis is accompanied with another mechanism responsible for the observed irreversible photodegradation.

In the hypothesis of domains described in Section 2.2.2, the tautomer, a mixture of the tautomer and the original dye molecule, or the original dye molecule may be the “pristine” dye species which decomposes into (multiple) pieces due to laser irradiation that recombine if the corresponding counterparts

meet each other [58, 59]. The presence of 1AAQ is confirmed in the fresh sample since both the C=O vibration and the two N−H stretching vibration bands are observed in the IR spectrum of the fresh 1AAQ/PMMA sample. Thus, the possible "pristine" dye species can be 1AAQ or a mixture of 1AAQ and its tautomer. This hypothesis posits that dye molecules are decomposed under irradiation and recovery occurs when the decomposed counterparts meet each other. Without knowing the possible products of the decomposed dye species, it is difficult to judge whether the observed change in the 1AAQ IR absorption peaks agrees with the hypothesis.

The hypothesis of photothermal-induced chemical reactions (PTCR) between dye and polymer involves changes in both dye and polymer simultaneously, so it will be discussed together with the irreversible photodegradation process below.

Reversible and irreversible photodegradation of dye and polymer

The PTCR hypothesis posits that 1AAQ undergoes photocycloaddition to MMA generated from photo-thermally degraded PMMA to form oxetane, the reversibly-damaged species, or undergoes other (photo)chemical reactions with fragments thermally degraded from PMMA to form the irreversibly-damaged species. Figure 7.8 illustrates the possible damage to 1AAQ and PMMA and the corresponding change in IR absorption peaks.

The reduction of C−C−O−C stretching vibrations of PMMA (1150∼1300 cm^{-1}) after irradiation indicates the scission of the methoxycarbonyl group ($COOCH_3$) from PMMA under irradiation. The decrease of CH_2 bending (1450 cm^{-1}) and α-CH_3 asymmetric deformation (1485 cm^{-1}) of PMMA after irradiation suggests that depolymerization and dissociation of polymer backbones take place under irradiation. Photocycloaddition between 1AAQ and the depolymerized MMA causes the decrease of the C=O vibration peak (1608 cm^{-1}) and the C−C−C stretch peak of ketone (1280 cm^{-1}) in 1AAQ. 1AAQ and other radicals and fragments dissociated from PMMA can also undergo (photo)chemical reaction to form irreversibly-damaged species and cause the same change in the IR peaks. Note that there is no change from the other C=O group of the 1AAQ molecule at frequency 1667 cm^{-1} [146] observed, which is consistent with the conclusion obtained from the linear absorption spectroscopy measurements and the TD-DFT calculation in DO11.

From the ground state geometry optimization of DO11 in the DFT calculation, the amine group in the reversibly- and irreversibly-damaged species, though still fairly planar, is observed to be slightly out-of-plane or slightly twisted instead of lying in-plane with the skeleton of DO11 as shown in Figure B.3 of Appendix B. It is reasonable to assume that the DFT calculation results of DO11 can be qualitatively applied to 1AAQ due to their similar molecular structures. Thus, the in-plane NH_2 scissoring of 1AAQ at 1546 cm^{-1} may be

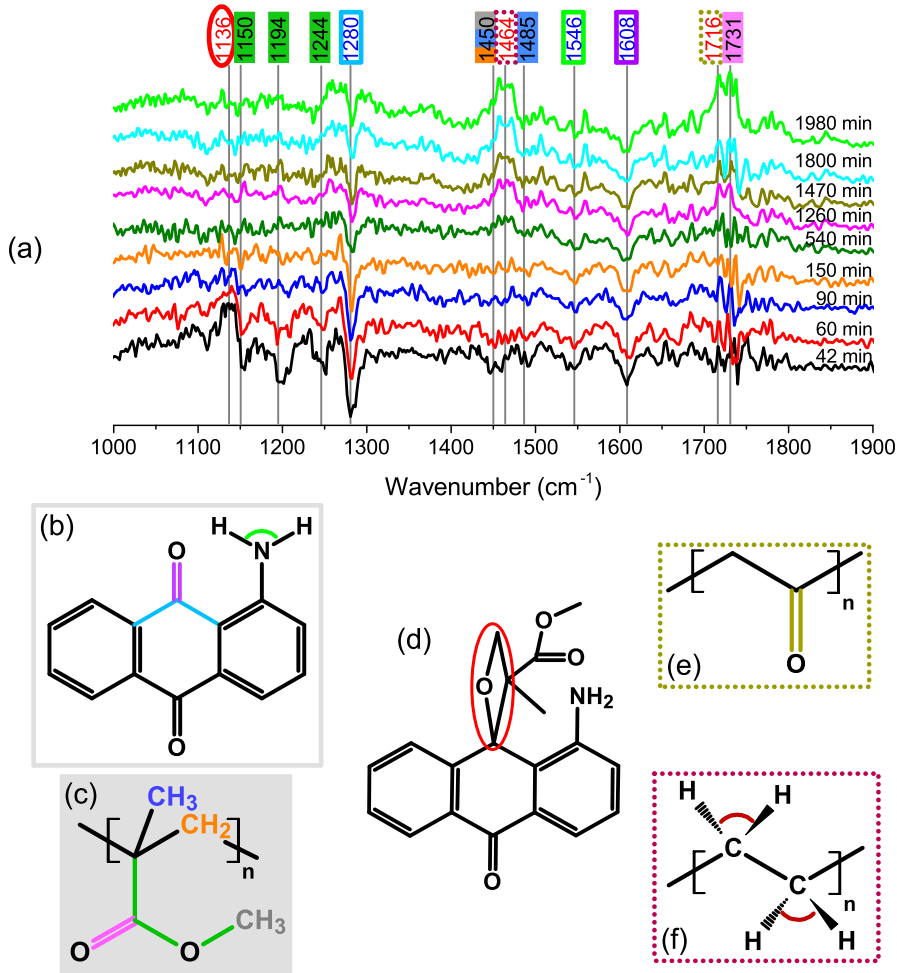

Figure 7.8: (a) Evolution of the change in the IR spectrum relative to the pristine 1AAQ/PMMA after 30 minutes of irradiation. Peaks belonging to 1AAQ have wavenumbers circled by hollow rectangles with colors corresponding to that in the 1AAQ structure in (b). Peaks belonging to PMMA are highlighted by rectangles with colors corresponding to that in the PMMA structure in (c). Peaks not belonging to PMMA and 1AAQ are illustrated with (d) 1AAQ-MMA oxetane using the red circle, (e) and (f) other structures originate from the background of the system using dotted rectangles with the corresponding colors shown in the structures. Details are described in the text.

weakened after irradiation. The IR absorption peaks of oxetane in the gas phase are located at 900 cm^{-1}, 995 cm^{-1}, and 2850∼3050 cm^{-1} [148]. The characteristic IR band of oxetane formed between 1AAQ and olefines was observed at 990 cm^{-1}, and for oxetane formed between 1AAQ and styrene was found at 970 cm^{-1} [68]. In this study, though, the change in the IR spectrum is relatively noisy in the frequency range below 1000 cm^{-1} and no significant change is observed between 800 cm^{-1} and 1000 cm^{-1} after irradiation. Since the vibration of chemical bonds may be affected by the environment, the growing peak at 1136 cm^{-1} after irradiation may be attributed to oxetane formed between 1AAQ and MMA as shown in Figure 7.8(d). The recovery of the peak at 1136 cm^{-1} indicates that 1AAQ-MMA oxetane molecules return to 1AAQ and MMA or further decay into irreversibly-damaged species.

Recall that the photocycloaddition between 1AAQ and MMA is just a possible photochemical reaction resulting in a possible reversibly-damaged structure. If photocycloaddition between 1AAQ and MMA does not occur, the reversibly-damaged species may be a metastable product of another photochemical reaction as discussed in Section 2.2.3. Thus, the peak at 1136 cm^{-1} could also be a red shift from 1150 cm^{-1} due to the dissociation of the $COOCH_3$ group from PMMA under irradiation.

The changing IR absorption peaks belonging to 1AAQ partially recover and the recovery is distinguishable until the 540^{th} minute except for the in-plane NH_2 scissoring band, which is difficult to resolve due to noise. However, as discussed in Appendix D, a growing peak near 1280 cm^{-1}, which corresponds to the C−C−C stretching vibration of ketone adjacent to the amine group in 1AAQ, is found to originate from the background of the system and become distinguishable starting at the 540^{th} minute in the IR spectrum. Thus, the recovery at the peak 1280 cm^{-1} may have stopped (i.e. become indistinguishable from noise) at the 150^{th} minute. The partial recovery of 1AAQ agrees with the observed absorption spectroscopy measurements. The reduced IR peaks belonging to PMMA fully recover at the 150^{th} minute. In addition to the changes in the background of the system, the "disagreement" of the recovery time in 1AAQ and PMMA may also originate from the small signal-to-noise (S/N) ratio of the spectrum and long time interval between two measurements, i.e. the recovery time for 1AAQ may agree with that for PMMA if the IR spectrum could have a better S/N ratio or be acquired more frequently. Other factors that may be responsible for the disagreement are uncertainties and artifacts that arise from the baseline process used for obtaining the spectra. Nonetheless, the experimental results qualitatively agree with the PTCR hypothesis.

Summary

FTIR results have provided the evidence that both dye and polymer undergo reversible photodegradation, instead of dye alone. The results rule out

the hypotheses that TICT states and anion formation are the responsible mechanisms for reversible photodegradation. Though the IPT hypothesis is not eliminated, it requires an additional mechanism and species to explain the observed irreversible process. As discussed in Chapter 2, the additional mechanism causing irreversible photodegradation likely originates from local heating due to light absorption. Instead of requiring two distinct mechanisms occurring simultaneously and producing two degraded dye species with similar absorbance or one of the two degraded species possessing a similar absorbance as the fresh dye, the domains or PTCR hypotheses provide possible mechanisms responsible for both reversible and irreversible photodegradation in dye-doped polymers. However, it is not clear how the dye molecules decompose within domains. On the other hand, FTIR experiments are in agreement with the PTCR hypothesis.

7.3 Further discussion on PTCR hypothesis

Among all possible mechanisms with specified reversibly- and/or irreversibly-damaged dye species to some extent as described in Chapter 2, the PTCR hypothesis is the only interpretation that simultaneously agrees with the study of 1AAQ/styrene, 1AAQ/MMA, DO11/styrene, 1AAQ/PMMA, DO11/PS and DO11/PMMA using linear absorption spectroscopy in Chapter 5 and Appendix A, the comparison between TD-DFT calculation and experimental UV-Vis spectra of DO11/PS and DO11/PMMA in Chapter 6, and the FTIR results presented here. The hypotheses of domains does not specify how dye molecules may decompose under irradiation which leaves it a possible candidate to be responsible for reversible photodegradation. Domains in this hypothesis are thought to satisfy the correlated chromophore domain model (CCDM) which predicts that higher dye concentration leads to slower photodegradation and faster recovery [50, 53, 55]. Additionally, the CCDM also emphasizes that the recovery of dye molecules is mediated by domain formation possibly with the assistance of the polymer host [53, 58, 59] which is in agreement with the conclusion that the photodegradation of DO11 in liquid solution is irreversible [49]. However, if the decomposition of dye molecules is due to locally accumulated heat contributed by nonradiative relaxation of excited dye molecules, higher concentration of dye should result in faster photodegradation, which is observed and will be shown in Chapter 8. It has also been observed that both 1AAQ and DO11 undergo reversible photodegradation in liquid monomer solutions as described in Chapter 5. Thus, even if there exist domains of dye molecules in polymer matrices, the kinetics of reversible photodegradation are unlikely described by the CCDM and the relations between domains and the mechanism responsible for reversible photodegradation should be further studied. On the other hand, the PTCR hypothesis is in agreement with the results in Chapter 5 and 8.

Considering the commonly observed reversible photodegradation from a large variety of doped polymers briefly reviewed in Section 1.2, it is possible that there exists a universal principle responsible for the phenomena. The energy transfer from photo-excited dopants to hosts can potentially occur in all solid solutions. Therefore, the photoinduced thermal degradation of polymer hosts is possibly a common mechanism responsible for reversible and irreversible photodegradation in various doped polymers. For instance, PMMA doped with AF455 dye was observed to recover from laser ablation including optical and physical damages within a month, but recovery was not observed from the damaged neat PMMA in six months [13]. Although the AF455 dye differs from dyes used in this study, which may lead to other potential mechanisms such as multiphoton induced electron ejection and recombination proposed in the literature [13], reversible chemical reactions were not considered. Charge ejection and recombination may explain the reversible process of the optical damage in dye-doped PMMA, but the reversible physical damage must involve dissociation and formation of chemical bonds in both AF455 dye and PMMA, which may not require charge ejection and recombination. If reversible (photo)chemical reactions between AF455 dye and MMA (the main product of thermally degraded PMMA) take place, the principle of the PTCR hypothesis can be applied to explain both reversible optical and physical damage in AF455/PMMA.

The principle of the PTCR hypothesis may be applicable to reversible photodegradation in various doped polymers. Based on this principle, the condition of thermal degradation for polymers and the (photo)chemical properties of dopants and the thermally degraded products of polymers are keys in searching for more robust polymer-based materials.

Chapter 8

Kinetics of reversible photodegradation

The correlated chromophore domain model (CCDM) describes the observed temperature and concentration dependence of decay and recovery as probed with ASE and transmittance image microscopy (TIM), which monitors the change in transmitted light, in DO11/PMMA with an ensemble average of single-exponential-like functions [50, 53, 55] as summarized in Chapter 1. However, the recovery process observed with linear absorption spectroscopy measurements for 1AAQ/PMMA, DO11/PMMA and DO11/PS described in Chapter 4 and 5 and Appendix A exhibits stretched exponential behavior. The CCDM predicts a lower decay rate at higher dye concentration and is in agreement with the concentration dependent decay rate as measured with ASE in DO11/PMMA, which contradicts the PTCR hypothesis that predicts a higher decay rate at higher dye concentration, which attributes the cause of photodegradation in doped polymers to heat transferred from excited dopants to surrounding polymer chains. These contradictions will be discussed in this chapter.

8.1 Stretched exponential recovery

Recovery of the photodegraded doped polymers, observed in linear absorption spectroscopy measurements, is found to fit a stretched exponential function. Assuming that fresh dye molecules undergo photodegradation and form a reversibly- and an irreversibly-damaged species, the absorbance, A, of the dye-doped polymer sample as a function of time, t, is expressed as

$$A(t) = A_0 n_0(t) + A_r n_r(t) + A_{irr} n_{irr}(t), \tag{8.1}$$

where A_0, A_r, A_{irr} and n_0, n_r, n_{irr} are the absorbance and the fractions of fresh, reversibly-damaged and irreversibly-damaged dye species, respectively. The absorbance at the time the laser is turned off, t_0, is given by

$$A(t_0) = A_0 n_0(t_0) + A_r n_r(t_0) + A_{irr} n_{irr}(t_0). \tag{8.2}$$

Assuming that the reversibly-damaged species converts only to the pristine dye after the laser is turned off, the absorbance is given by

$$\begin{aligned} A(t > t_0) &= A_0 n_0(t_0) + A_0 n_r(t_0) \left\{ 1 - \exp\left[-\left(\frac{t - t_0}{\tau} \right)^{\eta} \right] \right\} \\ &= A_r n_r(t_0) \exp\left[-\left(\frac{t - t_0}{\tau} \right)^{\eta} \right] + A_{irr} n_{irr}(t_0), \end{aligned} \tag{8.3}$$

where τ is the characteristic recovery time constant and η is an exponent which characterizes the dispersion of the distribution of the recovery time constants.

The change in absorbance relative to the absorbance at time t_0 is

$$\begin{aligned} \Delta A_{t_0}(t > t_0) &\equiv A(t) - A(t_0) \\ &= (A_0 - A_r) n_r(t_0) \left\{ 1 - \exp\left[-\left(\frac{t - t_0}{\tau} \right)^{\eta} \right] \right\}, \end{aligned} \tag{8.4}$$

and that relative to the absorbance at time $t = 0$ is

$$\begin{aligned} \Delta A(t > t_0) &\equiv A(t) - A(0) \\ &= (A_{irr} - A_0) n_{irr}(t_0) - (A_0 - A_r) n_r(t_0) \cdot \\ &\quad \exp\left[-\left(\frac{t - t_0}{\tau} \right)^{\eta} \right]. \end{aligned} \tag{8.5}$$

Based on the analysis in Appendix A, the difference between A_r and A_{irr} is negligible from about 460 nm to 365 nm; therefore, the change in absorbance in this range after the laser is turned off is due only to pure recovery.

Since the recovery process observed in previous ASE studies is described by the CCDM which exhibits a single-exponential-like function [50, 53, 55], we study recovery using ASE as a probe to determine if the stretched exponential recovery behavior is an artifact of the probing method. Using the experimental method described in Section 3.3.2, we simultaneously monitor the ASE signal and the absorbance change in a DO11/PMMA thin film sample during photodegradation and recovery. Figure 8.1 shows the results. The ASE intensity, I_{ASE}, is a

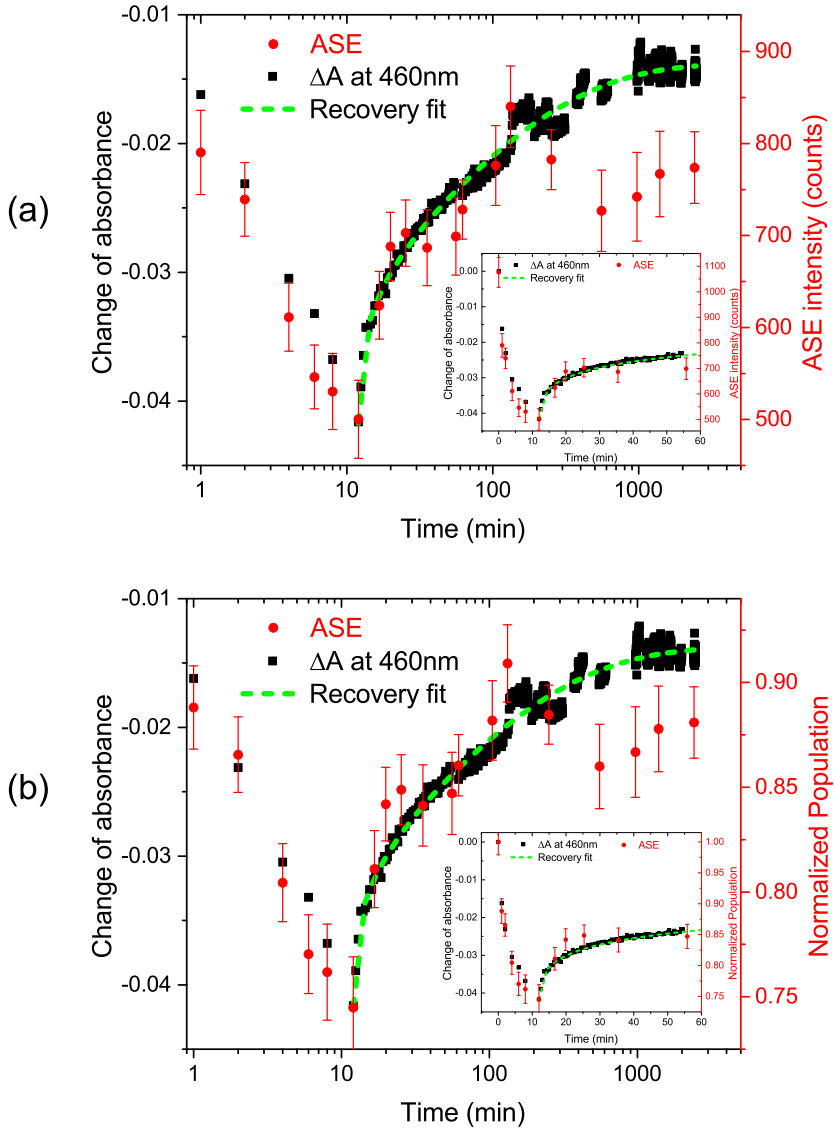

Figure 8.1: Photodegradation and recovery of a 9 g/L DO11/PMMA thin film sample. The experimental details are described in Section 3.3.2. (a) The black squares show the change in absorbance at 460 nm and the red points show the ASE intensity. The pump laser is on for the first 12 minutes to induce photodegradation. The green dashed line shows a fit using Equation 8.5 to the change in absorbance at 460 nm. The inset shows the first 60 minutes with a linear time scale. (b) Same as (a) but ASE intensity is converted to the population of DO11 molecules that generate ASE.

nonlinear function of the concentration of DO11, c, and the pump intensity in arbitrary unit, I_{pump}, according to the empirical relation

$$I_{ASE} = \frac{(c/c_0)^q}{1 + (I_0/I_{pump})^p}, \tag{8.6}$$

where fit parameters $c_0 = 5.0 \pm 0.6$ g/L, $p = 2.30 \pm 0.07$, $q = 2.6 \pm 0.5$ and I_0 has a value about 517 in arbitrary unit [53]. Thus, the population of pristine dye molecules, which is proportional to the dye concentration, is empirically determined to take the form

$$n_0 \propto (I_{ASE})^{1/2.6}, \tag{8.7}$$

where n_0 is the population of pristine DO11 molecules [53]. Note that Equation 8.6 and 8.7 were obtained from pristine bulk DO11/PMMA samples with thicknesses of 3 to 4 mm, so I_{ASE} is the integral of all layers in the sample that generate ASE. Both the ASE intensity and converted population of DO11 molecules that produce ASE according to Equation 8.7 follow the change in absorbance as shown in Figure 8.1. The last four data points of the ASE intensity fall below the trend, and are likely due to photodegradation of the sample caused by the pulsed laser used during probing. Since the overlap between the pulsed laser beam and the white light cross section is less than 7% of the white light area as illustrated in Figure 3.5, and the photodegradation caused by the pulsed laser may not necessarily overlap with the white light, so it is not surprising that this degradation is not observed in the absorbance data.

The ASE from DO11/PMMA was first observed to exhibit reversible photodegradation in earlier work in our group [9] and was later described by the CCDM, which assumes a single-exponential-like recovery function [50, 53]. Those ASE experiments were performed with DO11/PMMA bulk samples in the form of cylinders of about 1.3 cm diameter or disks with 3 to 4 mm thickness, and full recovery of the ASE signals was often observed. Though the CCDM seemed to fit the ASE recovery data, the fitting curve often recovers more slowly than the data at early times of recovery, as can be seen in Figure 8.2. Note that the ASE intensity in Figure 8.2 is converted to population of pristine DO11 according to Equation 8.7.

We fit the recovery data to the stretched exponential function given by

$$n_0(t) = 1 - n_r(t) \exp\left[-\left(\frac{t - t_0}{\tau}\right)^{\eta}\right], \tag{8.8}$$

and the results are plotted as blue lines in Figure 8.2. The stretched exponential fits clearly show better agreement with the experiment than the CCDM fits. Thus, the single-exponential-like recovery seems to fit because of the small number of data points acquired during recovery, a necessity to prevent photodegradation caused by the pulsed laser used to generate the ASE probe light.

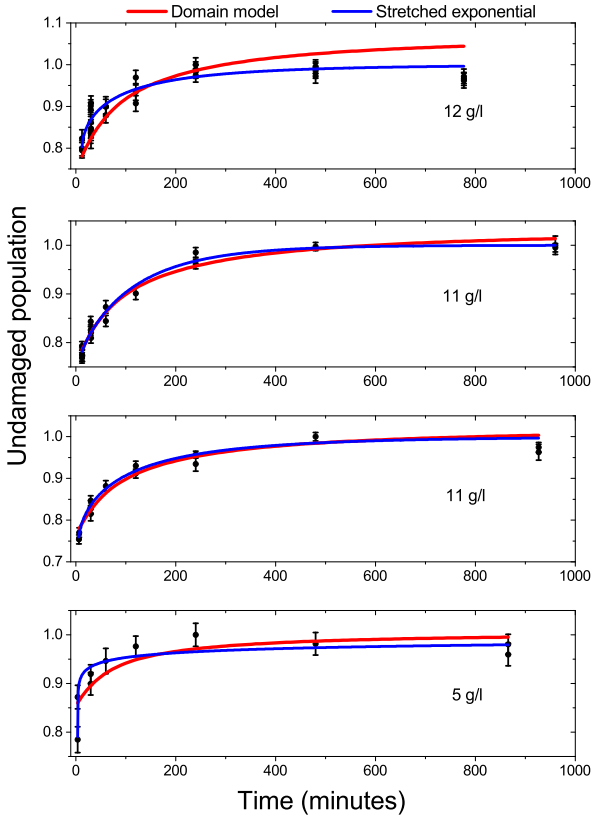

Figure 8.2: Recovery of DO11/PMMA with various concentrations fit using the CCDM (red lines) and Equation 8.8 (blue lines). Data and the CCDM fits are from the literature [53].

8.2 Photodegradation

The central difference between the predictions of the CCDM and the PTCR hypothesis is in the opposite predictions of the concentration dependence and temperature dependence of photodegradation and recovery. The decay rate obtained from a single exponential fit to the photodegradation caused by the pulsed laser of 532 nm wavelength in bulk DO11/PMMA samples (disks with thickness 3 to 4 mm) at various dye concentrations probed with ASE is found to be inversely proportional to the dye concentration [50, 53, 55]. This agrees with the CCDM and disagrees with the predictions of the PTCR hypothesis. A series of experiments were performed to control for possible artifacts.

Two thin film samples of DO11/PMMA with concentrations of 3 and 9 g/L were prepared with different thicknesses such that both samples have nearly

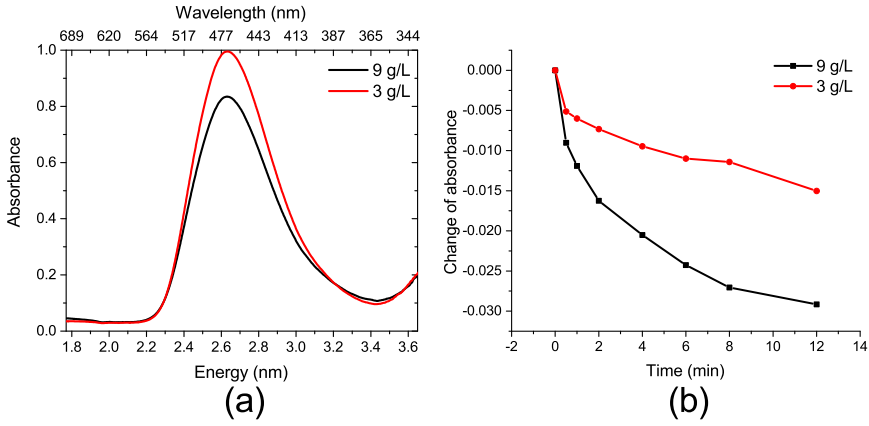

Figure 8.3: (a) Absorbance of DO11/PMMA thin film samples of 3 and 9 g/L concentrations. (b) The change of absorbance at 2.70 eV (460 nm) under irradiation with a cw laser of 532 nm wavelength at a peak intensity of 2.09 W/cm^2.

identical optical density, as shown in Figure 8.3(a), so that both samples have approximately the same number of dye molecules in the exposed volume. Note that the difference in shape of the two spectra, as can be assessed by the crossing at 2.29 and 3.21 eV, is likely an artifact due to the amount of white light collected by the optical fiber, which varies slightly each time a sample is placed in its holder due to changes in the thickness and angle of the sample and glass substrates and the resulting slight change in the portion of collected white light passing through the slit of the spectrometer. Both samples were irradiated with a cw laser of 532 nm wavelength at a peak intensity of 2.09 W/cm^2 using the linear absorption spectroscopy setup described in Section 3.3.2. The change in absorbance at 2.70 eV (460 nm) is plotted in Figure 8.3(b), which clearly shows that photodegradation is faster at higher dye concentration.

Using the ASE setup in Figure 3.2 and collecting the pulsed laser beam after passing the thin film sample to a photodetector, we obtained both the ASE intensity and the change in absorbance of the pump beam (532 nm) simultaneously for a DO11/PMMA thin film sample as shown in Figure 8.4. The ASE intensity is converted to the population of undamaged DO11 using Equation 8.7 and normalized. The time dependence of the ASE intensity shows a single-exponential-like decay as observed in previous ASE studies [9, 51, 53, 55]; but, the change in absorbance exhibits a non-exponential decay as observed with linear absorption spectroscopy using a cw laser as the pump laser.

The cause of this difference can be understood as follows. Excited dye molecules may return to their ground state by emitting photons or releasing energy through non-radiative relaxation, which may result in reversible or

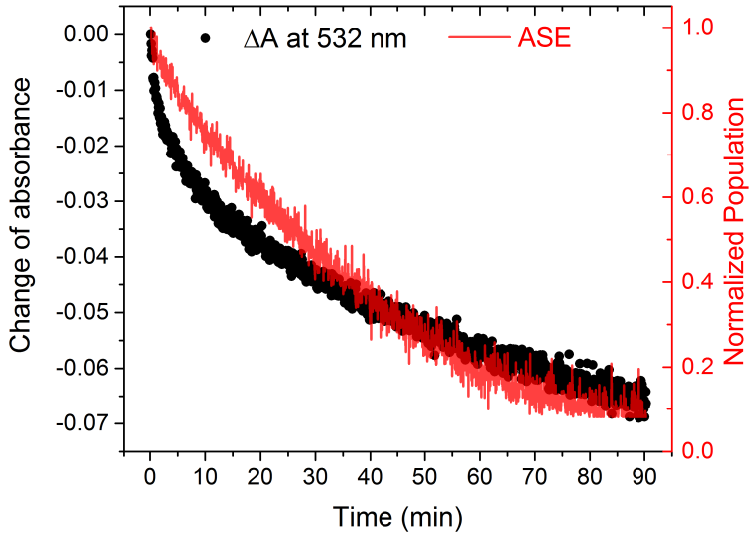

Figure 8.4: A 9 g/L DO11/PMMA thin film was irradiated with a pulsed laser with wavelength 532 nm at a peak intensity of 0.19 W/cm^2. The power of both the ASE light and the transmitted pulsed laser beam were recorded simultaneously. The transmitted pulsed laser beam was converted to a change in absorbance and the ASE intensity was converted into a normalized population of the undamaged DO11 molecules.

irreversible damage. According to Equation 8.6, the ASE intensity originating from the center of the focus will be brightest and drop off as a power law as a function of distance from the center of the focus. The ASE intensity also decreases as a power law of the pump intensity that reduces as an exponential function of the depth of the sample according to Lambert-Beer law. Thus, dye molecules in the most highly excited regions have the highest probability of being stimulated to emit photons, and thus are less likely to relax non-radiatively, which may suppress damage. In other words, ASE induces de-excitation, which decreases the time that molecules remain in the excited state, thus quenching non-radiative processes that lead to damage. A similar scenario can be found in second harmonic generation (SHG) microscopy, which does not require the population of excited-state dye molecules and thus the photostability of dye is improved [23, 24]. On the other hand, excited dye molecules in the darker regions will have longer lifetimes of their excited state, allowing for nonradiative transitions that result in reversible and irreversible photodegradation. This hypothesis will be further examined in future work. As such, the ASE probes only the population of (excited) dye molecules that emit stimulated photons along the narrow line of ASE. However, the transmitted pump beam experiences absorption from all dye molecules and damaged dye species. These two methods give different decay behavior because they probe different populations. Note

that the recovery of ASE intensity is a stretched exponential function of time, though still probing the portion of molecules that emit stimulated photons, independent of the pump laser (cw or pulsed) used to induce photodegradation as shown in Figure 8.1 and 8.2.

Another factor that may cause the difference in decay probed with ASE and linear absorption spectroscopy is the change of the environment of DO11 during decay. Since reversibly- and irreversibly-damaged dye species and thermally-degraded polymers are forming during decay, the fresh DO11 molecules experience different environments which may affect the efficiency of ASE. For example, there is no ASE signal observed in DO11/PS of the same dye concentration under the same pump condition as does in DO11/PMMA. In other words, Equation 8.6 and 8.7 are accurate for pristine DO11/PMMA, but it may not hold as sample decays. This may be difficult to verify since it requires known amount of each damaged species in the sample to determine the relation between the ASE intensity and the pump intensity. Nonetheless, it may not be a large effect in the early times of the decay as long as the amount of damaged products is still small along the narrow line of ASE.

To summarize, the photodegradation rate in DO11/PMMA is reduced when stimulated emission takes place. According to Equation 8.6, for fixed pump intensity, the ASE intensity increases as a nonlinear function of the DO11 concentration. As a result, the decay rate decreases as dye concentration increases when ASE is continuously generated during decay [50, 53]. This explanation does not require the CCDM to be invoked, which attributes the decreasing decay rate with increasing average domain size as the concentration increases [50, 53]. Thus, the difference in the concentration dependence of photodegradation of DO11/PMMA observed in the literature [50, 53] and Figure 8.3 is reconciled. Consequently, the conclusion obtained from the decay process accompanied with ASE should not be applied in the decay process without ASE taking place.

In TIM experiments, photodegradation of a dye-doped polymer sample is typically induced by a cw pump laser, and thus is not accompanied with ASE [50, 52]. TIM measurements use a wide range of pump intensity and typically a high average pump intensity (e.g. a peak intensity at 120 W/cm^2 [60]) due to low signal-to-noise ratio, which can cause a great amount of heat. In contrast, the pulsed laser used in ASE experiments has an average pump intensity of about 0.2 W/cm^2 [53], inducing less heating and therefore not exciting damage mechanisms that may come into play at higher average intensity and affect the decay and recovery kinetics (e.g. different degraded products might react with reversibly-damaged dye species). The CCDM, which was developed from studies in photodegradation and recovery accompanied with ASE [53], was later modified by introducing an irreversible photodegradation process based on the observation in TIM experiments [16, 57, 60]. The modified CCDM treats the reversible photodegradation with and without the accompany of ASE

using the same set of rate equations [16, 57, 60], which disregards the change in nonradiative decay pathways of the excited dye molecules. The modified CCDM also treats the reversible photodegradation observed under all pump intensities with the same set of rate equations [16, 57, 60], which implies the assumption of all observations obeying the same kinetic model. The calculated absorption cross section of the reversibly-damaged dye species, which is a fit parameter used in the modified CCDM for fitting the decay and recovery data obtained by TIM measurements, is close to that of pristine DO11 [60], which differs substantially from the conclusion in Chapter 6 and calculated results in Appendix A. The disagreement between TIM measurements and the current work will be discussed in Appendix E.

8.3 Kinetics of the recovery process

We further investigate the temperature dependence of reversible photodegradation in DO11/PMMA using linear absorption spectroscopy with a 532 nm

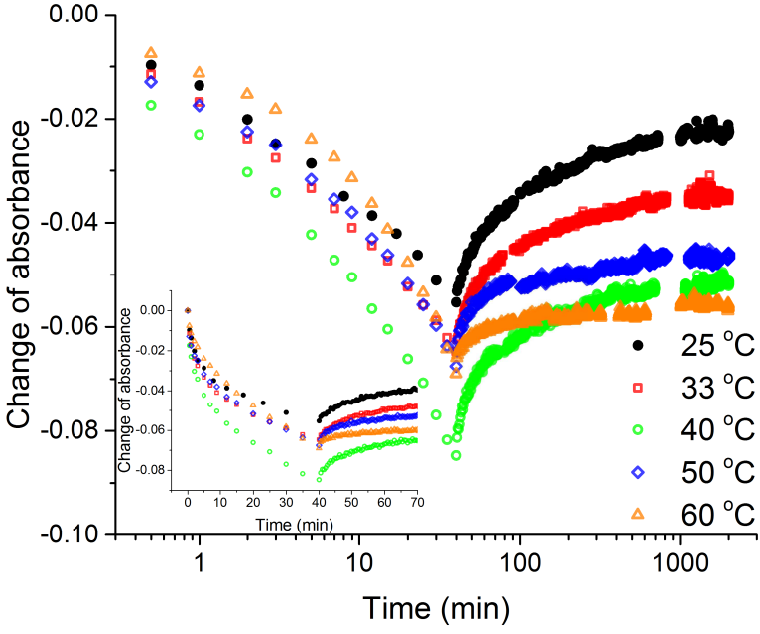

Figure 8.5: Changing absorbance at 460 nm relative to pristine DO11/PMMA thin film samples with concentration of 9 g/L at various temperatures. All samples were irradiated with a 532 nm wavelength cw laser of 2.09 W/cm^2 peak intensity for 40 minutes, then kept in the dark during recovery. The inset is the first 70 minutes with a linear time scale.

wavelength cw laser of 2.09 W/cm^2 peak intensity. Figure 8.5 shows a plot of the change in absorbance relative to each pristine sample at various temperature. The thickness of all samples used for this data set is estimated to be 27.1±0.6 μm except for the sample used in the 40 °C experiment, which has a thickness of 30.3 μm. The estimation method for the sample thickness is described in Appendix C.

8.3.1 The decay process

Figure 8.5 suggests that the decay rate does not increase monotonically with temperature, even if we disregard the data at 40 °C since it has about 10% deviation in thickness. Figure 8.6 shows photodegradation measurements of DO11/PMMA at various temperatures for a longer period of time. The thickness of all samples used for this data set is estimated to be 26.9±0.6 μm, except for the one used in the 25 °C experiment, which is 25.8 μm thick. Clearly the decay rate at early times, as seen in the inset, increases as temperature increases from

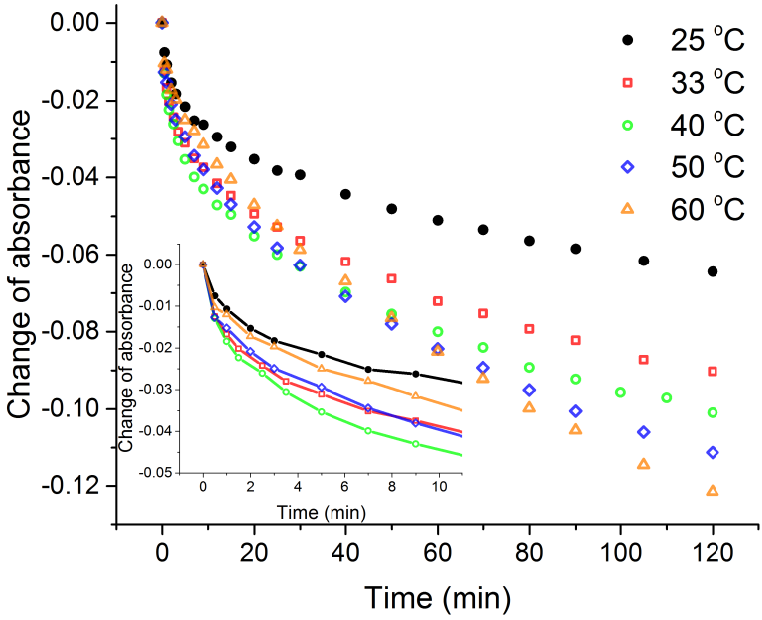

Figure 8.6: Change in absorbance at 460 nm relative to a pristine DO11/PMMA thin film samples of 9 g/L concentration at various temperatures. All samples were irradiated with a cw laser of 532 nm wavelength with 2.09 W/cm^2 peak intensity for 120 minutes. The inset shows the change in absorbance during the first 10 minutes of irradiation.

25 to 40 °C, but decreases as the temperature is increased to 50 °C and 60 °C. However, the decay rate monotonically increases with temperature at longer irradiation times.

The reversible decay rate of DO11/PMMA was previously assumed to be inversely proportional to the domain size, N, and is given by $\alpha I_{pump}/N$. As temperature increases, the CCDM predicts that the domains become smaller, so the decay rate increases with temperature [50, 53]. The CCDM was later modified to include an irreversible decay process that was first observed in the TIM experiment [16, 57, 60]. The irreversible decay rate was assumed to be of the form, $\varepsilon I_{pump} N$, where ε is the irreversible decay parameter [16, 57]. In this model, the irreversible decay rate decreases as the temperature increases due to the reduced domain size. A fit of the data to the modified CCDM finds that the reversible decay parameter α is about 2000 times larger than ε [57]. The average domain size of DO11/PMMA with concentration 9 g/L can be calculated according to the literature [55] and is about 32 dye molecules. Thus, the average reversible decay rate is about 2 times of the average irreversible decay rate for a 9 g/L DO11/PMMA sample. The reversible and irreversible decay rates are approximately the same when the concentration of DO11 is about 13 g/L. Additionally, the recovery rate $\beta' N$, where β' is the recovery parameter, decreases as temperature increases. Thus, photodegradation is dominated by the reversible decay in both CCDM and modified CCDM with the concentration of DO11 used in this investigation and previous studies (with the highest concentration of DO11 at 12 g/L) in the kinetics of reversible photodegradation in our group [16, 50, 51, 53, 55–57, 60]. This implies that the decay rate should increase monotonically with temperature, which is contradicted by the observation in Figure 8.6.

In the PTCR hypothesis, thermal energy accelerates all chemical reactions including reversible and irreversible decay and recovery. The non-monotonic temperature dependence of the absorbance change during the early stage of the decay process can be understood as a result of the competition between the recovery process and both decay processes. Long-time decay results in more irreversibly-damaged species and less reversibly-damaged species; therefore the recovery process can no longer compete with the decay processes and the decay rate increases as temperature increases. Due to the complexity of the non-exponential behavior of the time-dependence of the decay and recovery processes, the kinetics of the decay process will require additional studies that go beyond the scope of this dissertation. We will thus focus on the kinetics of the recovery process.

8.3.2 The recovery process

The microscopic explanation for the stretched exponential response functions observed in supercooled liquids has remained an unsolved puzzle for more than

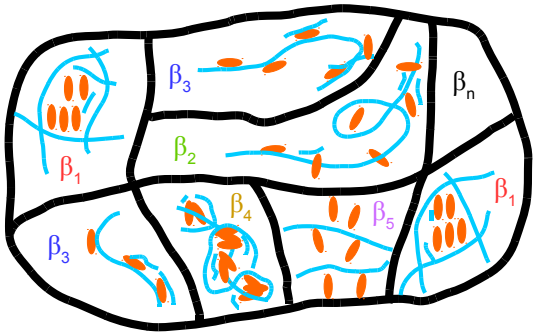

Figure 8.7: Illustration of the spatial heterogeneity of a DO11/PMMA sample after irradiation. The orange ellipses could be fresh DO11, reversibly-damaged or irreversibly-damaged dye species, and the light blue lines could be pristine polymer chains or thermally-degraded polymer segments. The reversibly-damaged dye molecules recover at different rates β_1, β_2, $\beta_3 \cdots \beta_n$ depending on the local environment.

a century [149, 150]. The stretched exponential kinetics was demonstrated by dynamic hole burning using nuclear magnetic resonance, photobleaching (orientational hole burning) and dielectric and magnetic (non-resonance) hole-burning; and by time-dependent emission energies (solvation dynamics), temperature dependence for molecular translational and rotational time scales, and photochromic probe molecules [150–152]. A reversible chemical reaction of a photochromic molecule doped in a polymer matrix exhibits the stretched exponential kinetics which was described by an energy barrier model [153]. We apply this model to analyze the recovery process observed in Figure 8.5 in the follows.

Due to the spatial heterogeneity of the polymer host, dopant dye molecules experience a continuous distribution of environments that affect material parameters such as decay and recovery rates, as illustrated in Figure 8.7 for the recovery process. Assuming that the reversibly-damaged species must overcome an energy barrier, E_b, to return to the pristine dye molecule, the recovery rate β is given by

$$\beta\left(E_r\right) = \nu_0 \exp\left[-\left(E_b - E_r\right)/k_B T\right], \tag{8.9}$$

where ν_0 is the frequency factor, which is related to the frequency of molecular collisions and the probability of proper molecular orientations for the reaction, E_r is the ground state energy of the reversibly-damaged dye species, k_B is Boltzmann constant and T is the absolute temperature. The activation energy is then given by $E_b - E_r$.

Assuming that the maximum of the energy barrier and the ground state energy of the reversibly-damaged species fluctuate statistically due to the spatial

heterogeneous environment with a Gaussian distribution characterized by its width ω. For the mathematical convenience, the fluctuation of the activation energy can be merely attributed to the Gaussian distribution of the ground state energy

$$G\left(E_r\right) = \frac{1}{\sqrt{2\pi}\omega} \exp\left[-\frac{\left(E_r - \langle E_r \rangle\right)^2}{2\omega^2}\right]. \tag{8.10}$$

The average ground state energy is assumed to be $\langle E_r \rangle = 0$ by appropriate choice of an energy offset. The change in absorbance with respect to the one taken at the time the pump laser turned off, t_0, can be expressed as

$$\begin{aligned} \Delta A_{t_0}\left(t > t_0\right) &= A\left(t\right) - A\left(t_0\right) \\ &= \left(A_0 - A_r\right) n_r\left(t_0\right) \cdot \\ &\quad \left\{1 - \int_{-\infty}^{\infty} G\left(E_r\right) \exp\left[-\beta\left(E_r\right)\left(t - t_0\right)\right] dE_r\right\}, \end{aligned} \tag{8.11}$$

where n_r is the fraction of reversibly-damaged dye species and A_r and A_0 are respectively the absorbance of the reversibly-damaged dye species and the fresh dye defined in Equation 8.1.

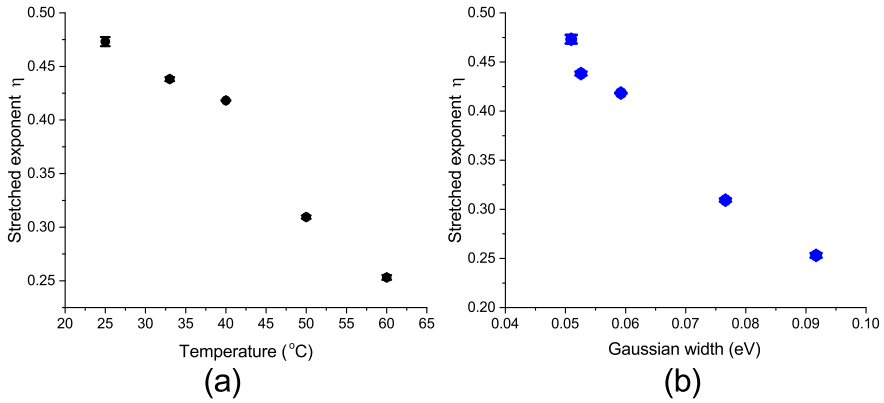

Figure 8.8: Fitted stretched exponent as a function of (a) temperature and (b) Gaussian width.

Fitting the time-dependence of the recovery data between 459 and 461 nm obtained subsequent to 40 minutes of irradiation at various temperatures to Equations 8.4 and 8.11, we obtain the fitting parameters η and $1/\tau$ from Equation 8.4 and ω and the activation energy from Equation 8.11, as shown in Figures 8.8 and 8.9. The recovery rate, $\beta\left(E_r = 0\right)$, is calculated from the fitting parameters and plotted in Figure 8.9(b). The frequency factor $\nu_0 = 1.14 \times 10^{14}$

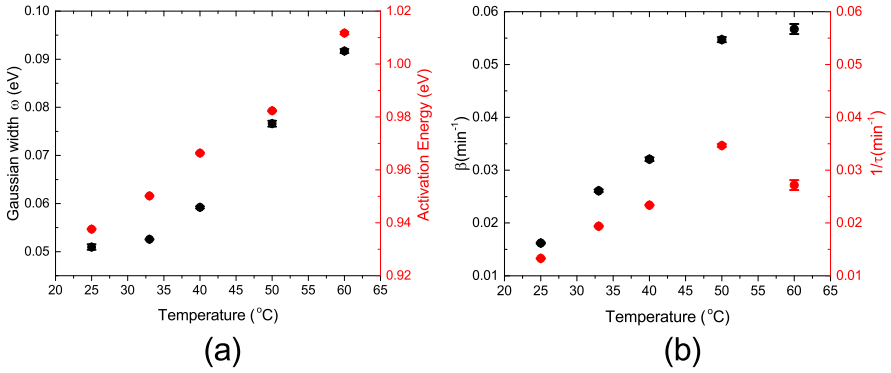

Figure 8.9: (a) Gaussian width ω and the activation energy in Equation 8.11. (b) Recovery rate $\beta\,(E_r = 0)$ calculated using Equation 8.9 and inverse recovery time constant $1/\tau$ as defined by Equation 8.4.

min^{-1} was found to fit all recovery data for all temperatures, though it may vary slightly with temperature, as reported in the literature [153].

The stretched exponent η is typically found in the range of $0 < \eta \leq 1$ and represents the breadth of the distribution of the underlying time constants, τ. When $\eta = 1$, the stretched exponential function is a single exponential function with a single time constant. As η decreases, the stretched exponential function includes a broader distribution of single exponential functions of various time constants [154]. Relaxation for supercooled liquid is characterized by $\eta\,(T) \to 1$ at high temperature and decreases monotonically to $\eta\,(T \to T_g) < 1$ as the temperature decreases to the glass transition temperature, T_g, then stabilizes at $\eta\,(T_g)$ when the temperature is below T_g, since the solution at high temperature is a homogeneous liquid solution and the structural variation increases as the temperature drops and reaching a constant after T_g [149, 155].

While most studies focus on the relaxation of glassy solids at, near, or above T_g, the interaction between dopant and host in a guest-host system may affect the relaxation of the dopant and host. The observation in Figure 8.8(a) indicates the distribution of the recovery time constants spreads when the temperature increases, which is in agreement with the reversible chemical reaction observed in a photochromic molecule-doped polymer [153], though the reason was not explained. There are many possible sources of inhomogeneity that could lead to an increase in the breadth of the distribution of sites. For example, the distribution of void sizes broadens as temperature increases, so mechanisms of healing that are affected by molecule/polymer interactions would be similarly broadened. If domains of molecules, as illustrated in Figure 8.7, are involved, similar broadening would be expected to be observed. Note that domains of molecules in a polymer matrix are independent from the CCDM which

is a kinetic model that relates the concept of domains with the reversible photodegradation process. In addition, larger amount of the irreversibly-damaged species produced at higher temperature may also contribute to the inhomogeneity of the environment. Figures 8.8(a) and 8.9(a) show that η decreases and the Gaussian width ω increases as the temperature rises, and thus η decreases as ω increases as seen in Figure 8.8(b). These observations imply that the inhomogeneity of the dye-doped polymer matrix increases as the temperature rises in the temperature range in this study. However, the the activation energy increases with temperature as shown in Figure 8.9(a) is inconsistent with an energy barrier process that is governed by a characteristic energy, which should remain constant. Although the recovery rate β and the inverse recovery time constant $1/\tau$ are observed to increase with temperature shown in Figure 8.9(b), as expected for an energy barrier process, their behaviors diverge further as the temperature increases. While the energy barrier model successfully describes the reversible chemical reaction observed in the literature [153], it comes up short in the analysis of reversible photodegradation of DO11/PMMA.

The temperature dependence in both η and $1/\tau$ comes from a phenomenological expression, given by Equation 8.4, and the energy barrier model is applied to modeling the behavior of η and $1/\tau$. Hence, the increase of heterogeneity of the recovery process and the increase of the recovery rate $(1/\tau)$ with temperature shown in Figure 8.8(a) and 8.9(b) are measured properties of the material independent of the kinetic models that are later applied. However, the temperature dependence of $1/\tau$ disagrees with the CCDM, which correctly predicts that the recovery rate decreases with increasing temperature as observed from fitting the recovery of ASE intensity in bulk DO11/PMMA samples measured at temperatures between -10 °C and 60 °C to a single exponential function [50, 55]. To prevent photodegradation caused by the pulsed laser used in ASE probing, the number of data points taken is limited, making the fit to a single exponential function appear good. Furthermore, the single-exponential-like CCDM is heavily weighted by the long-time behavior of the recovery process as shown in Figure 8.2. The assumption of a single exponential recovery and the limited number of data points might mask the stretched exponential form and yield parameters that contradict those determined with absorbance measurements.

Figure 8.10 shows a plot of a stretched exponential function used to model the recovery process of a system prepared with an initial population of only reversibly-damaged dye species that fully recovers. The stretched exponential recovery function at $t > \tau$ agrees with the CCDM, i.e. the recovery rate increases as temperature decreases (corresponding to increasing η). However, at $t < \tau$, the recovery rate increases with temperature which disagrees with the CCDM. Note that the magnitude of recovery in the region $t > \tau$ is only $1/e$ of the full magnitude of recovery.

The failure of the energy barrier height to remain constant may be due to

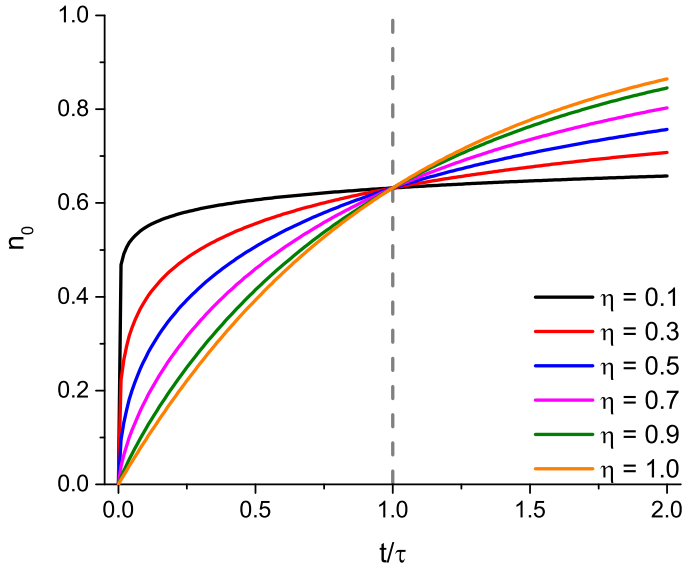

Figure 8.10: Stretched exponential recovery as a function of time for several stretched exponents, η. n_0 is the fraction of dye that is undamaged.

the assumption of a Gaussian distribution of the ground state energy. The divergence between β and $1/\tau$ in Figure 8.9(b) suggests that the the distribution of β obtained from the energy barrier model does not agree with the distribution of recovery rates when re-constructed from the stretched exponential function, which is known to be difficult [154]. Using Equation 8.11, the density of states of the reversibly-damaged dye species can be expressed as

$$\rho_r\left(t, E_b\right) \propto \left(A_0 - A_r\right) n_r\left(t_0\right) G\left(E_r\right) \exp\left[-\beta\left(E_r\right)\left(t - t_0\right)\right]. \tag{8.12}$$

By analyzing the absorbance data at 460 nm, the wavelength that further decay of the reversibly-damaged species is negligible as described in Appendix A, the calculated $\rho_r\left(t, E_b\right)$ corresponds to the portion of reversibly-damaged species that recovers but not decays into irreversibly-damaged species.

Figure 8.11(a) shows $\rho_r\left(t_0, E_b\right)$ after 40 minutes of irradiation at different temperatures and after 120 minutes of irradiation at 25 °C. The population of reversibly-damaged dye species decreases as temperature is increased except for the sample used at 40 °C, which is thicker than the others. Figure 8.11(b) shows normalized $\rho_r\left(t_0, E_b\right)$. At 25 °C, $\rho_r\left(t_0, E_b\right)$ after 120 minutes of irradiation, the energy barrier and its width are close to the one obtained at 33 °C after 40 minutes of irradiation. Figure 8.12 shows the evolution of $\rho_r\left(t, E_b\right)$ during recovery after 40 minutes of irradiation at 25 °C and 60 °C. Notice that the population with lower activation energy recovers sooner than the ones with higher activation energy, and the peak of the remaining population of the

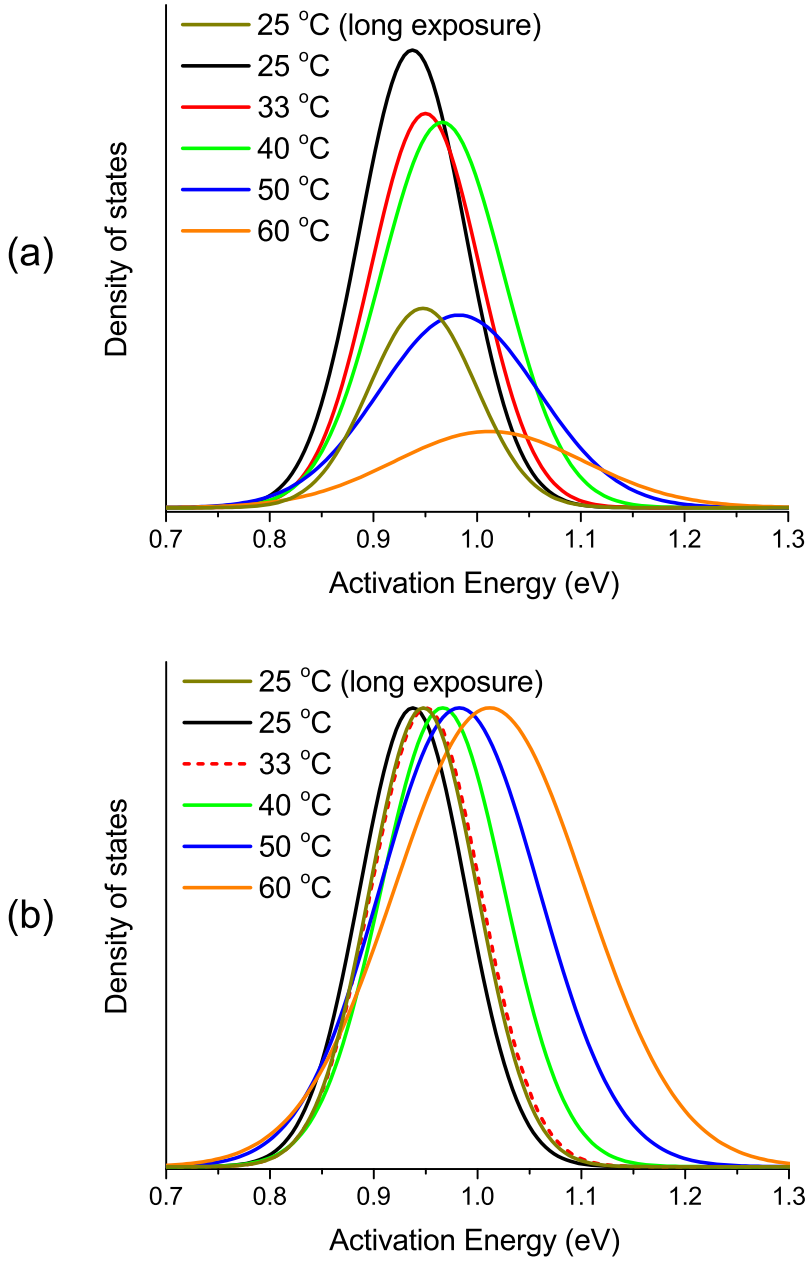

Figure 8.11: (a) Density of states of the reversibly-damaged dye species $\rho_r\,(t_0, E_b)$ at various temperature after 40 minutes of irradiation. (b) Normalized $\rho_r\,(t_0, E_b)$. The "long exposure" curve is obtained from the recovery data after 120 minutes of irradiation at 25 °C.

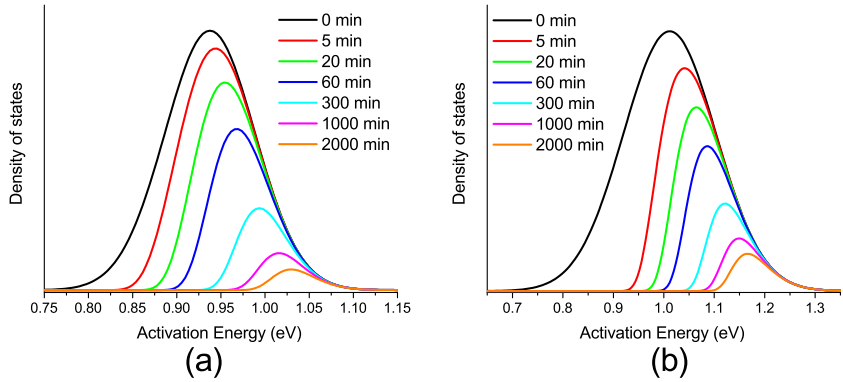

Figure 8.12: Density of states of the reversibly-damaged dye species evolving over time subsequent to 40 minutes of irradiation to damage the sample at (a) 25 °C and (b) 60 °C.

reversibly-damaged species shifts to higher activation energy. These observations suggest that the increasing activation energy with temperature is possibly a result of the loss of the reversibly-damaged dye species with lower activation energy when the sample is still exposed to the pump laser. Since the population with lower activation energy recovers quickly, the remaining reversibly-damaged dye species after the pump laser is turned off is populated predominantly in a local environment of higher activation energy, which causes β to deviate from $1/\tau$ as seen in Figure 8.9(b).

The correct density of states, rather than being a Gaussian distribution, may have a long tail at high activation energy. By inspecting Figure 8.11(a), we speculate that the population of the reversibly-damaged dye species at lower temperature is dominated by the population associated with lower activation energy and the contribution from the long tail at the high activation energy end may be negligible, so the Gaussian width is efficiently narrower when the data is forced to fit a Gaussian distribution. As temperature increases, the contribution from the long tail at high activation energy becomes more significant, so the Gaussian width increases when forced to fit to a Gaussian distribution. The observed stretched exponential recovery implies that a distribution of sites is contributing to the process so it is likely that stretched exponential behavior will be observed during photodegradation. The kinetics of reversible and irreversible photodegradation requires further study to resolve these issues.

Chapter 9

Conclusion

Previous studies in reversible photodegradation of DO11/PMMA using amplified spontaneous emission (ASE) and transmittance image microscopy (TIM) techniques led to the (modified) correlated chromophore domain model (CCDM), which describes the time dependence of reversible and irreversible photodegradation and recovery with an ensemble average of single-exponential-like functions using a distribution of domains [16, 50, 53, 57]. Using linear absorption spectroscopy as a probe, a stretched exponential time dependence is observed for the recovery process. Photodegradation may also involve a stretched exponential time dependence, but this hypothesis was not tested.

Orientational hole burning [51] and "normal" diffusion [52, 54] have been ruled out as possible mechanisms responsible for reversible photodegradation in earlier studies from our group, and both "normal" and "anomalous" diffusion are excluded as the responsible mechanisms for the observed stretched exponential recovery in this study.

In this dissertation, we proposed a series of photothermal-induced chemical reactions (PTCR) as the responsible mechanism for reversible photodegradation of 1-substituded aminoanthraquinones-doped polymers. In the PTCR hypothesis, the photodegradation of dye is caused by (photo)chemical reactions between fresh dye molecules and thermally-degraded polymers, and recovery is due to the metastable (photo)chemical reaction products returning back to fresh dye. It is also proposed that both reversible and irreversible damage to 1-substituded aminoanthraquinones occur in the carbonyl group adjacent to the amine group. The PTCR hypothesis is qualitatively verified by the agreement between calculated oscillator strength and the corresponding excitation energy of the pristine and possible damaged dye species using time-dependent density functional theory (TD-DFT), and experiments using linear absorption spectroscopy and Fourier transform infrared (FTIR) spectroscopy.

The PTCR hypothesis also suggests that reversible photodegradation of dye molecules may occur in dye dissolved in liquid monomer solutions, and the present studies have provided supportive evidence. In contrast, previous studies found that photodegradation of DO11 dissolved in dimethylformamide solution is fully irreversible [49], an observation that was used in the development of the CCDM, in which domains assist the recovery process [53].

Reversible photodegradation in DO11/PMMA probed simultaneously with ASE and linear absorption spectroscopy confirmed that the observed stretched exponential time dependence of the recovery process is the same one observed in previous ASE studies. Studies of the recovery of DO11/PMMA using ASE as a probe is found to fit the stretched exponential function better than previously fit to the CCDM [53].

Photodegradation of DO11/PMMA irradiated with a cw laser and probed with linear absorption spectroscopy is found to decay at a faster rate at higher dye concentration, which agrees with the PTCR hypothesis but contradicts previous observations when the sample is pumped with a pulsed laser and probed using ASE [50, 53]. By comparing the decay of the ASE intensity and absorption of the pulsed pump laser beam during photodegradation of DO11/PMMA and finding them to behave differently leads us to propose that the disagreement originates from the reduced degree of non-radiative relaxation when ASE dominates over the other pathways. Hence, the kinetic relation, i.e. rate equations, of photodegradation in the same material may vary depending on whether the irradiation is accompanied with ASE. This observation also indicates that the kinetic model developed from ASE experiments, the CCDM, is not necessarily applicable for situations where ASE is absent.

The PTCR hypothesis suggests an energy barrier mechanism for the kinetics of decay and recovery since chemical reactions are usually accelerated at elevated temperatures. In this scenario, the reversibly-damaged dye species must overcome an energy barrier to return to the ground state of the pristine dye. The decay rate in DO11/PMMA is a non-monotonic function of temperature at early stages of photodegradation, then the decay rate monotonically increases with temperature at long times. This is explained by the varying amounts of reversibly-damaged products at different stages of photodegradation and the competition between the decay processes (reversible and irreversible decay rates) and the recovery process (recovery rate) at various temperatures described by an energy barrier mechanism. The temperature dependence in the recovery time constant obtained from stretched exponential fits is also consistent with the energy barrier mechanism in the temperature between 25 °C and 60 °C studied in this work. These results disagree with the CCDM, which predicts slower recovery at higher temperature and is supported with a single exponential function fits to recovery measurements in DO11/PMMA probed with ASE between -10 °C and 60 °C [50, 53, 55]. The disagreement may originate from the limited number of data points collected to prevent photodegradation caused

by the pulsed laser used to generate the ASE probe light.

A simple energy barrier model [153] is applied to analyze the temperature dependent recovery of DO11/PMMA by assuming a Gaussian distribution of activation energies. The final results do not fully agree with the energy barrier model, and a possible cause is that the energy barrier may not be a Gaussian distribution. Nonetheless, the failure of this analysis does not eliminate the energy barrier model, which is supported by the phenomenological results (stretched exponential fits) of the temperature dependent recovery time constant.

Outlook

Photostability of dyes, polymers and doped polymer materials is an important criteria for applications that require light exposure as discussed in Chapter 1. Although the proposed PTCR hypothesis is qualitatively verified by this study, the reversibly- and irreversibly-damaged species are not determined. In addition, the principle of PTCR may be generalized to other doped polymer materials exhibiting reversible photodegradation. According to the PTCR hypothesis, the key to prevent photodegradation of dopants in doped polymers is to eliminate the possibility of (photo)chemical reactions between dopants and thermally-degraded polymers taking place, in addition to the effects of oxygen, moisture etc. Thus, a more robust doped polymer material can be made by reducing the probability of non-radiative relaxation from dopants, increasing the thermal degradation temperature of the polymer host, increasing the heat dissipation rate of polymer chains, selecting proper dopants that do not react with thermally degraded polymers under the operating condition (if local thermal degradation of polymer chains is not a concern) etc. An interesting perspective is that the probability of non-radiative relaxation from dopants may be reduced by providing the excited dopants other relaxation pathways such as stimulated emission, which provides a way to simultaneously achieve high optical output and photo-stable doped polymers.

The energy barrier picture is qualitatively supported by experimental results, but a simple model has failed to describe the observed behavior during recovery of photodegraded DO11/PMMA. The distribution of recovery rates (possibly reversible and irreversible decay rates as well), which are determined by the distribution of the activation energy, should originate from the spatial heterogeneity of the dye-doped polymer. Thus, the role of the spatial heterogeneity of doped polymers is to be explored. Does the spatial heterogeneity affect the nonradiative decay of an excited dopant? Does the energy transfer or dissipation in the material depend on the spatial heterogeneity? For example, some configurations of dopants and the host polymer may result in fast dissipation of photon energy absorbed by dopants and thus reduce the decay rate, while other configurations may result in preserving the energy locally

and thus increase the decay rate. Answers to these questions help advancing the understanding in the science of spatial heterogeneous materials and may provide new perspectives and avenues to applications. To reconstruct the rate distribution from the experimental results is known to be a difficult task [154]. Studying the distribution and structures of dye molecules in polymer hosts may provide a better insight for understanding the microscopic origin of rate distribution, a problem that is more than a century old.

Appendix A

Absorbance of photodegraded dye species

The absorption band of 1AAQ in the visible regime is known to originate from intramolecular charge transfer (ICT) between the amine group and carbonyl groups [63]. From the results of TD-DFT calculations in Chapter 6, the oscillator strength and absorption peak position of degraded DO11 only agree with the experimental results when the ICT between the amine group and the neighboring carbonyl group becomes forbidden by breaking the double bond of the carbonyl group adjacent to the amine group, leaving both carbon and oxygen atoms singly bound to fragments of decomposed polymer. TD-DFT calculations also suggest that the absorption spectrum in the visible band is not sensitive to what is singly bound to the carbon and oxygen atoms upon photodegradation as illustrated in the PTCR hypothesis in Chapter 2, which implies that there could be multiple reversibly- and irreversibly-damaged products exhibiting similar visible absorption spectra. In this appendix, we qualitatively verify the absorbance of reversibly- and irreversibly-photodegraded dye species from experimental results by assuming that there is effectively one reversibly-damaged species and one irreversibly-damaged species, and further discuss the conversion between these three species (including the pristine dye) during decay and recovery. It is also assumed that the damage to the polymer does not contribute to the probed UV-Vis absorption spectrum, i.e. it excludes the possibility of any absorption or light scattering due to scattering centers generated from damaged polymer. The calculated absorbance can be regarded as the results of the dominant damage products or the average of several products with similar absorbance.

The absorbance A measured during decay and recovery at time t can be expressed as

$$A(t) = n_0(t)A_0 + n_r(t)A_r + n_{irr}(t)A_{irr}, \tag{A.1}$$

where n_0, n_r, n_{irr}, and A_0, A_r, A_{irr} are the fraction and the absorbance of fresh, reversibly-damaged and irreversibly-damaged dye species, respectively. Since we assume that dye molecules only convert between three species, we can obtain A_0 and A_{irr} experimentally by taking the absorption spectra of a fresh sample and a sample that has been exposed to the pump laser for a long enough time such that the absorption spectrum no longer changes. The maximum fraction of irreversibly-damaged dye molecules $n_{irr}(t \to \infty) \equiv n_{irr}^{\infty}$ can be determined in a recovery experiment by the absorbance at the time that recovery approaches completion,

$$A(t \to \infty) = n_0(t \to \infty)A_0 + n_{irr}(t \to \infty)A_{irr} = A_0 + n_{irr}^{\infty}(A_{irr} - A_0), \quad \text{(A.2)}$$

where we have used the assumption that the presence of only three species yields $n_0(t) + n_r(t) + n_{irr}(t) = 1$ and $n_r(t \to \infty) = 0$. Thus, n_{irr}^{∞}, A_0, and A_{irr} are obtained experimentally. The absorbance of the reversibly-damaged species A_r, however, depends on how the three species convert into each other and can be calculated by rewriting Equation A.1 at the time, t_0, that the laser is turned off,

$$A_r = \frac{A(t_0) - n_0(t_0)A_0 - n_{irr}(t_0)A_{irr}}{n_r(t_0)}. \quad \text{(A.3)}$$

If we further assume that n_{irr} is a constant after the pump laser is turned off, i.e. $n_{irr}(t \geq t_0) = n_{irr}^{\infty}$, which implies that the reversibly-damaged species only recovers back to the fresh dye but does not decay further into the irreversibly-damaged species as illustrated in Figure A.1(a). With this assumption, $n_r\,(t_0)$ and $n_{irr}\,(t_0)$ are constants proportional to the change in absorbance when

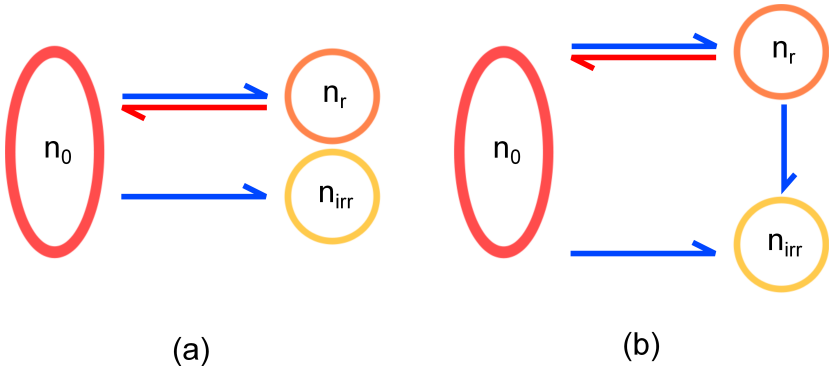

Figure A.1: n_0, n_r and n_{irr} are the fraction of fresh, reversibly-damaged and irreversibly-damaged dye species, respectively. (a) The fresh dye may photodegrade to both damaged species and the reversibly-damaged species only recovers to the fresh dye but does not decay further to the irreversibly-damaged species. (b) The same as (a) but the reversibly-damaged species may recover to the fresh dye or decay to the irreversibly-damaged species.

the recovery approaches completion as n_r and n_{irr} shown in Figure A.2, thus A_r can be calculated from Equation A.3. This assumption can be relaxed to $n_{irr}(t \geq t_0) \leq n_{irr}^{\infty}$, in which case the reversibly-damaged species may either decay to the irreversibly-damaged species or recover to the fresh dye as illustrated in Figure A.1(b), and $n_r\,(t_0)$ and $n_{irr}\,(t_0)$ can be numerically adjusted to generate A_r using Equation A.3. Notice that the total fraction of damaged molecules after the laser is turned off at time t_0, $n_r(t \geq t_0) + n_{irr}(t \geq t_0)$, in the later case is not necessarily the same as in the former case since $n_r\,(t_0)$ can convert into n_0 and n_r.

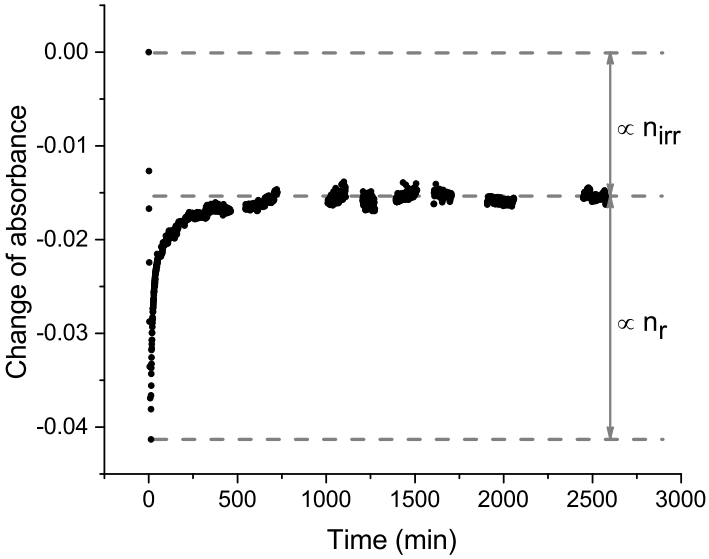

Figure A.2: Change in absorbance of DO11/PMMA during recovery at 2.57 eV (482 nm). The sample was irradiated with a 532 nm cw laser for 12 minutes then kept in the dark.

In practice, A_r and A_{irr} were determined from two individual experiments, i.e. we used two samples or one sample but at two different spots on the sample, since A_r requires the damaged sample to recover and A_{irr} requires the sample to be irreversibly damaged. Two white light probe sources were used at different periods of data collection: all A_{irr}'s were obtained using the Ocean Optics PX2 pulsed lamp, and all A_r's were obtained using the Ocean Optics LS1 lamp. These factors increase the experimental uncertainty in addition to the noise from a single white light source and the spectrometer. However, we can still determine approximately the absorption spectra of the damaged species.

A.1 DO11/PMMA

A_{irr} of a 9 g/L DO11/PMMA sample was approximated by the absorption spectrum obtained after 59 minutes of irradiation using a 532 nm cw laser with peak intensity of 37.56 W/cm^2 as shown in FigureA.3(a). The changing peaks of absorbance at 2.57 eV (482 nm) and 3.09 eV (401 nm) during 59 minutes of irradiation are shown in Figure A.3(b).

In the recovery experiment, a sample with the same concentration was irradiated using the same laser with a peak intensity 2.09 W/cm^2 for 12 minutes then kept in the dark. The change of absorbance at 2.57 eV (482 nm) is shown in Figure A.2. The absorption spectra between 2520 and 2550 minutes were averaged as an approximation of $A(t \to \infty)$ in Equation A.2, and $A(t \to \infty)$ between 477 nm and 487 nm were used to determine the averaged ratio of n_1/n_2. Using Equation A.2 and Figure A.3(a), n_{irr} can be determined and also averaged between 477 nm and 487 nm. Thus, A_r is determined using Equation A.3 with the assumption that $n_{irr}(t \geq t_0)$ is constant, as $A_r^{(1)}$ shows in Figure A.4(a). A large deviation between $A_r^{(1)}$ and A_{irr} near the UV region is observed indicating that absorbance between reversibly- and irreversibly-damaged dye species are more distinguishable there than in the visible region. However, this statement is based on the assumption that there is (effectively) only one reversibly- and one irreversibly-damaged dye species generated during photodegradation and the damaged PMMA does not contribute to the absorption spectrum.

In the visible region, $A_r^{(1)}$ and A_{irr} are similar which is consistent with TD-DFT calculations. The difference between $A_r^{(1)}$ and A_{irr} shown in Figure A.4(b) indicates a peak at about 2.4 eV. The dip near 2.56 eV is a defect of the pulsed white light source used to determine A_{irr}. We further relax the assumption $n_{irr}(t \geq t_0) = n_{irr}^{\infty}$ (corresponding to Figure A.1(a)) to be $n_{irr}(t_0) \leq n_{irr}^{\infty}$ (corresponding to Figure A.1(b)) so as to allow the reversibly-damaged species to either decompose to irreversibly-damaged species or recover to fresh dye. We also assume that the total fraction of damaged molecules after time t_0, $n_r(t \geq t_0) + n_{irr}(t \geq t_0)$, is the same as previously calculated, which may not be true but used as a guess to study A_r. Two other values of $n_{irr}(t_0)$ have been chosen to calculate A_r, and we tabulate parameters n_0, n_r and n_{irr} at time t_0 in Table A.1 and add the calculated $A_r^{(2)}$ and $A_r^{(3)}$ in Figure A.4(a). $A_r^{(1)}$, $A_r^{(2)}$ and $A_r^{(3)}$ in the visible region only differ from A_{irr} in the low energy shoulder near 2.4 eV as expected since the reversibly-damaged species is allowed to decay into the irreversibly-damaged species.

Note that the difference between A_r and A_{irr} is much smaller than that between A_r and A_0 in visible region as shown in Figure A.4(b), therefore degradation of the reversibly-damaged dye species may be difficult to measure. Figure A.5 shows the change in absorbance with respect to the spectrum taken at the end of irradiation during recovery. The shoulder between 2.4 eV and 2.5

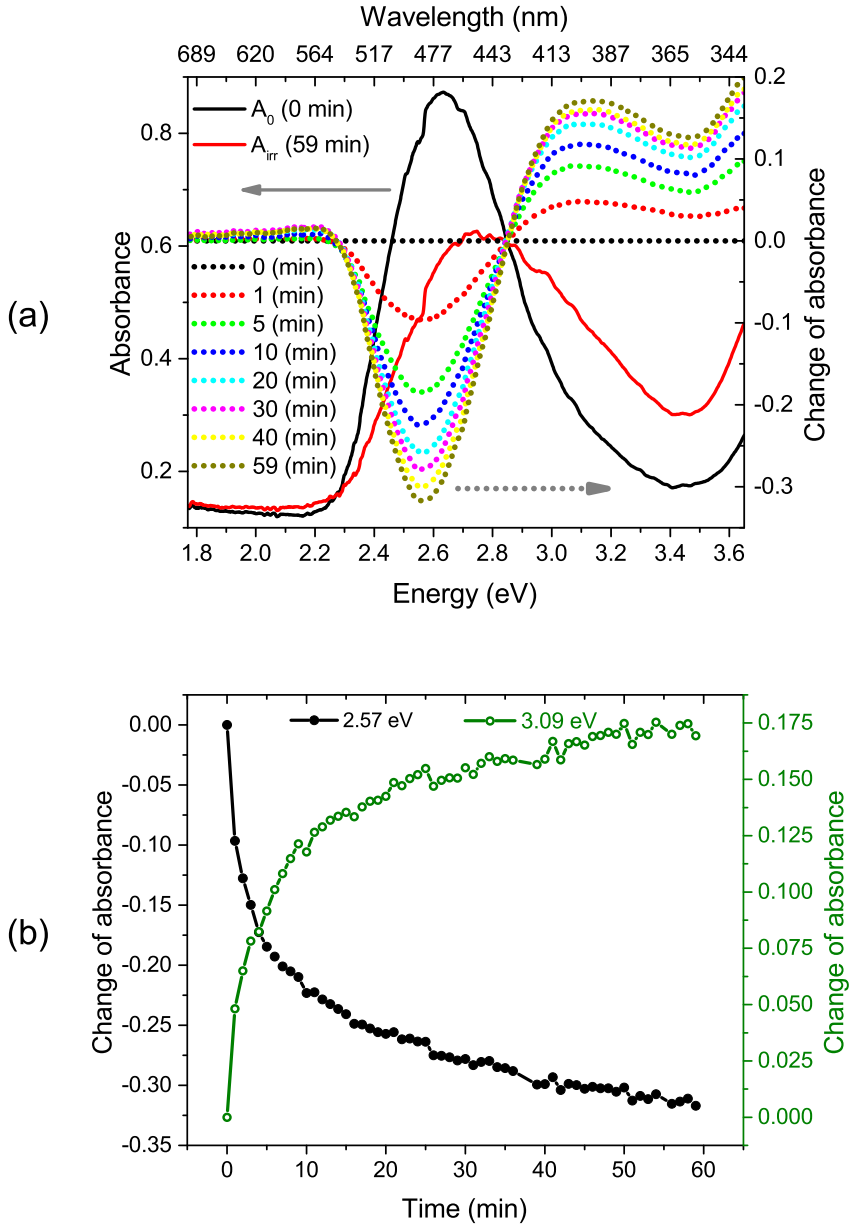

Figure A.3: (a) A_0 and A_{irr} (adjusted according to the relative thickness of both samples) of a 9 g/L DO11/PMMA thin film sample. (b) Change in absorbance at 2.57 eV (482 nm) and 3.09 eV (401 nm) during decay.

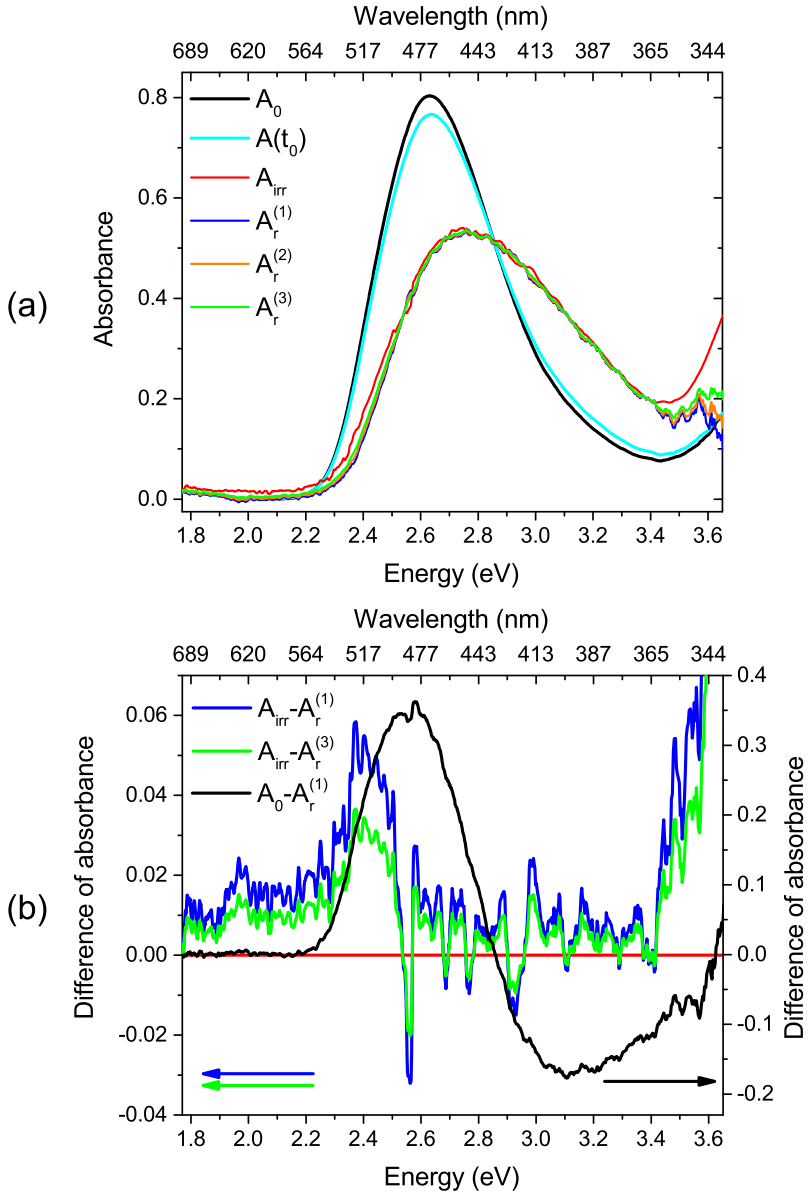

Figure A.4: (a) Absorbance of the pristine DO11/PMMA (A_0), the reversibly-damaged DO11/PMMA ($A_r^{(1)}$, $A_r^{(2)}$ and $A_r^{(3)}$, depending on the pathway of further decay described in the text) and the irreversibly-damaged DO11/PMMA (A_{irr}). $A\,(t_0)$ is the absorbance of DO11/PMMA sample measured at time t_0, at which time the pump laser was turned off. (b) Difference of absorbance between the reversibly-damaged species and the reversibly-damaged species $A_r^{(1)}$ and $A_r^{(3)}$ (see text and Table A.1), and between the pristine dye and the reversibly-damaged species $A_r^{(1)}$.

	$n_0(t_0)$	$n_r(t_0)$	$n_{irr}(t_0)$	$n_r(t \geq t_0) + n_{irr}(t \geq t_0)$
$A_r^{(1)}$	0.88258	0.07347	0.04395 ($n_{irr}(t \geq t_0) = n_{irr}^{\infty}$)	0.11742
$A_r^{(2)}$	0.88258	0.0879	0.02952	0.11742
$A_r^{(3)}$	0.88258	0.11742	0	0.11742

Table A.1: Fractions of three species n_0, n_r and n_{irr} at time t_0 that result in the corresponding absorbance of the reversibly-damaged DO11/PMMA species $A_r^{(1)}$, $A_r^{(2)}$ and $A_r^{(3)}$ shown in Figure A.4(a).

eV having nearly the same amplitude as the peak at about 2.57 eV in the first minute (12 - 13 min) suggests certain amount of the reversibly-damaged species decay to the irreversibly-damaged species. A much clearer result is observed in a spin-coated 1AAQ/PMMA during the recovery in Figure 7.2. The difference in absorbance between the reversibly- and irreversibly-damaged species is at the region below 2.70 eV and above 3.40 eV as shown in Figure A.4(b), i.e. the observed change in absorbance between 2.70 eV and 3.40 eV is due to the reversibly-damaged species recovers back to the fresh dye.

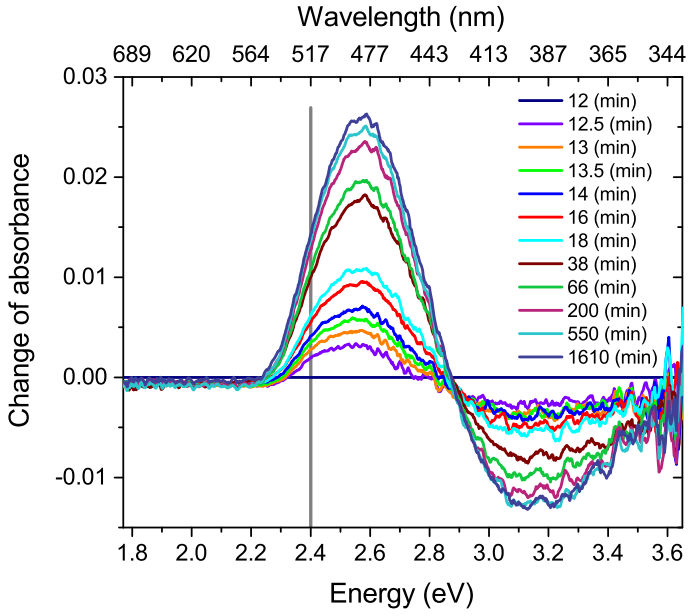

Figure A.5: Change in absorbance of a 9 g/L DO11/PMMA thin film relative to the spectrum taken at the 12$^{\text{th}}$ minute, the time at which the pump beam is turned off.

A.2 DO11/PS

A_{irr} of a 9 g/L DO11/PS sample was approximated by the absorption spectrum obtained after 90 minutes of irradiation using a 532 nm cw pump laser with peak intensity 35.01 W/cm^2 as shown in Figure A.6(a). The changing peaks of absorbance at 2.64 eV (470 nm) and 3.22 eV (385 nm) during 90 minutes of irradiation are shown in Figure A.6(b).

In the recovery experiment, a sample with same concentration was irradiated using the same laser with peak intensity 0.43 W/cm^2 for 7 minutes then kept in the dark. The change of absorbance at 2.64 eV (470 nm) and 3.22 eV (385 nm) are shown in Figure A.7. The absorption spectra of the last 20 minutes were averaged as an approximation of $A(t \to \infty)$ in Equation A.2, and $A(t \to \infty)$ between 465 nm and 475 nm were used to determine the averaged ratio of n_1/n_2. Using Equation A.2 and Figure A.6(a), n_{irr} can be determined and also averaged between 465 nm and 475 nm. Thus, $A_r^{(1)}$ is determined using Equation A.3 with the assumption $n_{irr}(t \geq t_0) = n_{irr}^{\infty}$ (corresponding to Figure A.1(a)) and plotted in Figure A.8. As we did for DO11/PMMA, we also loosen the assumption to $n_{irr}(t \geq t_0) \leq n_{irr}^{\infty}$ (corresponding to Figure A.1(b)) and tabulate n_0, n_r and n_{irr} at time t_0 in Table A.2, assuming that the total fraction of damaged molecules after time t_0, $n_r(t \geq t_0) + n_{irr}(t \geq t_0)$, is the same as previously calculated. The calculated $A_r^{(2)}$, $A_r^{(3)}$ and $A_r^{(4)}$ are plotted in Figure A.8(a), and some of the difference in absorbance between different species are shown in Figure A.8(b).

The absorbance of reversibly-damaged dye species varies drastically with $n_r(t_0)$ and $n_{irr}(t_0)$ in the near UV region. Figure A.8(a) shows that only $A_r^{(4)}$ crosses the isosbestic point at 3.01 eV, which is obtained from decay measurement as shown in Figure A.9 and Figure 5.8(a), among all A_r's. This implies that no irreversibly-damaged species was formed during the 7 minutes irradiation and all the reversibly-damaged species degraded into reversibly-damaged species after the pump laser was turned off. Though the isosbestic point provides a constraint to estimate A_r, the uncertainty due to different samples and white light probe sources used in the experiments as described earlier in this appendix makes it difficult to determine A_r accurately. The result may also change if we further relax the assumption that the total fraction of damaged dye molecules after time t_0, $n_r(t \geq t_0) + n_{irr}(t \geq t_0)$, is a constant as shown in Table A.2. Since the reversibly-damaged species can recover back to the fresh dye, $n_r(t_0)$ could be larger than what is obtained in Table A.2 as long as $n_{irr}(t \geq t_0) \leq n_{irr}^{\infty}$ and the calculated A_r crosses the isosbestic point. Nonetheless, we can still conclude from the above analysis that A_r is similar to A_{irr} in the visible region and there is a great portion of reversibly-damaged dye species further degraded into irreversibly-damaged species in the DO11/PS sample after the pump laser is turned off.

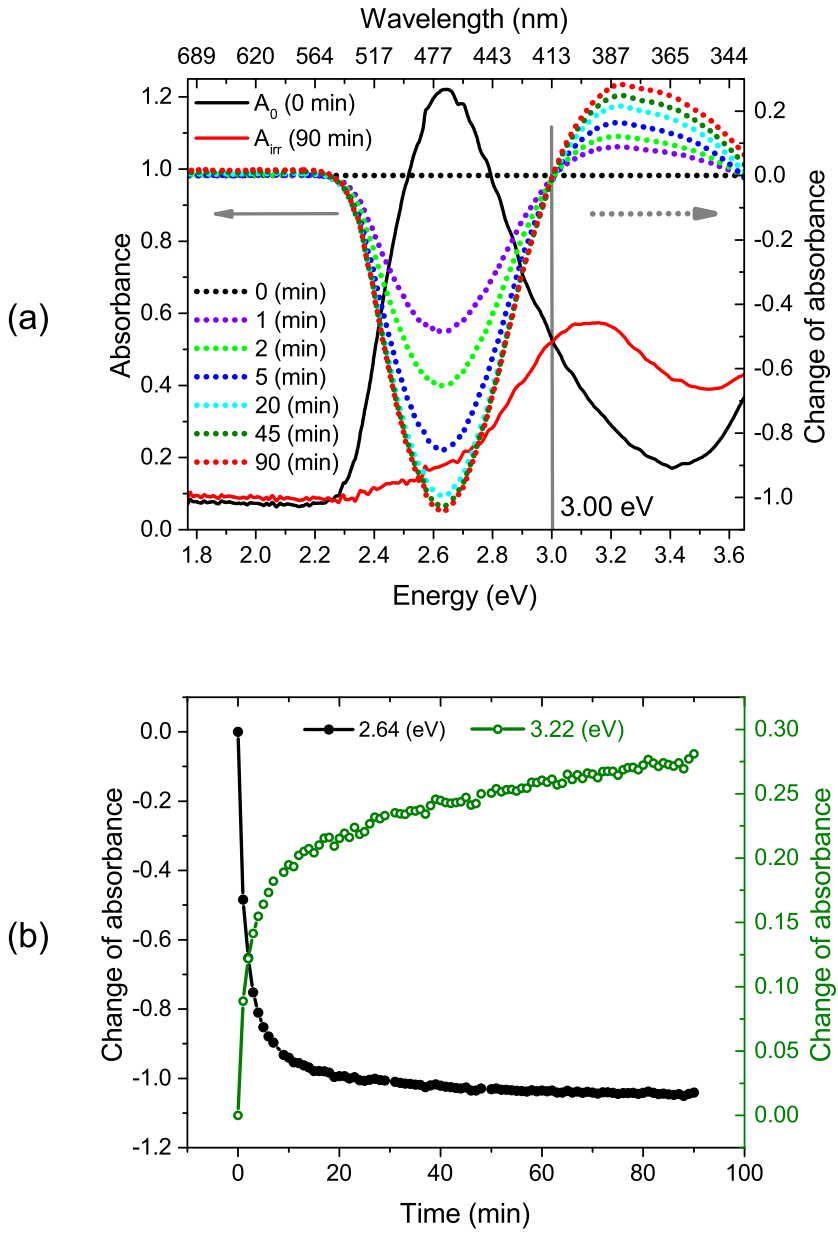

Figure A.6: (a) A_0 and A_{irr} of a 9 g/L DO11/PS thin film sample. (b) Change in absorbance at 2.64 eV (470 nm) and 3.22 eV (385 nm) during decay.

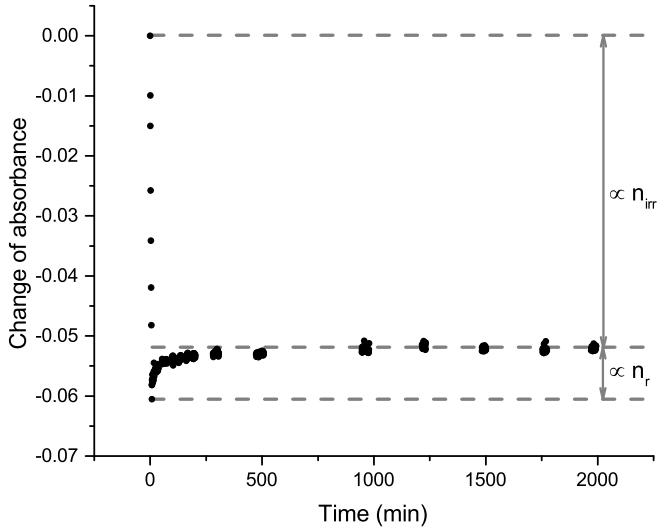

Figure A.7: Change in absorbance of DO11/PS at 2.64 eV (470 nm). The sample was irradiated with a 532 nm cw pump laser for 7 minutes then kept in the dark except for the time intervals during which absorbance was measured.

The change of absorbance relative to the spectrum taken at t_0 is shown in Figure A.9. The changing absorbance peak at near 2.6 eV during recovery is slightly red-shifted from that during decay. This can be rationalized by the results from the difference of absorbance in Figure A.8(b). When the reversibly-damaged species further decay into irreversibly-damaged species, a peak near 2.46 eV forms and the feature near 2.75 eV decays. Consequently the change in absorbance after the pump laser is turned off, including a large portion of further decay and a small portion of recovery, exhibits a red-shift. Notice that if there is no recovery at all, the change in absorbance should behave like the colored curves in Figure A.8(b). The isosbestic point moves from 3.01 eV during decay to 2.93 eV during recovery, as seen in Figure A.9, which corresponds to the isosbestic point between A_0 and A_r's and between A_r's and A_{irr} in Figure A.8, respectively. The shift in the isosbestic point for DO11/PS is in excellent agreement with the shift observed for DO11 in styrene as shown in Figure 5.9.

In this appendix, the absorbance of the reversibly-damaged dye species of DO11/P-MMA and DO11/PS are calculated based on the experimental results with simple assumptions. The results indicate that the reversibly- and irreversibly-damaged dye species in each polymer host have similar absorption spectra in the visible region, which is in agreement with the TD-DFT calculation that is presented in Chapter 6.

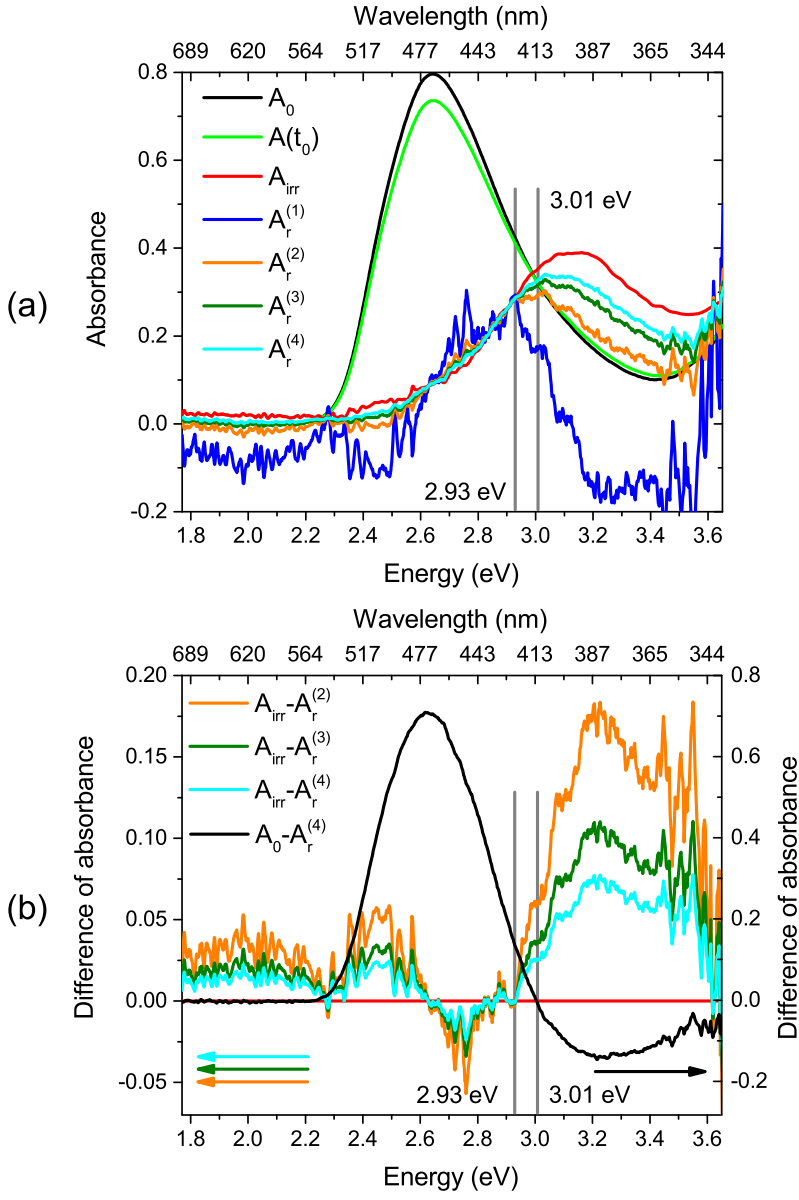

Figure A.8: (a) Absorbance of the pristine DO11/PS (A_0), the reversibly-damaged DO11/PS ($A_r^{(1)}$, $A_r^{(2)}$, $A_r^{(3)}$ and $A_r^{(4)}$, depending on the pathway of further decay described in the text) and the irreversibly-damaged DO11/PS (A_{irr}). $A\,(t_0)$ is the absorbance of DO11/PS sample measured at time t_0, at which time the pump laser was turned off. (b) Difference of absorbance between the reversibly-damaged species and the reversibly-damaged species $A_r^{(2)}$, $A_r^{(3)}$ and $A_r^{(4)}$ (see text and Table A.2), and between the pristine dye and the reversibly-damaged species $A_r^{(4)}$.

	$n_0(t_0)$	$n_r(t_0)$	$n_{irr}(t_0)$	$n_r(t \geq t_0) + n_{irr}(t \geq t_0)$
$A_r^{(1)}$	0.91412	0.01208	0.0738 ($n_{irr}(t \geq t_0) = n_{irr}^{\infty}$)	0.08588
$A_r^{(2)}$	0.91412	0.03624	0.04964	0.08588
$A_r^{(3)}$	0.91412	0.06039	0.02549	0.08588
$A_r^{(4)}$	0.91412	0.08588	0	0.08588

Table A.2: Fractions of three species n_0, n_r and n_{irr} at time t_0 that result in the corresponding absorbance of the reversibly-damaged DO11/PS species $A_r^{(1)}$, $A_r^{(2)}$, $A_r^{(3)}$ and $A_r^{(4)}$ shown in Figure A.8(a).

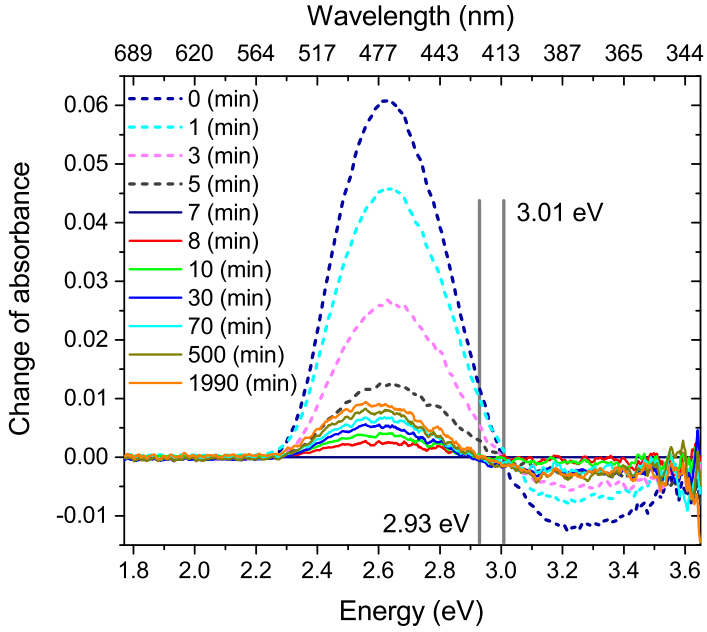

Figure A.9: Change in absorption spectrum of a 9 g/L DO11/PS thin film relative to the spectrum taken at the 7^{th} minute, the time when the pump laser is turned off.

Appendix B

Molecular orbitals and structures

The HOMO and LUMO electron density plots of the DO11 molecule and the proposed reversibly (Figure B.1) and irreversibly (Figure B.2) degraded species obtained by the TD-DFT calculations described in Chapter 6 are presented in this appendix. The lone-pair electron clouds of the amine group in the DO11 HOMO are reduced in its LUMO and oxygen atoms of both carbonyl groups, the center ring and the unsubstituted ring gain electron density in the LUMO. However, for all reversibly- and irreversibly-damaged species proposed in the PTCR hypothesis, the oxygen atom in the carbonyl group adjacent to the amine group does not gain electron density in the LUMO, hence the electron accepting power is lowered after photodegradation. As a result, the visible absorption spectra of all reversibly- and irreversibly-damaged species proposed in the PTCR hypothesis are similar due to the same portion of the ICT pathway remaining, as illustrated in Figure 2.7.

The ground state molecular structures of the DO11 molecule and the reversibly- and irreversibly-damaged species proposed in the PTCR hypothesis are obtained from the ground state geometry optimization described in Chapter 6. The results and the calculated dipole moments are shown in Figure B.3. Note that the amine group lies in the plane of the anthraquinone skeleton in the pristine DO11 molecule, and it is slightly out-of-plane and in some cases slightly twisted for the reversibly- and irreversibly-damaged species though it is still fairly planar. This may cause the decrease in the IR absorption peak of the in-plane NH_2 scissoring vibration as discussed in Chapter 7.

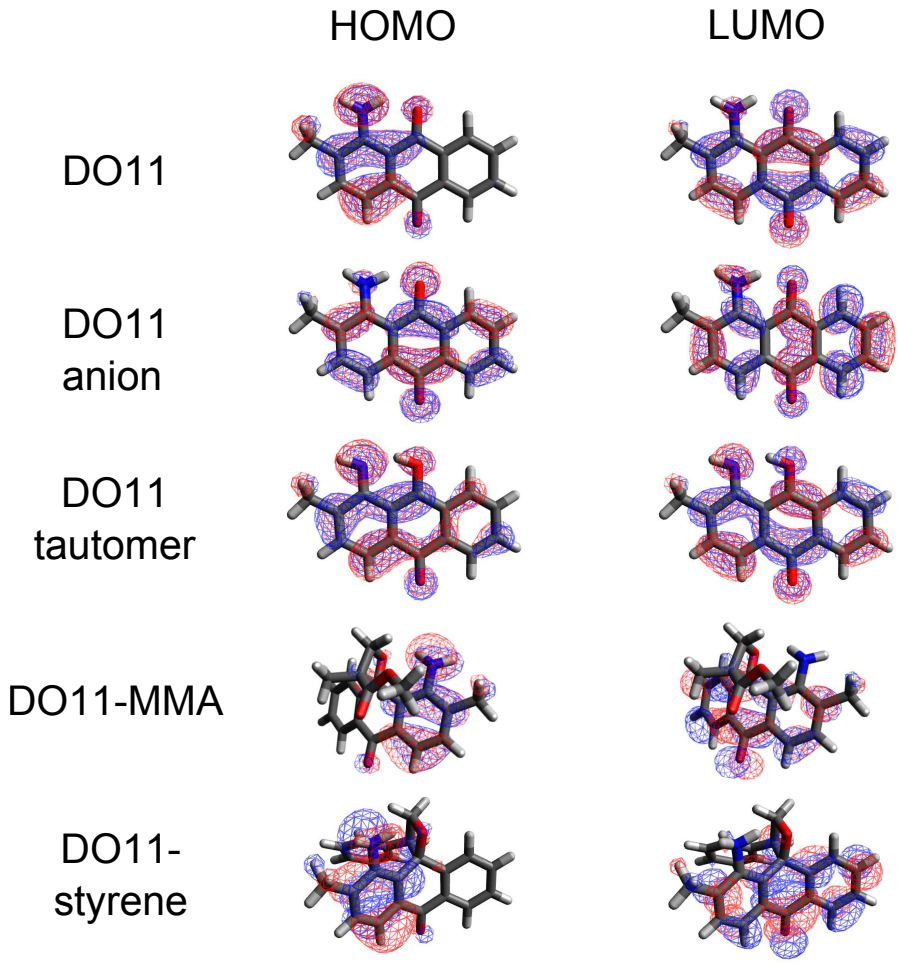

Figure B.1: HOMO and LUMO electron density of DO11 and the proposed reversibly-damaged species. Red and blue lobes indicate the electron density with opposite phases in the electron wavefunction. Colors in molecular structures: black represents the carbon atom, gray is the hydrogen atom, red is the oxygen atom and blue is the nitrogen atom.

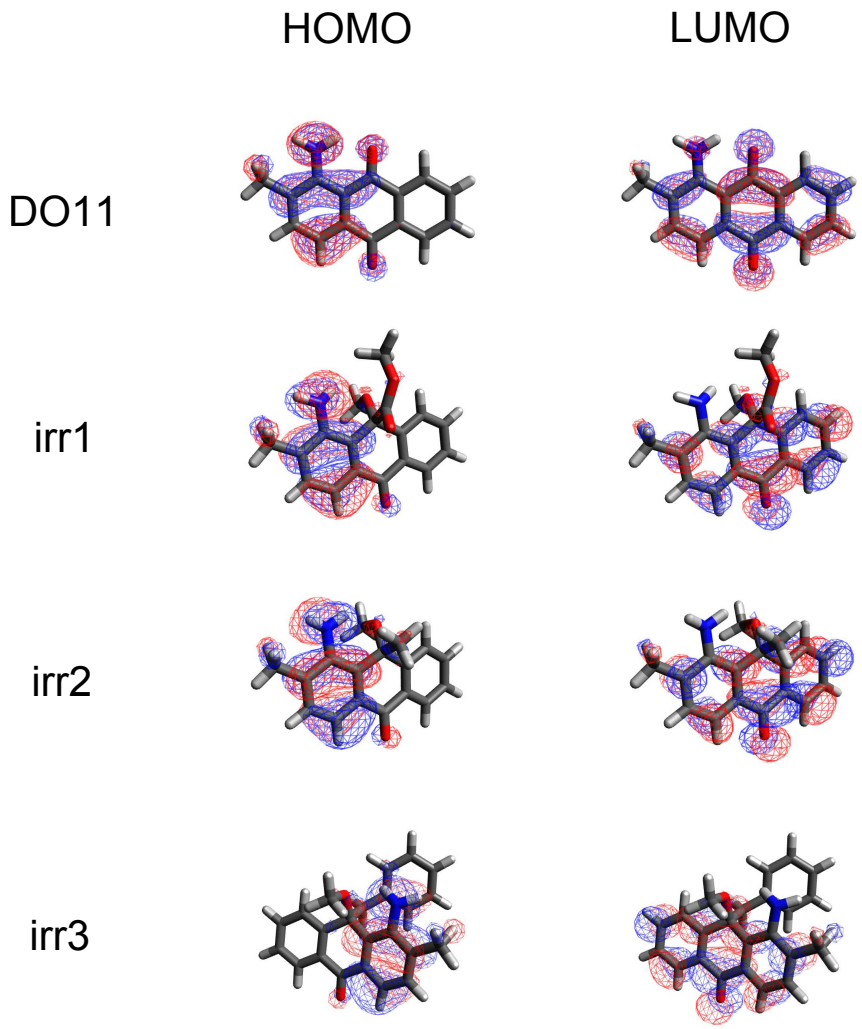

Figure B.2: HOMO and LUMO electron density of DO11 and the proposed irreversibly-damaged species. Red and blue lobes and colors in molecular structures have the same meaning as in Figure B.1.

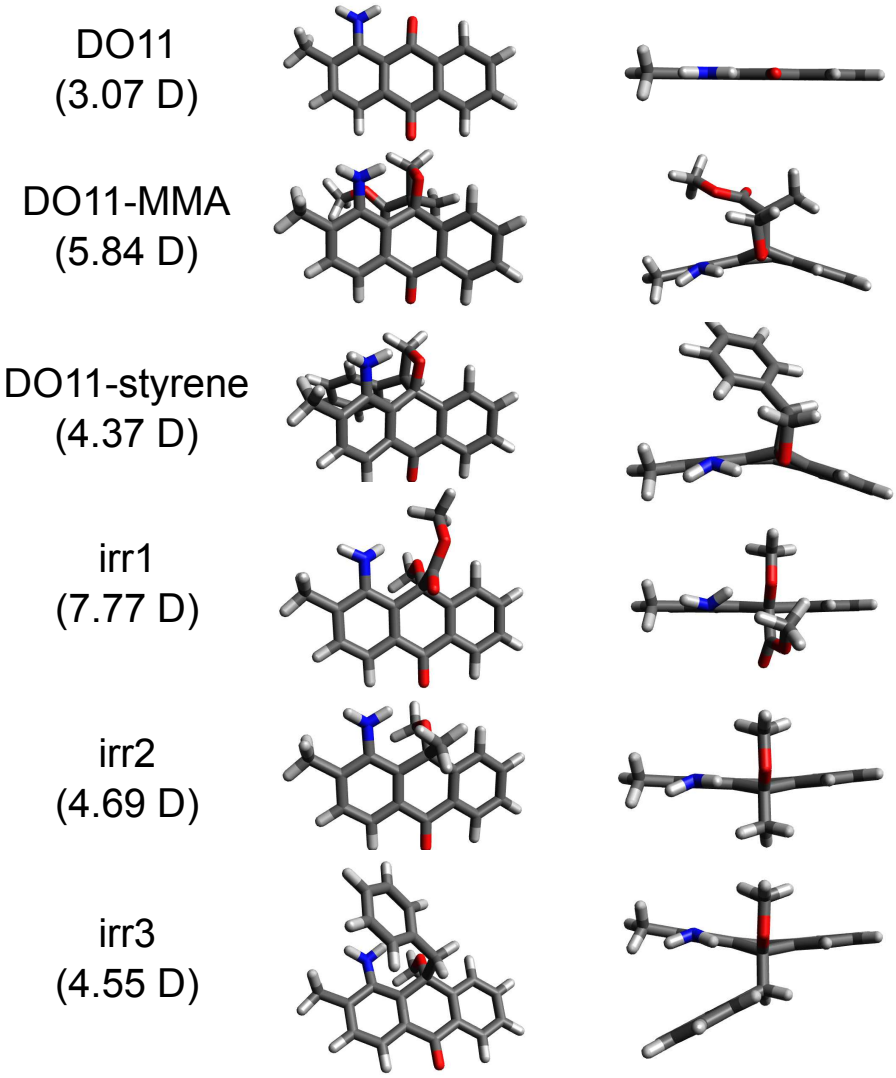

Figure B.3: Molecular structures of DO11 and the proposed reversibly- and irreversibly-damaged species optimized by DFT calculation. The calculated dipole moment (Debye) for each species is indicated in the parentheses. Colors in molecular structures have the same meaning as in Figure B.1.

Appendix C

Thickness of dye-doped polymer films

The thickness of all dye-doped polymer films sandwiched between two glass substrates and spin-coated on one glass substrate are estimated by the following method [60] using DO11/PMMA as an example.

A nearly constant baseline of the absorption spectrum is found between 450 and 470 nm for a glass slide and for a PMMA thin film sandwiched between two glass slides, which includes the effects of reflection and scattering. This offset is noticeably enlarged in the short wavelength region (wavelength shorter than 450 nm), but this does not affect the estimation of sample thickness since the DO11 absorption peak is centered at 471 nm. The constant offset can be obtained by averaging the spectrum in the long wavelength region, where DO11/PMMA samples do not absorb, and is subtracted when calculating the thickness of the thin film samples using the peak of the absorbance. The absorption spectrum of DO11/PMMA has the same peak position as that of DO11/MMA solution within the resolution limit of the spectrometer. The extinction coefficient of DO11 is obtained by averaging the results from four measurements of DO11/MMA liquid solutions with various concentrations. Note that the absorption of PMMA in the visible region is negligible in thin film samples. Thus, the thickness of DO11/PMMA thin films can be calculated using Lambert-Beer law.

Appendix D

Changes in the background of the FTIR system

The long-time changes in the background of the FTIR system are examined and compared with changes in the IR absorption peaks that do not belong to PMMA and 1AAQ in Figure D.1. The changes in the background may originate from pump oil depositing on the system.

A 1AAQ/PMMA spin-coated on a silicon substrate sample with concentration 105g/L was used in this control experiment. The sample was not irradiated throughout the experiment. Figure D.1(a) shows the change of IR absorption spectrum of 1AAQ/PMMA at the 1020^{th} minute and the 2580^{th} minute relative to the spectrum acquired at the beginning of the experiment (the 0^{th} minute), and thus they are the changes in the background of the system. A similar change in IR absorbance of a pure silicon substrate is also observed. Increasing IR peaks at 1464 cm^{-1}, 1716 cm^{-1}, 1731 cm^{-1}, and between 2850 and 3000 cm^{-1}, which are observed during recovery of 1AAQ/PMMA after photodegradation as shown in Chapter 7, are observed in this control experiment. The IR absorption bands at 1244 cm^{-1}(belonging to PMMA), 1280 cm^{-1} and 1546 cm^{-1}(belonging to 1AAQ) are also observed to increase in this control experiment.

The recovery in IR absorption bands is distinguishable during the first 150 or 540 minutes, and the increase of the IR peaks due to changes in the background of the system is only distinguishable starting at the spectrum taken at the 540^{th} minute as can be seen in Figure 7.6(b) and 7.7(b) in Chapter 7. Additionally, there are no growing IR peaks observed in this control experiment at 1608 cm^{-1}, which corresponds to the stretching vibration of the C=O adjacent to the amine group of 1AAQ, and at other frequencies corresponding to PMMA as observed during the recovery of photodegraded 1AAQ/PMMA. Therefore, the long-time

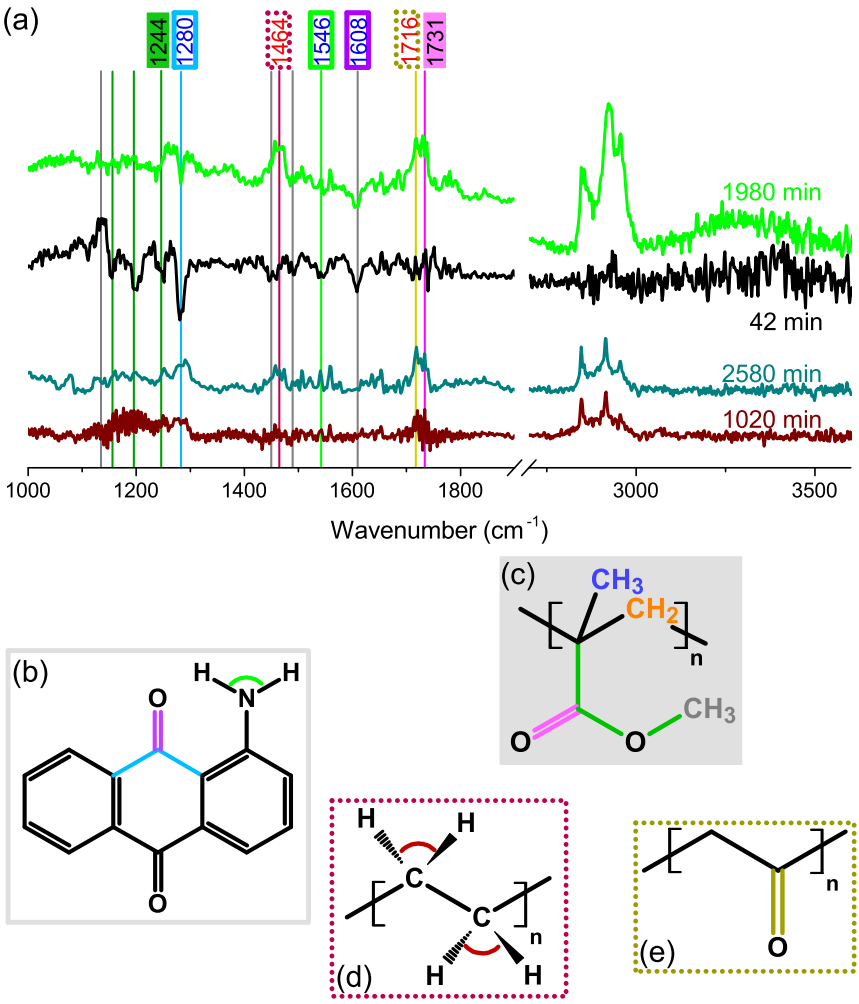

Figure D.1: (a) Comparison of change in IR absorbance of 1AAQ/PMMA during recovery (42 and 1980 min) and the background signals of the FTIR system (1020 and 2580 min). Peaks belonging to 1AAQ have wavenumbers circled by hollow rectangles with colors corresponding to that in the 1AAQ structure in (b). Peaks belonging to PMMA overlapping with the background signals are highlighted by rectangles with colors corresponding to that in the PMMA structure in (c). Peaks not belonging to PMMA and 1AAQ are illustrated with structures (d) and (e) using dotted rectangles with the corresponding colors shown in the structures.

increasing IR absorption bands are most likely due to the FTIR system.

The smaller amplitude of the change in IR absorbance observed in this control experiment than in the recovery experiment is possibly due to the renovation of the FTIR system including changing the vacuum pump. If that does not account for all the difference in amplitudes of the change in IR absorbance, the difference could be understood with the following reasons. The increasing CH_2 scissoring band of hydrocarbons at 1464 cm^{-1}, sp^3 CH stretch between 2850∼3000 cm^{-1}, and C=O stretch at 1716 cm^{-1} after irradiation suggest molecules or segments of polymer chains other than 1AAQ and PMMA are continuously formed after irradiation. This is possibly due to dissociated MMA, radicals and other fragments from reversibly-damaged dye species and PMMA reacting with each other and with the unsaturated chain ends of PMMA as described in Section 2.4. According to Grassie and Scott, approximately 50% of PMMA molecular chains have unsaturated chain ends [83], which can contribute to the increasing CH_2 scissoring band of hydrocarbons and the sp^3 CH stretching vibration. Unfortunately absorption bands of decreasing amplitude due to unsaturated carbon-carbon bonds and the corresponding C−H bending vibrations are not observed, perhaps hidden in the noise especially for wavenumbers below 1000 cm^{-1}. Note that the results and discussions in Chapter 7 are not affected whether this explanation is required here.

Appendix E

Disagreement between linear measurements

As discussed in Chapter 8, studies of photodegradation and recovery of DO11/PMMA using linear absorption spectroscopy disagree with the modified correlated chromophore domain model (CCDM) [16, 57], which was developed using data from transmittance image microscopy (TIM) [16, 52, 56]. In this appendix, we discuss the possible causes of the contradiction between the two linear measurements.

In TIM experiments, the transmittance of a narrow band light-emitting diode (LED) or a narrow wavelength range of a white light source selected with optical filters through a DO11/PMMA thin film sample is monitored using a charge-coupled device (CCD) during photodegradation or recovery [16, 52, 56]. The pump lasers used in TIM measurements are typically cw lasers with a wavelength between 464 and 514 nm, though there are also experiments done with pulsed laser at wavelength 532 nm [14, 16, 52, 60]. Irreversible damage [50] was observed after photodegradation of DO11/PMMA in TIM experiments in addition to the reversibly-damaged dye species observed in ASE experiments [9, 51, 53]. The reversible photodegradation of DO11/PMMA studied using the TIM technique was quantitatively described by the modified CCDM [16, 57] with the evolution among three species, as schematically illustrated in Figure E.1. The rate equations are given by

$$\begin{aligned} \frac{dn_0}{dt} &= -\left(\frac{\alpha I_p}{N} + \varepsilon I_p N\right) n_0 + \beta' N n_r, \\ \frac{dn_r}{dt} &= \frac{\alpha I_p}{N} n_0 - \beta' N n_r, \end{aligned} \tag{E.1}$$

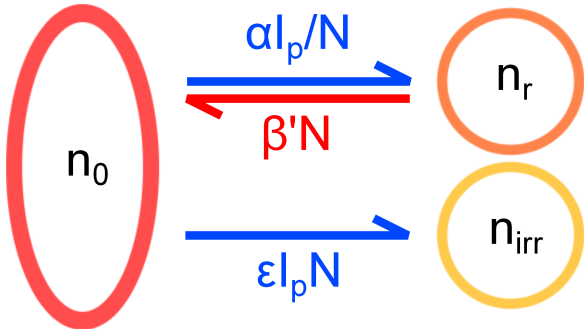

Figure E.1: Three species model with reversible decay rate $\alpha I_p/N$, recovery rate $\beta' N$ and irreversible decay rate $\varepsilon I_p N$. n_0, n_r and n_{irr} are the population fractions of undamaged, reversibly-damaged and irreversibly-damaged species, respectively.

and

$$\frac{dn_{irr}}{dt} = \varepsilon I_p N n_0, \tag{E.2}$$

where α is the reversible decay parameter, β' is the recovery parameter, ε is the irreversible decay parameter, I_p is the pump intensity, N is the domain size, n_0, n_r, n_{irr} are the fraction of fresh, reversibly-damaged and irreversibly-damaged dye species, respectively [16]. The domain distribution [53] is briefly reviewed in Chapter 1.

As described in Chapter 8, the photodegradation of DO11/PMMA undergoes different pathways with and without the accompany of ASE and thus exhibits completely opposite concentration dependence. A wide range of pump intensity in the order of 0.2 to 100 W/cm^2 has been used in TIM experiments with a wavelength between 464 and 532 nm [14, 16, 52, 60]. High pump intensity may cause a large amount of heat accumulation and activate damage mechanisms that are less possible to take place with low pump intensity. Different damage mechanisms may produce various damaged dye and polymer species that may affect the recovery process. The main issue with the modified CCDM is to describe all observations with the same set of rate equations [16, 57, 60] disregarding possible variations in the processes of photodegradation and recovery and in the products of photodegradation.

The peak intensity used in TIM experiments is typically in the order of 100 W/cm^2 at wavelengths between 464 and 514 nm (for example, 120 W/cm^2 at wavelength 488 nm was used as a pump [60]), but the peak intensity used in linear absorption spectroscopy experiments is 2-40 W/cm^2 at a wavelength of 532 nm. The absorbance of DO11/PMMA peaks at 471 nm; therefore, the absorbed power in a TIM experiment at 488 nm can be about 20 to 300 times greater than in linear absorption spectroscopy experiments, which results in a

large difference in the amount of accumulated heat. It is important to study the influence of the pump intensity on photodegradation of DO11/PMMA to determine whether the damage mechanisms or products are affected by pump intensity.

By fitting the decay and recovery data obtained from TIM measurements in DO11/PMMA with pump intensity 120 W/cm^2 at wavelength 488 nm to the modified CCDM and taking into account the depth effect using the Lambert-Beer law, incorporated with decay and recovery data obtained from linear absorption measurements with lower pump intensity (possibly between 2-40 W/cm^2) at wavelength 532 nm, the absorption cross sections of the pristine DO11 molecule, the reversibly-damaged and irreversibly-damaged species have been found [60]. Note that the absorption cross sections of both damaged species are found by assuming that there is no substantial difference in reversible photodegradation of DO11/PMMA with different pump intensities. The absorption cross section is referred to the absorbance in this appendix since they are proportional for the same species. The absorbance of the reversibly-damaged species, A_r^{TIM}, was found to be close to the absorbance of the pristine molecule, A_0^{TIM}. A_{irr}^{TIM}, the absorbance of the irreversibly-damaged species, was found to be similar to that obtained in Appendix A [60]. The calculated A_r^{TIM} suggests that the intramolecular charge transfer (ICT) between the amine group and both carbonyl groups in DO11 is minimally affected by reversible damage, yet the reversibly-damaged species does not produce ASE. However, the absorbance of the reversibly-damaged species, A_r, obtained using the linear absorption spectroscopy method as described in Appendix A is close to the absorbance of the irreversibly-dmamaged species, A_{irr}, which implies the ICT pathway being partially damaged in the reversibly-damaged species and is in agreement with the calculation results using TD-DFT in Chapter 6. The disagreement between A_r^{TIM}, which is a fit parameter for fitting TIM results using the modified CCDM, obtained using the TIM method incorporated with linear absorption spectroscopy method and A_r obtained using the linear absorption spectroscopy method is a substantial discrepancy. Unfortunately it is difficult to measure A_r^{TIM} and A_r directly. In contrast, A_{irr}^{TIM} and A_{irr} can be approximated from long time irradiation, where the other species are mostly depleted.

Photodegradation of DO11/PMMA samples is induced with a pump laser of 488 nm wavelength at peak intensity of 79.1 W/cm^2 using the linear absorption spectroscopy setup described in Section 3.3.2, and the result is shown in Figure E.2. The absorption spectrum at the 90$^{\text{th}}$ minute is approximately the absorbance of the irreversibly-damaged species since it is the long-time steady state spectrum. This spectrum differs from both A_{irr}^{TIM} calculated in the literature[60] and A_{irr} obtained in Appendix A. Note that the different pump laser wavelength used here does not cause a drastic difference in the absorption spectrum of the damaged species as can be seen in the same experiment performed with a peak intensity of 18.5 W/cm^2 shown in Figure E.3, in which the evolution in absorption spectrum is similar to that observed with the pump

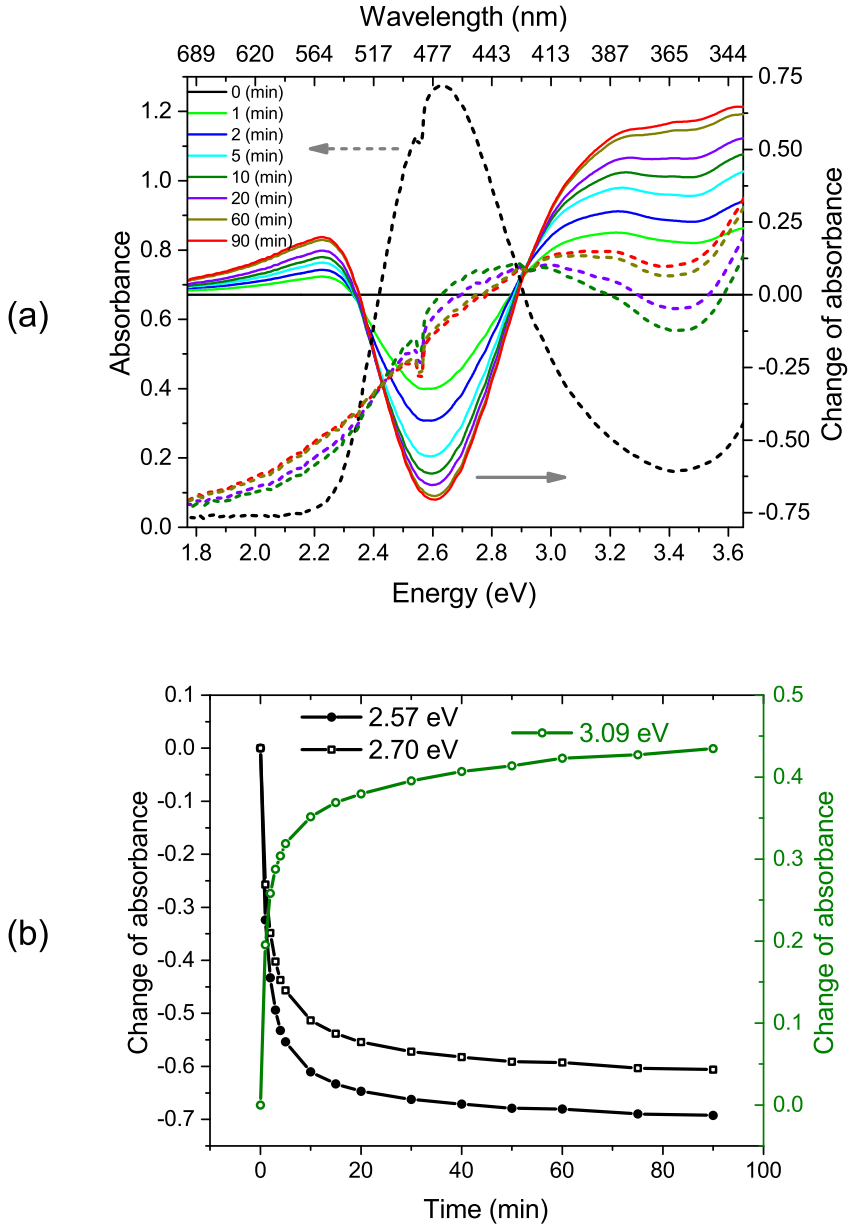

Figure E.2: Photodegradation of a 9 g/L DO11/PMMA sample irradiated with a 488 nm wavelength cw laser at 79.1 W/cm^2 intensity. (a) Absorbance and change of absorbance recorded at various times. (b) Change of absorbance as a function of time at 2.57 eV (482 nm), 2.70 eV (460 nm), and 3.09 eV (401 nm).

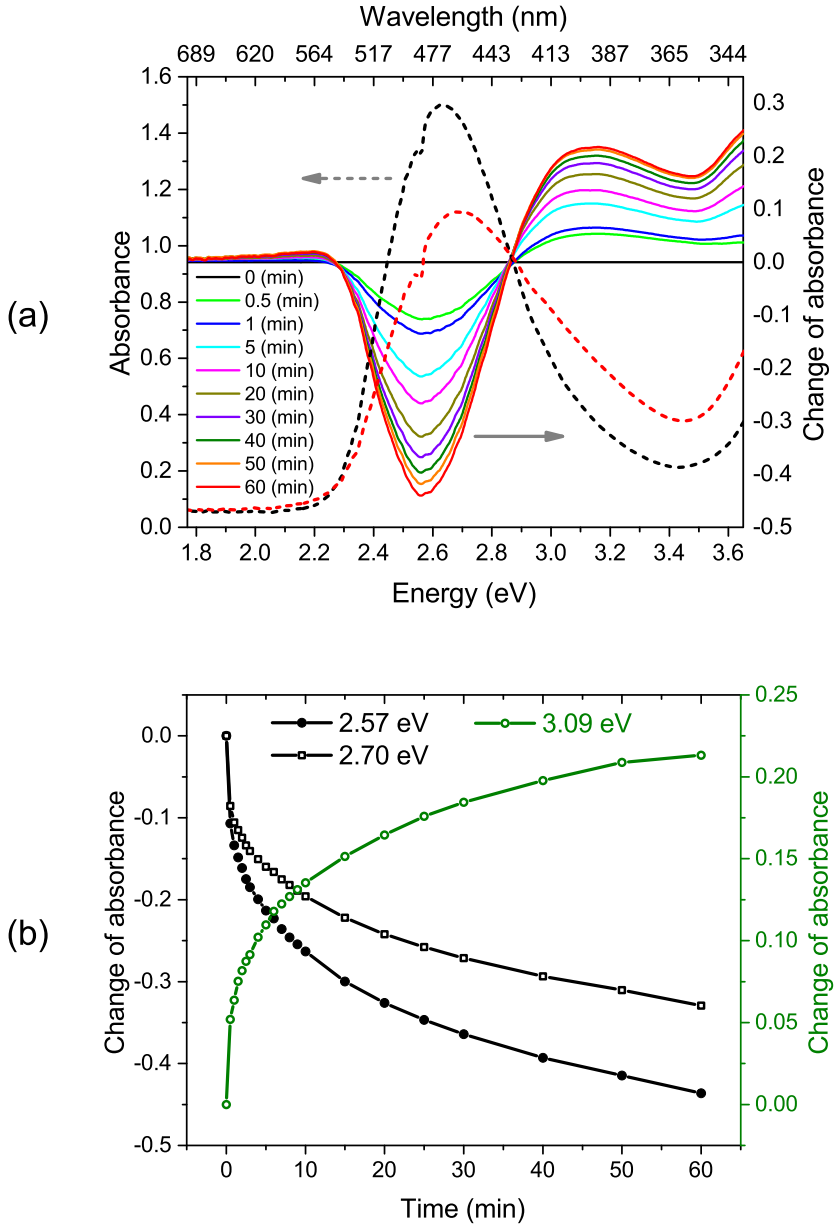

Figure E.3: Photodegradation of a 9 g/L DO11/PMMA sample irradiated with a 488 nm wavelength cw laser at 18.5 W/cm^2 intensity. (a) Absorbance and change of absorbance recorded at various times. (b) Change of absorbance as a function of time at 2.57 eV (482 nm), 2.70 eV (460 nm), and 3.09 eV (401 nm).

laser wavelength of 532 nm as described in Appendix A. Thus, the drastic difference in the absorbance of the end products seen in Figure E.2 results from the high pump intensity.

The above results suggest that the large amount of accumulated heat due to high pump intensity may activate more kinds of reactions between DO11 and thermally-degraded PMMA than when the pump intensity is much lower. In other words, the amount of deposited heat may result in different degradation process and damaged products. Note that the absorbance of the irreversibly-dmamaged species found in Appendix A (approximately A_{irr}) and in Figure E.2 (approximately A_{irr}^{TIM} for a typical TIM experiment) is obtained experimentally; hence it is independent of the kinetic model. Even if the irreversibly-damaged dye species were dominated by one species in a typical TIM measurement with pump intensity in the order of 100 W/cm^2, the calculated A_{irr}^{TIM} disagrees with the experimental result in Figure E.2.

The calculated A_r, as discussed in Appendix A, depends on the assumption that there are effectively three species converting into each other, and the result qualitatively agrees with the time-dependent density functional theory (TD-DFT) calculation described in Chapter 6. The calculated A_r^{TIM} depends on the assumptions of three populations, the form of the rate equations given by Equation E.1 and E.2 and no substantial difference in photodegradation of DO11/PMMA through a wide range of pump intensity. Since A_{irr}^{TIM} does not agree with the experimental result, A_r^{TIM} should also be re-examined. Additionally, none of the candidates of the possible reversibly-damaged species exhibit an absorption spectrum similar to the pristine DO11 spectrum (as A_r^{TIM} does) calculated using the TD-DFT calculation as described in Chapter 6.

TIM experiments probe the transmittance in a narrow wavelength range and can be approximated as a single wavelength, therefore the observations are similar to Figure E.2(b) and E.3(b) at various pump intensities. When fitting the results of TIM experiments to the modified CCDM, the absorption cross sections of reversibly- and irreversibly-damaged dye are fit parameters assumed to be the same for all observations, and the results obtained from different pump intensities, e.g. Figure E.2(b) and E.3(b), are assumed to satisfy the same set of rate equations in Equations E.1 and E.2. Thus, the modified CCDM was established by experimental results that do not distinguish the substantial difference of the processes and products of (reversible) photodegradation under various conditions.

Bibliography

[1] AnneL. Boreen, WilliamA. Arnold, and Kristopher McNeill. Photodegradation of pharmaceuticals in the aquatic environment: A review. *Aquatic Sciences*, 65(4):320–341, 2003.

[2] Chin-Chuan Liu, Yung-Hsu Hsieh, Pao-Fan Lai, Chia-Hsin Li, and Chao-Lang Kao. Photodegradation treatment of azo dye wastewater by uv/tio2 process. *Dyes and Pigments*, 68(2):191 – 195, 2006.

[3] Hiroyuki Daido. Review of soft x-ray laser researches and developments. *Reports on Progress in Physics*, 65(10):1513, 2002.

[4] Jun Hyuk Moon, Jamie Ford, and Shu Yang. Fabricating three-dimensional polymeric photonic structures by multi-beam interference lithography. *Polymers for Advanced Technologies*, 17(2):83–93, 2006.

[5] Banqiu Wu and Ajay Kumar. Extreme ultraviolet lithography: A review. *Journal of Vacuum Science & Technology B*, 25(6):1743–1761, 2007.

[6] Gang Ding Peng, Zhengjun Xiong, and Pak L. Chu. Fluorescence decay and recovery in organic dye-doped polymer optical fibers. *J. Lightwave Technol.*, 16(12):2365, Dec 1998.

[7] Olga V. Przhonska, Jin Hong Lim, David J. Hagan, Eric W. Van Stryland, Mikhail V. Bondar, and Yurij L. Slominsky. Nonlinear light absorption of polymethine dyes in liquid and solid media. *J. Opt. Soc. Am. B*, 15(2):802–809, Feb 1998.

[8] P K Singh and S T Lakshmikumar. Quenching and recovery of photoluminescence intensity of silicon nanoparticles embedded in optically transparent polymers. *Semiconductor Science and Technology*, 17(10):1123, 2002.

[9] Brent F. Howell and Mark G. Kuzyk. Amplified spontaneous emission and recoverable photodegradation in polymer doped with disperse orange 11. *J. Opt. Soc. Am. B*, 19(8):1790 – 1793, Aug 2002.

[10] P. Kobrin, R. Fisher, and A. Gurrola. Reversible photodegradation of organic light-emitting diodes. *Applied Physics Letters*, 85(12):2385–2387, 2004.

[11] Matteo Biancardo, Keld West, and Frederik C. Krebs. Optimizations of large area quasi-solid-state dye-sensitized solar cells. *Solar Energy Materials and Solar Cells*, 90(16):2575–2588, 2006.

[12] Ye Zhu, Juefei Zhou, and Mark G. Kuzyk. Two-photon fluorescence measurements of reversible photodegradation in a dye-doped polymer. *Opt. Lett.*, 32(8):958–960, Apr 2007.

[13] Logan DesAutels, Mark G. Kuzyk, and Chrisopher Brewer. Femtosecond bulk transparent material processing and recovery. *Opt. Express*, 17(21):18808 – 18819, Oct 2009.

[14] BR Anderson, SK Ramini, and MG Kuzyk. Imaging studies of photodamage and self-healing of anthraquinone derivative dye doped polymers. *SPIE Laser Damage Symposium Proc.*, 8190-16:81900N, 2011.

[15] Sheng-Ting Hung, Shiva K. Ramini, David G. Wyrick, Koen Clays, and Mark G. Kuzyk. The role of the polymer host on reversible photodegradation in disperse orange 11 dye. *Proc. SPIE*, 8474:84741A, 2012.

[16] Benjamin R Anderson. *Testing a generalized domain model of photodegradation and self-healing using novel optical characterization techniques and the effects of an applied electric field.* PhD thesis, WASHINGTON STATE UNIVERSITY, 2013.

[17] I Ayesta, M.A Illarramendi, J. Arrue, F. Jimenez, and J. Zubia. Two-photon-excited emission in polymer optical fibers doped with a conjugated polymer. *Photonics Journal, IEEE*, 6(4):1–9, Aug 2014.

[18] Benjamin R. Anderson, Ray Gunawidjaja, and Hergen Eilers. Self-healing organic-dye-based random lasers. *Opt. Lett.*, 40(4):577–580, Feb 2015.

[19] J G White, W B Amos, and M Fordham. An evaluation of confocal versus conventional imaging of biological structures by fluorescence light microscopy. *The Journal of Cell Biology*, 105(1):41–48, 1987.

[20] Winfried Denk, James H Strickler, and Watt W Webb. Two-photon laser scanning fluorescence microscopy. *Science*, 248(4951):73–76, 1990.

[21] Warren R Zipfel, Rebecca M Williams, and Watt W Webb. Nonlinear magic: multiphoton microscopy in the biosciences. *Nature biotechnology*, 21(11):1369–1377, 2003.

[22] Bo Huang, Mark Bates, and Xiaowei Zhuang. Super resolution fluorescence microscopy. *Annual review of biochemistry*, 78:993–1016, 2009.

[23] James E. Reeve, Hazel A. Collins, Kurt De Mey, Michael M. Kohl, Karl J. Thorley, Ole Paulsen, Koen Clays, and Harry L. Anderson. Amphiphilic porphyrins for second harmonic generation imaging. *Journal of the American Chemical Society*, 131(8):2758–2759, 2009. PMID: 19209855.

[24] James E. Reeve, Harry L. Anderson, and Koen Clays. Dyes for biological second harmonic generation imaging. *Phys. Chem. Chem. Phys.*, 12:13484–13498, 2010.

[25] Evelien De Meulenaere, Wei-Qiang Chen, Stijn Van Cleuvenbergen, Mei-Ling Zheng, Sotiris Psilodimitrakopoulos, Rik Paesen, Jean-Marc Taymans, Marcel Ameloot, Jos Vanderleyden, Pablo Loza-Alvarez, Xuan-Ming Duan, and Koen Clays. Molecular engineering of chromophores for combined second-harmonic and two-photon fluorescence in cellular imaging. *Chem. Sci.*, 3:984–995, 2012.

[26] Ismael Lopez-Duarte, James E. Reeve, Javier Perez-Moreno, Igor Boczarow, Griet Depotter, Jan Fleischhauer, Koen Clays, and Harry L. Anderson. "push-no-pull" porphyrins for second harmonic generation imaging. *Chem. Sci.*, 4:2024–2027, 2013.

[27] Sebastien Redon, Julien Massin, Sandrine Pouvreau, Evelien De Meulenaere, Koen Clays, Yves Queneau, Chantal Andraud, Agnes Girard-Egrot, Yann Bretonnière, and Stéphane Chambert. Red emitting neutral fluorescent glycoconjugates for membrane optical imaging. *Bioconjugate Chemistry*, 25(4):773–787, 2014. PMID: 24528385.

[28] Anders Hagfeldt, Gerrit Boschloo, Licheng Sun, Lars Kloo, and Henrik Pettersson. Dye-sensitized solar cells. *Chemical Reviews*, 110(11):6595–6663, 2010. PMID: 20831177.

[29] Daniel N. Congreve, Jiye Lee, Nicholas J. Thompson, Eric Hontz, Shane R. Yost, Philip D. Reusswig, Matthias E. Bahlke, Sebastian Reineke, Troy Van Voorhis, and Marc A. Baldo. External quantum efficiency above 100singlet-exciton-fission-based organic photovoltaic cell. *Science*, 340(6130):334–337, 2013.

[30] Harald Hoppe and Niyazi Serdar Sariciftci. Organic solar cells: An overview. *Journal of Materials Research*, 19(7):1924–1945, 7 2004.

[31] Serap Günes, Helmut Neugebauer, and Niyazi Serdar Sariciftci. Conjugated polymer-based organic solar cells. *Chemical Reviews*, 107(4):1324–1338, 2007. PMID: 17428026.

[32] Gang Li, Rui Zhu, and Yang Yang. Polymer solar cells. *Nature Photonics*, 6(3):153–161, 2012.

[33] BH Soffer and BB McFarland. Continuously tunable, narrow-band organic dye lasers. *Applied physics letters*, 10(10):266–267, 1967.

[34] Fritz Peter Schäfer, editor. *Dye lasers.* 3rd edition, 1990.

[35] FJ Duarte and LW Hillman, editors. *Dye laser principles with applications.* Academic Press, Boston, 1990.

[36] A. Costela, I. Garcia-Moreno, and R. Sastre. Polymeric solid-state dye lasers: Recent developments. *Phys. Chem. Chem. Phys.*, 5:4745–4763, 2003.

[37] Sébastien Chénais and Sebastien Forget. Recent advances in solid-state organic lasers. *Polymer International*, 61(3):390–406, 2012.

[38] Abhishek P. Kulkarni, Christopher J. Tonzola, Amit Babel, and Samson A. Jenekhe. Electron transport materials for organic light-emitting diodes. *Chemistry of Materials*, 16(23):4556–4573, 2004.

[39] Kiran T Kamtekar, Andrew P Monkman, and Martin R Bryce. Recent advances in white organic light-emitting materials and devices (woleds). *Advanced Materials*, 22(5):572–582, 2010.

[40] Dev Kumar Chatterjee, Li Shan Fong, and Yong Zhang. Nanoparticles in photodynamic therapy: An emerging paradigm. *Advanced Drug Delivery Reviews*, 60(15):1627–1637, 2008. 2008 Editors' Collection.

[41] Niagara Muhammad Idris, Muthu Kumara Gnanasammandhan, Jing Zhang, Paul C Ho, Ratha Mahendran, and Yong Zhang. In vivo photodynamic therapy using upconversion nanoparticles as remote-controlled nanotransducers. *Nature medicine*, 18(10):1580–1585, 2012.

[42] Gerald Donnert, Jan Keller, Rebecca Medda, M Alexandra Andrei, Silvio O Rizzoli, Reinhard Lührmann, Reinhard Jahn, Christian Eggeling, and Stefan W Hell. Macromolecular-scale resolution in biological fluorescence microscopy. *Proceedings of the National Academy of Sciences*, 103(31):11440–11445, 2006.

[43] RA Hoebe, CH Van Oven, Th WJ Gadella, PB Dhonukshe, CJF Van Noorden, and EMM Manders. Controlled light-exposure microscopy reduces photobleaching and phototoxicity in fluorescence live-cell imaging. *Nature biotechnology*, 25(2):249–253, 2007.

[44] Helena Greijer Agrell, Jan Lindgren, and Anders Hagfeldt. Degradation mechanisms in a dye-sensitized solar cell studied by uv-vis and ir spectroscopy. *Solar Energy*, 75(2):169–180, 2003.

[45] Mikkel Jørgensen, Kion Norrman, and Frederik C Krebs. Stability/degradation of polymer solar cells. *Solar Energy Materials and Solar Cells*, 92(7):686–714, 2008. Degradation and Stability of Polymer and Organic Solar Cells.

[46] Mohammad Ahmad, Terence A King, Do-Kyeong Ko, Byung Heon Cha, and Jongmin Lee. Performance and photostability of xanthene and pyrromethene laser dyes in sol-gel phases. *Journal of Physics D: Applied Physics*, 35(13):1473–1476, 2002.

[47] Edward Van Keuren and Wolfgang Schrof. Fluorescence recovery after two-photon bleaching for the study of dye diffusion in polymer systems. *Macromolecules*, 36(13):5002–5007, 2003.

[48] Dewu Long, Hongzhen Lin, and Ivan G. Scheblykin. Carbon nanotubes as photoprotectors of organic dyes: reversible photoreaction instead of permanent photo-oxidation. *Phys. Chem. Chem. Phys.*, 13:5771–5777, 2011.

[49] Brent F. Howell and M.G. Kuzyk. Lasing action and photodegradation of disperse orange 11 dye in liquid solution. *Applied Physics Letters*, 85(11):1901–1903, Sep 2004.

[50] Shiva K. Ramini, Benjamin Anderson, Sheng-Ting Hung, and Mark G. Kuzyk. Experimental tests of a new correlated chromophore domain model of self-healing in a dye-doped polymer. *Polym. Chem.*, 4:4948–4954, 2013.

[51] Natnael B. Embaye, Shiva K. Ramini, and Mark G. Kuzyk. Mechanisms of reversible photodegradation in disperse orange 11 dye doped in pmma polymer. *The Journal of Chemical Physics*, 129(5):054504, 2008.

[52] Benjamin Anderson, Shiva K. Ramini, and Mark G. Kuzyk. Imaging studies of photodamage and self-healing in disperse orange 11 dye-doped pmma. *J. Opt. Soc. Am. B*, 28(3):528–532, Mar 2011.

[53] Shiva K. Ramini and Mark G. Kuzyk. A self healing model based on polymer-mediated chromophore correlations. *The Journal of Chemical Physics*, 137(5):054705, 2012.

[54] Shiva K. Ramini, Nathan Dawson, and Mark G. Kuzyk. Testing the diffusion hypothesis as a mechanism of self-healing in disperse orange 11 doped in poly(methyl methacrylate). *J. Opt. Soc. Am. B*, 28(10):2408–2412, Oct 2011.

[55] Shiva Kumar Ramini. *Experimental investigations of a proposed chromophore correlation model of self healing of Disperse Orange 11 doped in Poly(methyl methacrylate)*. PhD thesis, Washington State University, 2012.

[56] Benjamin Anderson, Sheng-Ting Hung, and Mark G. Kuzyk. Influence of an electric field on photodegradation and self-healing in disperse orange 11 dye-doped pmma thin films. *J. Opt. Soc. Am. B*, 30(12):3193 – 3201, Dec 2013.

[57] Benjamin Anderson and Mark G Kuzyk. Generalizing the correlated chromophore domain model of reversible photodegradation to include the effects of an applied electric field. *Physical Review E*, 89(3):032601, 2014.

[58] Mark G. Kuzyk and Shiva Ramini. Correlated aggregate model of self-healing in dye-doped polymers. *Proc. SPIE*, 8519:85190E, 2012.

[59] Mark G. Kuzyk and Shiva Ramini. The role of polymer-mediated dopant correlations in damage moderation and self healing. *Proc. SPIE*, 8530:853014, 2012.

[60] Benjamin Anderson, Sheng-Ting Hung, and Mark G Kuzyk. The effect of pump depletion on reversible photodegradation. *Optics Communications*, 318:180–185, 2014.

[61] J. Malcolm Bruce. *The chemistry of the quinonoid compounds*. Part I. John Wiley & Sons, 1974. Chapter 9.

[62] Paul Francis Gordon and Peter Gregory. *Organic chemistry in colour*. Springer-Verlag, 1983. Chapter 4.

[63] Hiroyasu Inoue, Toshihiko Hoshi, Junko Yoshino, and Yoshie Tanizaki. The polarized absorption spectra of some α-aminoanthraquinones. *Bulletin of the Chemical Society of Japan*, 45(4):1018–1021, 1972.

[64] Hiroyasu Inoue, Toshihiko Hoshi, Junko Yoshino, and Yoshie Tanizaki. The polarized absorption spectra of some β-substituted anthraquinones. *Bulletin of the Chemical Society of Japan*, 46(2):380–384, 1973.

[65] Nathan J. Westfall and Carl W. Dirk. The photochemistry of the self-healing chromophore disperse orange 11. *Journal of Physical Organic Chemistry*, 25(8):704 – 712, 2012.

[66] M.B Hocking and S.M Mattar. Electron paramagnetic resonance examination of aqueous anthrasemiquinone radical anion. *Journal of Magnetic Resonance (1969)*, 47(2):187 – 199, 1982.

[67] Haruo Inoue, Atsuo Ezaki, Haruo Tomono, and Mitsuhiko Hida. Photocycloaddition of 1-aminoanthraquinones to dienes by visible light irradiation. *J. Chem. Soc., Chem. Commun.*, pages 860–861, 1979.

[68] Haruo Inoue, Atsuo Ezaki, Daiji Nakajima, Haruo Tomono, and Mitsuhiko Hida. Photocycloaddition of 1-aminoanthraquinones to dienes by visible light irradiation. *J. Chem. Soc., Perkin Trans. 1*, pages 1771–1773, 1982.

[69] Haruo Inoue, Atsuo Ezaki, and Mitsuhiko Hida. Mechanism of the photocycloaddition of 1-aminoanthraquinones to olefins by visible light irradiation; oxetan formation via an exciplex. *J. Chem. Soc., Perkin Trans. 2*, pages 833–839, 1982.

[70] Steven R. Flom and Paul F. Barbara. Proton transfer and hydrogen bonding in the internal conversion of s1 anthraquinones. *The Journal of Physical Chemistry*, 89(21):4489–4494, 1985.

[71] Dipak K. Palit, Haridas Pal, Tulsi Mukherjee, and Jai P. Mittal. Photodynamics of the s1 state of some hydroxy- and amino-substituted naphthoquinones and anthraquinones. *J. Chem. Soc., Faraday Trans.*, 86:3861–3869, 1990.

[72] T. P. Carter, M. H. Van Benthem, and G. D. Gillispie. Fluorescence and fluorescence excitation spectra of 1-aminoanthraquionone in an n-heptane shpol'skii matrix. *The Journal of Physical Chemistry*, 87(11):1891–1898, 1983.

[73] Shinichi Nagaoka and Umpei Nagashima. Effects of node of wave function upon excited-state intramolecular proton transfer of hydroxyanthraquinones and aminoanthraquinones. *Chemical Physics*, 206(3):353 – 362, 1996.

[74] B Abbas and MA Khalis. Dichroism of poly (methyl methacrylate) thin films doped with disperse orange 11 molecules. *Acta Phys. Pol. A*, 115:857–863, 2010.

[75] D Zarzeczańska, P Niedziałkowski, A Wcisło, L Chomicz, J Rak, and T Ossowski. Synthesis, redox properties, and basicity of substituted 1-aminoanthraquinones: spectroscopic, electrochemical, and computational studies in acetonitrile solutions. *Structural Chemistry*, 25(2):625–634, 2014.

[76] Sebastian van de Linde, Ivan Krstic, Thomas Prisner, Soren Doose, Mike Heilemann, and Markus Sauer. Photoinduced formation of reversible dye radicals and their impact on super-resolution imaging. *Photochem. Photobiol. Sci.*, 10:499–506, 2011.

[77] Chanchal Samanta. Direct synthesis of hydrogen peroxide from hydrogen and oxygen: An overview of recent developments in the process. *Applied Catalysis A: General*, 350(2):133 – 149, 2008.

[78] F. M. Fowkes, D. O. Tischler, J. A. Wolfe, L. A. Lannigan, C. M. Ademu-John, and M. J. Halliwell. Acid-base complexes of polymers. *Journal of Polymer Science: Polymer Chemistry Edition*, 22(3):547–566, 1984.

[79] Nicholas J. Turro. *Modern molecular photochemistry*. University Science Books, 1991.

[80] Larry Peck Kenneth W. Whitten, Raymond E. Davis and George G. Stanley. *Chemistry*. Thomson Brooks/Cole, 8th edition, 2007.

[81] Haruo Inoue, Mitsuhiko Hida, Nobuaki Nakashima, and Keitaro Yoshihara. Picosecond fluorescence lifetimes of anthraquinone derivatives. radiationless deactivation via intra- and intermolecular hydrogen bonds. *The Journal of Physical Chemistry*, 86(16):3184–3188, 1982.

[82] P. Dahiya, M. Kumbhakar, D.K. Maity, T. Mukherjee, A.B.R. Tripathi, N. Chattopadhyay, and H. Pal. Solvent polarity and intramolecular hydrogen bonding effects on the photophysical properties of 1-amino-9,10-anthraquinone dye. *Journal of Photochemistry and Photobiology A: Chemistry*, 181(2):338 – 347, 2006.

[83] Norman Grassie and Gerald Scott. *Polymer degradation and stabilisation*. Cambridge University Press, 1985.

[84] I.C. McNeill, M. Zulfiqar, and T. Kousar. A detailed investigation of the products of the thermal degradation of polystyrene. *Polymer Degradation and Stability*, 28(2):131 – 151, 1990.

[85] Lewis E. Manring. Thermal degradation of poly(methyl methacrylate). 4. random side-group scission. *Macromolecules*, 24(11):3304–3309, 1991.

[86] Jeffery D Peterson, Sergey Vyazovkin, and Charles A Wight. Kinetics of the thermal and thermo-oxidative degradation of polystyrene, polyethylene and poly (propylene). *Macromolecular Chemistry And Physics*, 202(6):775–784, 2001.

[87] M. Ferriol, A. Gentilhomme, M. Cochez, N. Oget, and J.L. Mieloszynski. Thermal degradation of poly(methyl methacrylate) (pmma): modelling of {DTG} and {TG} curves. *Polymer Degradation and Stability*, 79(2):271 – 281, 2003.

[88] Stanislav I. Stoliarov, Phillip R. Westmoreland, Marc R. Nyden, and Glenn P. Forney. A reactive molecular dynamics model of thermal decomposition in polymers: I. poly(methyl methacrylate). *Polymer*, 44(3):883 – 894, 2003.

[89] Lewis E. Manring. Thermal degradation of saturated poly(methyl methacrylate). *Macromolecules*, 21(2):528–530, 1988.

[90] Lewis E. Manring. Thermal degradation of poly(methyl methacrylate). 2. vinyl-terminated polymer. *Macromolecules*, 22(6):2673–2677, 1989.

[91] Lewis E. Manring, Dotsevi Y. Sogah, and Gordon M. Cohen. Thermal degradation of poly(methyl methacrylate). 3. polymer with head-to-head linkages. *Macromolecules*, 22(12):4652–4654, 1989.

[92] Takashi Kashiwagi, T. Hirata, and J. E. Brown. Thermal and oxidative degradation of poly(methyl methacrylate) molecular weight. *Macromolecules*, 18(2):131–138, 1985.

[93] Takashi Kashiwagi, Atsushi Inaba, James E. Brown, Koichi Hatada, Tatsuki Kitayama, and Eiji Masuda. Effects of weak linkages on the thermal and oxidative degradation of poly(methyl methacrylates). *Macromolecules*, 19(8):2160–2168, 1986.

[94] T. Hirata, Takashi Kashiwagi, and J. E. Brown. Thermal and oxidative degradation of poly(methyl methacrylate): weight loss. *Macromolecules*, 18(7):1410–1418, 1985.

[95] B.J. Holland and J.N. Hay. The kinetics and mechanisms of the thermal degradation of poly(methyl methacrylate) studied by thermal analysis-fourier transform infrared spectroscopy. *Polymer*, 42(11):4825 – 4835, 2001.

[96] B.J Holland and J.N Hay. The effect of polymerisation conditions on the kinetics and mechanisms of thermal degradation of {PMMA}. *Polymer Degradation and Stability*, 77(3):435 – 439, 2002.

[97] Yu-Hsiang Hu and Chuh-Yung Chen. The effect of end groups on the thermal degradation of poly(methyl methacrylate). *Polymer Degradation and Stability*, 82(1):81–88, 2003.

[98] Jan F Rabek and Bengt Rånby. Studies on the photooxidation mechanism of polymers. ii. the role of quinones as sensitizers in the photooxidative degradation of polystyrene. *Journal of Polymer Science: Polymer Chemistry Edition*, 12(2):295–306, 1974.

[99] Itaru Mita, Toshie Takagi, Kazuyuki Horie, and Yoichi Shindo. Photosensitized degradation of polystyrene by benzophenone in benzene solution. *Macromolecules*, 17(11):2256–2260, 1984.

[100] Itaru Mita, Tetsuhiko Hisano, Kazuyuki Horie, and Akio Okamoto. Photoinitiated thermal degradation of polymers. i. elementary processes of degradation of polystyrene. *Macromolecules*, 21(10):3003–3010, 1988.

[101] H Kaczmarek, A Kamińska, M Świątek, and S Sanyal. Photoinitiated degradation of polystyrene in the presence of low-molecular organic compounds. *European Polymer Journal*, 36(6):1167 – 1173, 2000.

[102] Itaru Mita, Kazuhito Obata, and Kazuyuki Horie. Photoinitiated thermal degradation of polymers ii. poly (methyl methacrylate). *Polymer Journal*, 22(5):397–410, 1990.

[103] O. Chiantore, L. Trossarelli, and M. Lazzari. Photooxidative degradation of acrylic and methacrylic polymers. *Polymer*, 41(5):1657 – 1668, 2000.

[104] Hiroshi Fukumura, Nobuko Mibuka, Shigeru Eura, and Hiroshi Masuhara. Mass spectrometric studies on laser ablation of polystyrene sensitized with anthracene. *The Journal of Physical Chemistry*, 97(51):13761–13766, 1993.

[105] C Egami, Y Kawata, Y Aoshima, H Takeyama, F Iwata, O Sugihara, M Tsuchimori, O Watanabe, H Fujimura, and N Okamoto. Visible-laser ablation on a nanometer scale using urethane-urea copolymers. *Optics Communications*, 157(1):150 – 154, 1998.

[106] M. S. Silverstein, I. Visoly, O. Kesler, M. Janai, and Y. Cassuto. Plasma polymer films for 532 nm laser micromachining. *Journal of Vacuum Science & Technology B*, 16(6):2957–2967, 1998.

[107] Sergei Popov. Dye photodestruction in a solid-state dye laser with a polymeric gain medium. *Appl. Opt.*, 37(27):6449–6455, Sep 1998.

[108] Anthony E Siegman. *Lasers*. University Science Books, 1986.

[109] John David Jackson. *Classical electrodynamics*. John Wiley & Sons, 3rd edition, 1999.

[110] Peter R Griffiths and James A De Haseth. *Fourier Transform Infrared Sepectrometry*. John Wiley & Sons, 1986.

[111] Marcus T. Cicerone, F. R. Blackburn, and M. D. Ediger. Anomalous diffusion of probe molecules in polystyrene: Evidence for spatially heterogeneous segmental dynamics. *Macromolecules*, 28(24):8224–8232, 1995.

[112] Andrey V. Veniaminov and Hans Sillescu. Polymer and dye probe diffusion in poly(methyl methacrylate) below the glass transition studied by forced rayleigh scattering. *Macromolecules*, 32(6):1828–1837, 1999.

[113] H. E. Rose. Breakdown of the lambert-beer law. *Nature*, 169:287–288, 1952.

[114] Robert G Parr and Weitao Yang. *Density-functional theory of atoms and molecules*. Oxford university press, 1989.

[115] Daniel Joubert, editor. *Density functionals: theory and applications*. Springer-Verlag, 1998.

[116] Eberhard Engel and Reiner M Dreizler. *Density functional theory*. Springer, 2011.

[117] Pierre Hohenberg and Walter Kohn. Inhomogeneous electron gas. *Physical review*, 136(3B):B864, 1964.

[118] Brian Harold Bransden and Charles Jean Joachain. *Physics of atoms and molecules*. Pearson Education, 2nd edition, 2003.

[119] Walter Kohn and Lu Jeu Sham. Self-consistent equations including exchange and correlation effects. *Physical Review*, 140(4A):A1133, 1965.

[120] Walter Kohn. Nobel lecture: Electronic structure of matter-wave functions and density functionals. *Reviews of Modern Physics*, 71(5):1253–1266, 1999.

[121] Erich Runge and E. K. U. Gross. Density-functional theory for time-dependent systems. *Phys. Rev. Lett.*, 52:997–1000, Mar 1984.

[122] M. Petersilka, U. J. Gossmann, and E. K. U. Gross. Excitation energies from time-dependent density-functional theory. *Phys. Rev. Lett.*, 76:1212–1215, Feb 1996.

[123] Denis Jacquemin, Julien Preat, Magali Charlot, Valérie Wathelet, Jean-Marie André, and Eric A Perpète. Theoretical investigation of substituted anthraquinone dyes. *The Journal of Chemical Physics*, 121(4):1736–1743, 2004.

[124] Denis Jacquemin, Valérie Wathelet, Julien Preat, and Eric A Perpète. Ab initio tools for the accurate prediction of the visible spectra of anthraquinones. *Spectrochimica Acta Part A: Molecular and Biomolecular Spectroscopy*, 67(2):334 – 341, 2007.

[125] Denis Jacquemin, Eric A. Perpète, Gustavo E. Scuseria, Ilaria Ciofini, and Carlo Adamo. Td-dft performance for the visible absorption spectra of organic dyes: conventional versus long-range hybrids. *Journal of Chemical Theory and Computation*, 4(1):123–135, 2008.

[126] Denis Jacquemin, Eric Brémond, Aurélien Planchat, Ilaria Ciofini, and Carlo Adamo. Td-dft vibronic couplings in anthraquinones: From basis set and functional benchmarks to applications for industrial dyes. *Journal of Chemical Theory and Computation*, 7(6):1882–1892, 2011.

[127] Denis Jacquemin, AurÃ©lien Planchat, Carlo Adamo, and Benedetta Mennucci. Td-dft assessment of functionals for optical 0â€“0 transitions in solvated dyes. *Journal of Chemical Theory and Computation*, 8(7):2359–2372, 2012.

[128] Denis Jacquemin, Eric Brémond, Ilaria Ciofini, and Carlo Adamo. Impact of vibronic couplings on perceived colors: Two anthraquinones as a working example. *The Journal of Physical Chemistry Letters*, 3(4):468–471, 2012.

[129] Eric A Perpète, Valerie Wathelet, Julien Preat, Christophe Lambert, and Denis Jacquemin. Toward a theoretical quantitative estimation of the λmax of anthraquinones-based dyes. *Journal of Chemical Theory and Computation*, 2(2):434–440, 2006.

[130] Jürgen Fabian. Tddft-calculations of vis/nir absorbing compounds. *Dyes and Pigments*, 84(1):36 – 53, 2010.

[131] Laura L. Walkup, Krishanthi C. Weerasinghe, Minli Tao, Xueqin Zhou, Minhua Zhang, Dongzhi Liu, and Lichang Wang. Importance of dynamics in electron excitation and transfer of organic dyes. *The Journal of Physical Chemistry C*, 114(45):19521–19528, 2010.

[132] Piotr Cysewski and Tomasz Jeliński. Accuracy of color prediction of anthraquinone dyes in methanol solution estimated from first principle quantum chemistry computations. *Journal of Molecular Modeling*, 19(10):4089–4097, 2013.

[133] John P Lowe and Kirk A Peterson. *Quantum chemistry*. Academic Press, 3rd edition, 2006.

[134] Axel D. Becke. Density-functional thermochemistry. iii. the role of exact exchange. *The Journal of Chemical Physics*, 98(7):5648–5652, 1993.

[135] P. J. Stephens, F. J. Devlin, C. F. Chabalowski, and M. J. Frisch. Ab initio calculation of vibrational absorption and circular dichroism spectra using density functional force fields. *The Journal of Physical Chemistry*, 98(45):11623–11627, 1994.

[136] S Miertuš, E Scrocco, and J Tomasi. Electrostatic interaction of a solute with a continuum. a direct utilizaion of {AB} initio molecular potentials for the prevision of solvent effects. *Chemical Physics*, 55(1):117 – 129, 1981.

[137] E Cances, B Mennucci, and J Tomasi. A new integral equation formalism for the polarizable continuum model: Theoretical background and applications to isotropic and anisotropic dielectrics. *The Journal of Chemical Physics*, 107(8):3032–3041, 1997.

[138] Benedetta Mennucci and Jacopo Tomasi. Continuum solvation models: A new approach to the problem of solute's charge distribution and cavity boundaries. *The Journal of Chemical Physics*, 106(12):5151–5158, 1997.

[139] Chemical Rubber Company. *CRC handbook of chemistry and physics (Online)*. Boca Raton, Fla. : CRC Press : Taylor & Francis, electronic edition, 1978.

[140] Hiroshi Nagai, Haruaki Watanabe, and Atsuo Nishioka. Infrared spectra of deuterated polymethyl methacrylates. *Journal of Polymer Science*, 62(174):S95–S98, 1962.

[141] H. Nagai. Infrared spectra of stereoregular polymethyl methacrylate. *Journal of Applied Polymer Science*, 7(5):1697–1714, 1963.

[142] H.A Willis, V.J.I Zichy, and P.J Hendra. The laser-raman and infra-red spectra of poly(methyl methacrylate). *Polymer*, 10(0):737 – 746, 1969.

[143] Robert Silverstein and Francis Webster. *Spectrometric identification of organic compounds*. John Wiley & Sons, 6th edition, 1998.

[144] Jerry Workman. *Handbook of Organic Compounds: UV-Vis and NIR spectra*, volume 1. Academic press, 2001.

[145] Bohdan Schneider, Jan Štokr, Pavel Schmidt, Marian Mihailov, Stoil Dirlikov, and Nadezhda Peeva. Stretching and deformation vibrations of ch2, c(ch3) and o(ch3) groups of poly(methyl methacrylate). *Polymer*, 20(6):705 – 712, 1979.

[146] M St C Flett. The application of infra-red spectroscopy to structural problems in the anthraquinone field. *J. Chem. Soc.*, pages 1441–1448, 1948.

[147] Daimay Lin-Vien, Norman B Colthup, William G Fateley, and Jeanette G Grasselli. *The handbook of infrared and Raman characteristic frequencies of organic molecules*. Elsevier, 1991.

[148] P.J. Linstrom and W.G. Mallard, editors. *NIST Mass Spec Data Center, S.E. Stein, director, "Infrared Spectra" in NIST Chemistry WebBook, NIST Standard Reference Database Number 69*. National Institute of Standards and Technology, Gaithersburg MD, 20899, retrieved February 5, 2015. http://webbook.nist.gov.

[149] J C Phillips. Stretched exponential relaxation in molecular and electronic glasses. *Reports on Progress in Physics*, 59(9):1133, 1996.

[150] Ranko Richert. Heterogeneous dynamics in liquids: fluctuations in space and time. *Journal of Physics: Condensed Matter*, 14(23):R703, 2002.

[151] M. D. Ediger. Spatially heterogeneous dynamics in supercooled liquids. *Annual review of physical chemistry*, 51(1):99–128, 2000.

[152] Peter G Wolynes and Vassiliy Lubchenko, editors. *Structural Glasses and Supercooled Liquids: Theory, Experiment, and Applications*. John Wiley & Sons, 2012. Chapter 1.

[153] R Richert and H Bässler. Merocyanine - spiropyran transformation in a polymer matrix: an example of a dispersive chemical reaction. *Chemical Physics Letters*, 116(4):302 – 306, 1985.

[154] M.N. Berberan-Santos, E.N. Bodunov, and B. Valeur. Mathematical functions for the analysis of luminescence decays with underlying distributions 1. kohlrausch decay function (stretched exponential). *Chemical Physics*, 315(1-2):171 – 182, 2005.

[155] C. A. Angell, K. L. Ngai, G. B. McKenna, P. F. McMillan, and S. W. Martin. Relaxation in glassforming liquids and amorphous solids. *Journal of Applied Physics*, 88(6):3113–3157, 2000.

FACULTEIT WETENSCHAPPEN
DEPARTEMENT CHEMIE
AFDELING MOLECULAIRE VISUALISATIE EN FOTONICA
Afdeling Moleculaire Visualisatie en Fotonica, Celestijnenlaan 200D
B-3001 Heverlee